International
Progress Report

IPR-06-11

Äspö Hard Rock Laboratory

Temperature Buffer Test

Evaluation modeling – Mock-up test

Edited by

Mattias Åkesson
Clay Technology AB

March 2006

Svensk Kärnbränslehantering AB
Swedish Nuclear Fuel
and Waste Management Co
Box 5864
SE-102 40 Stockholm Sweden
Tel 08-459 84 00
+46 8 459 84 00
Fax 08-661 57 19
+46 8 661 57 19

Äspö Hard Rock
Laboratory

Report no.
IPR-06-11
Author
Mattias Åkesson
Checked by
Bertrand Vignal
Approved
Anders Sjöland

No.
F12K
Date
March 2006
Date
April 2006
Date
2006-08-15

Äspö Hard Rock Laboratory

Temperature Buffer Test

Evaluation modeling – Mock-up test

Edited by

Mattias Åkesson
Clay Technology AB

March 2006

Keywords: Buffer, Bentonite, THM, Modeling, Mock-up, Test, Temperature, Hydration, Stress, Strain

Résumé

TBT (Test de Barrière ouvragée en Température) est un projet mené dans le Hard Rock Laboratory d'Äspö en Suède par SKB et l'ANDRA, soutenu par ENRESA et DBE, qui vise à comprendre et modéliser le comportement thermo-hydro-mécanique de barrières ouvragées à base d'argile gonflante soumises à des températures élevées (> 100°C) pendant le processus de leur hydratation.

Depuis le début du projet, différentes tâches de modélisation ont été continûment développées. Les calculs de dimensionnement et les modélisations prédictives de la désaturation initiale du test *in situ* ont été antérieurement rapportés.

Le présent rapport traite de la modélisation prédictive relative à un essai sur maquette (TBT_2) réalisé par le CEA à Saclay (France) concernant le processus de désaturation de la bentonite observé dans l'essai *in situ* autour de la sonde chauffante inférieure. Cette tâche a été réalisée en 2005.

Toutes les prédictions, comme les résultats du test sur maquette, indiquent que la redistri-bution de l'eau dans la bentonite intervient dès qu'apparaît un gradient thermique. Ainsi les résultats infirment l'hypothèse selon laquelle existerait un seuil de gradient thermique. Les modèles montrent en outre que, plus que le gradient thermique, c'est la différence de température entre les faces "froide" et "chaude" qui détermine l'étendue de la redistribu-tion d'eau.

Abstract

TBT (Temperature Buffer Test) is a joint project between SKB/ANDRA, supported by ENRESA and DBE, carried out in granitic rock at Äspö Hard Rock Laboratory, Sweden.

The test aims at understanding and modeling the thermo-hydro-mechanical behavior of buffers made of swelling clay exposed to high temperatures (over 100°C) during the water saturation process.

Since the beginning of the project, different modeling tasks have continuously been carried out. Previously, scoping design calculations, predictive modeling of initial field test desaturation and evaluation modeling of field test issues have been reported.

The present report covers the predictive modeling of a mock-up test (TBT_2), carried out by CAE in Saclay (France), addressing the desaturation process observed in the field test around the lower heater. This task was carried out during 2005.

All predictions and test results showed that moisture redistribution takes place as soon as there are thermal gradients. Results therefore do not support the notion of thermal threshold gradients. Models also showed that it is the difference in temperature between the hot and cold ends, rather than the thermal gradient, that determines the extent of moisture redistribution.

Sammanfattning

TBT (Temperature Buffer Test) är ett gemensamt SKB/ANDRA projekt, med deltagande av ENRESA och DBE, vilket utförs i granitiskt berg vid Äspö HRL i Sverige. Syftet är att öka förståelsen för, och att modellera, de termiska, hydrauliska och mekaniska processerna i en buffert av svällande lera som utsätts för höga temperaturer (över 100°C) under bevätningsfasen.

Olika modelleringsinsatser har utförts kontinuerligt sedan projektet startades. Tidigare har inledande beräkningar (scoping design) samt prediktiva modelleringar av den initiella uttorkningen av fältförsöket rapporterats.

Den föreliggande rapporten omfattar en prediktiv modellering av ett mock-up försök (TBT_2), utfört av CEA i Saclay (Frankrike), vilket efterliknade den uttorkningsprocess som observerades runt den nedre värmaren i fältförsöket. Insatsen utfördes under 2005.

Alla prediktioner och experimentella resultat visar att en fuktomfördelning äger rum så snart det föreligger en termisk gradient. Resultaten stödjer därför inte föreställningen om en termisk tröskelgradient. Modellerna visade också att det är temperaturskillnaden mellan den kalla och varma sidan, snarare än den termiska gradienten, som avgör av fuktomfördelningens omfattning.

Contents

1 Introduction and background

1.1 Outline of work

Within the framework of the TBT modeling task force, it has been decided to consider particularly the thermo-hydraulic conditions around the lower heater in the TBT test. In the field experiment, there was a significant and fast dehydration in an approximately 0.15 m wide annular zone around the heater /Goudarzi et al., 2005/. The temperature increased to just below 130 °C during the first 20 days. The temperature gradients were almost 4.5 °C/cm in the region where desaturation appeared to have taken place. Figure 1 shows measured temperatures and calculated thermal gradients at different distances from the heater axis.

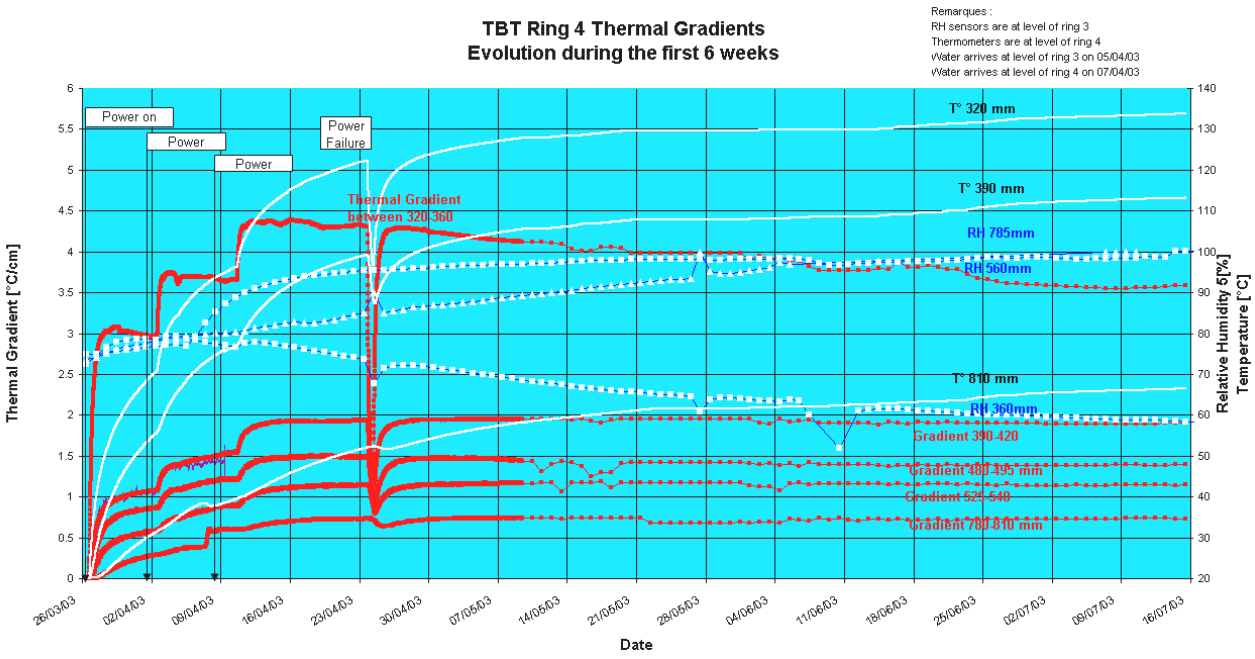

***Figure 1**. Temperatures and thermal gradients at different distances from the lower heater axis.*

The pattern of desaturation and its time-scale has raised the question whether the thermal gradient alone or the combination of high temperatures and high thermal gradients is responsible for the process. However, it is not possible to infer any such information directly from Figure 1. The high gradient close to the heater was partly an effect of the drying, and not the clear-cut cause of it. At some distance from the heater, there was no drying. This may well be an effect of moisture moving in from the regions close to the heater, rather than an indication of insufficient thermal gradients.

The approach decided by ANDRA and the TBT modeling teams was two-fold, with a lab-scale mock-up test combined with a predictive modeling task, and addressed the phenomenon of desaturation and the relative importance of temperature gradients and temperature levels.

The mock-up test was planned and designed at the CEA laboratory in Paris, France. The basic idea was to subject a confined sample of MX 80 bentonite material to thermal gradients similar to those around the lower heater in the TBT field experiment, and to monitor the development of temperatures, relative humidities and stresses during a well-defined sequence of thermal loading.

1.2 Experimental setup and thermal protocol

The used cell is illustrated in Figure 2 and was composed of:

- A stainless steel cylinder
- A 17 mm thick PTFE lining cylinder for thermal insulation.
- A stainless steel fixed base with temperature control
- A moving piston with temperature control
- An isostatically compacted ortho-cylindrical MX 80 bentonite sample of 200 mm height and diameter.

The cell was instrumented with sensors for measurements of temperature, relative humidity, pore-water pressure, radial pressure and the axial vertical stress.

The thermal loading was divided in three phases: a nominal, an optional and a transient phase. In the nominal phase, a thermal gradient was gradually increased from zero to a maximum of 1.8°C/cm. The protocol for the optional phase aimed at establishing a 3°C/cm gradient in the sample, then at elevating temperature keeping the thermal gradient constant. Finally, in the transient phase, a gradient identical to the final gradient in the nominal phase was established momentarily (see Figure 3).

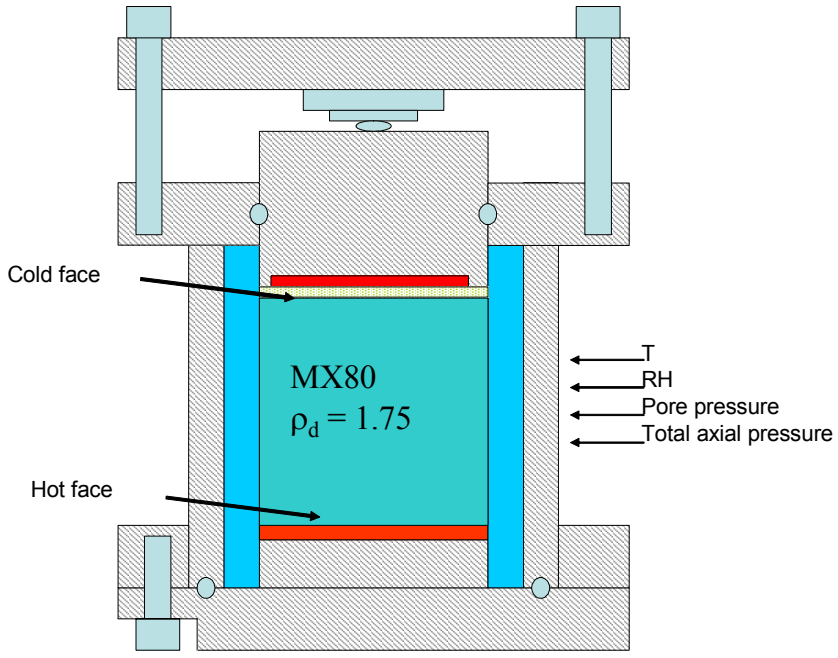

***Figure 2**. Diagram of the TBT_2 Mock-up.*

2 Model predictions

A modeling program for the specified task was issued in April 2005 (Appendix I). Predictions were completed in July 2005. Contributions were given by two modeling teams: UPC (Appendix II) and ClayTech (Appendix III). Both the UPC and ClayTech teams used the Code_Bright code.

The problem was further elucidated with the use of an analytical solution of steady-state conditions, i.e. a state at which the suction driven advective flow equals the diffusive vapor flow in all points (see Appendix III).

All predictions and test results showed that moisture redistribution takes place as soon as there are thermal gradients. The results therefore do not support the notion of thermal threshold gradients.

As far as long-term effects are concerned, the difference in temperature between the hot and cold ends, rather than the gradient determines the extent of desaturation at the hot end. This is a consequence of the applied conceptual models and was demonstrated both by use of FEM codes and by use of an independent analytical solution.

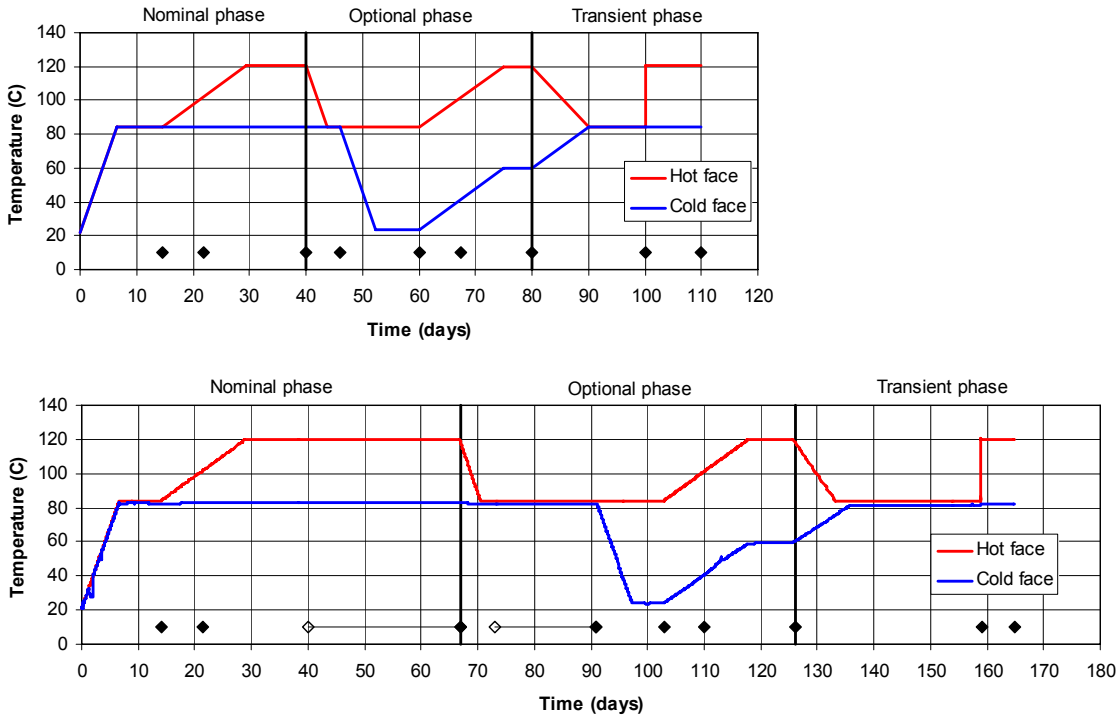

Figure 3. *Prescribed (upper) and applied (lower) thermal protocol. Points in time for which predictions were requested marked with ♦. Alternative translation (see text) marked ◊.*

3 Evaluation of predictions and experimental data

3.1 Protocol and models

The applied thermal protocol differed to some extent from the protocol prescribed in the modeling program. The difference is illustrated in Figure 3. The largest deviation was made at the end of the nominal phase, with a longer time period for equilibration. A significant deviation was also made for the isothermal period at the beginning of the optional period.

In order to compare experimental results with model prediction, the time-scale of the experiment was translated to the one used in the models. The points in time for which predictions were requested are marked in Figure 3, upper graph. The corresponding points in the applied protocol are marked in the lower graph. These translations are set so that events with corresponding changes in boundary temperature will be regarded as identical. Two exceptions from this rule were applied for the two periods mentioned above. These alternative points in time were instead chosen to give equal timeframes during the transient conditions. These alternative point in time are only regarded as important for the relative humidity data.

A few comments can be made regarding the used material properties and the initial conditions.

It can be noted that the flow coefficient values used in the ClayTech model were 2 – 3 times lower than the corresponding values used in the UPC model (Table 1), while the ratio between the intrinsic permeability and the vapor tortousity was only approx. 50 % higher in the ClayTech model than in the UPC model. Provided that the models were identical in other respects, one could expect that the steady-state solutions should be very similar. The timescale of the transient process to reach steady-state conditions, however, can be expected to be shorter in the UPC model than in the ClayTech model, due to the higher vapor diffusion tortousity used in this model.

The applied initial degree of saturation differed to some extent in the different models. A value of 62 %, was actually stated in the modeling program. During the course of the modeling work it turned up that this value was based on a particle density value of 2.65 g/cm^3. In the models from UPC and ClayTech, the initial degree of saturation was therefore adjusted to correspond to a particle density of 2.78 g/cm^3.

Finally, it can be noted that the retention curves used in the different models are quite similar (Figure 4).

Table 1. Critical flow coefficients (k and τ) and initial degree of saturation (S_{init}).

	ClayTech	UPC
k (m^2)	$1.6 \cdot 10^{-21}$	$3.6 \cdot 10^{-21}$
τ	0.3	1
S_{init} (%)	57	55

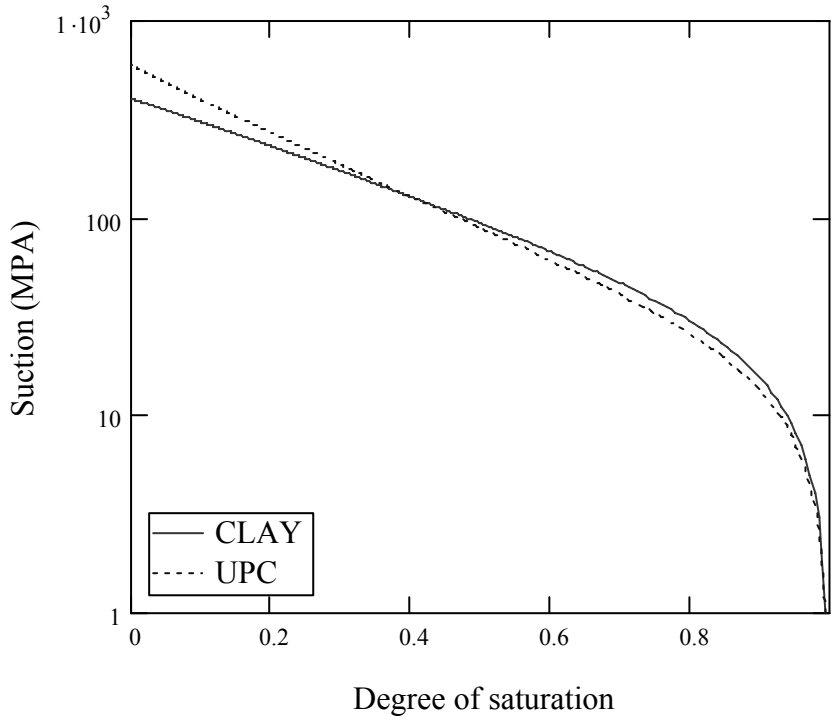

Figure 4. *Retention curves used in predictions.*

3.2 Comparison of results

Scan-lines for predicted and experimental *temperatures* are shown in Figure 5. It can be noted that the predicted values are mutually identical, whereas they differ significantly from the experimental data. Scan-lines with expected isothermal conditions (day 14.5, 46 and 100) are clearly non-isothermal, indicating a thermal leakage. The thermocouple at the 149 mm level exhibits the lowest temperature at these occasions, as well as on day 22, which indicate that this is the location of the leakage. At strong thermal gradients, i.e. day 60, 67.5 and 80, the deviation are less pronounced.

Moreover, the difference between the experimental and the calculated temperatures at the mid-section (height 100 mm) was with a few exceptions generally approx. 8°C. With a fully developed thermal gradient during the nominal phase (day 40) the difference was 5 °C, while during corresponding periods of the optional phase with maximal gradient (day 60, 67.5 and 80) the difference was minor.

These temperature differences would certainly influence the redistribution of water and affect the results of *relative humidity*. This is readily apparent in the first scan-line (day 14.5), for which the relative humidity should be constant (see Figure 6). Results from the three models are grouped within the interval 66 – 69 %. The experimental results indicate however that redistribution already had occurred at that time. The temperature minimum at the 149 mm level can be expected to correspond to a maximum RH value, and this is also generally the case. However, the irregular distribution of RH values, with several

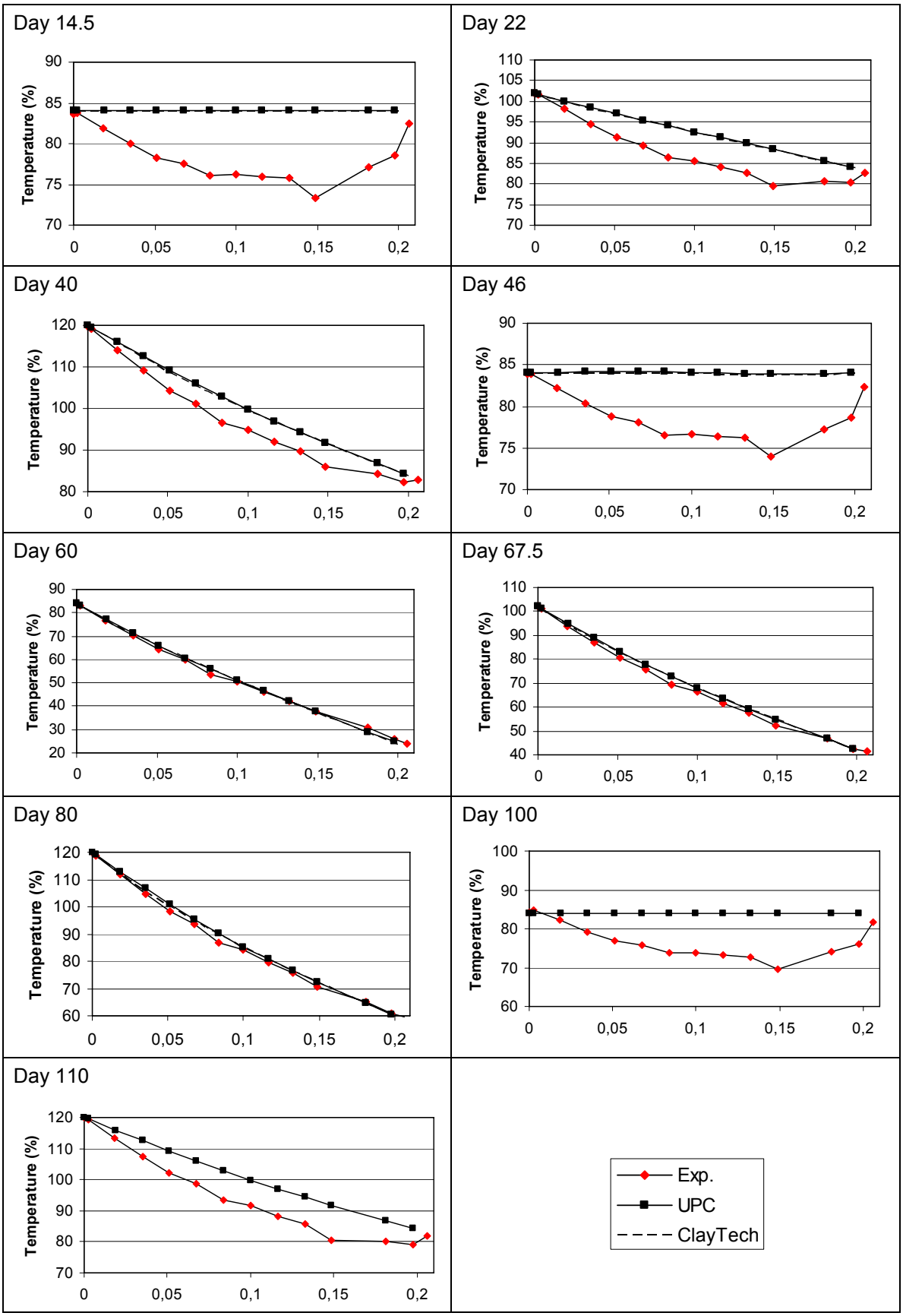

Figure 5. *Temperature.*

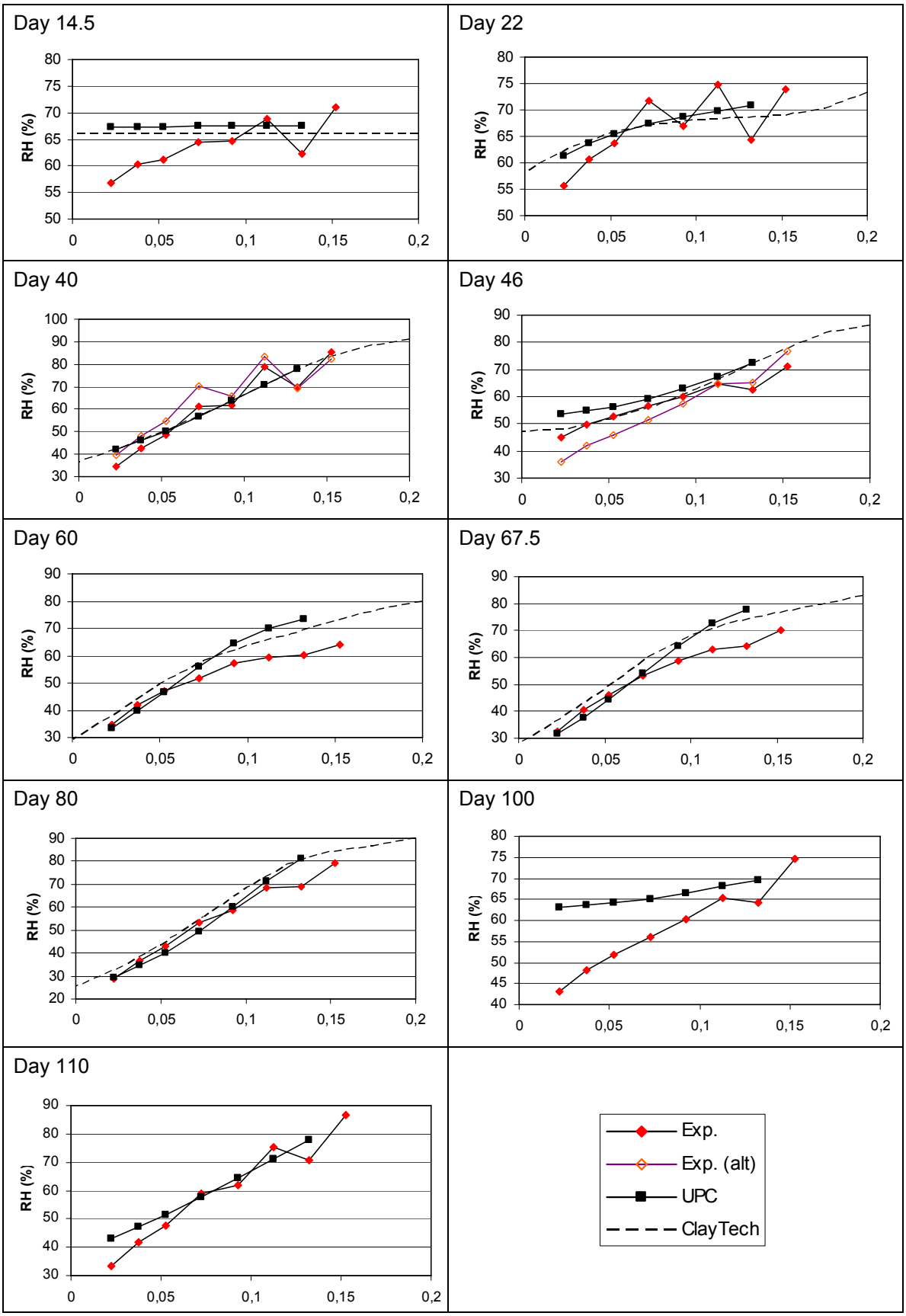

Figure 6. *Relative humidity.*

extreme points in the midsection, is more difficult to explain. This distribution is especially noticeable for the day 22 scan-line. The distribution of RH values was nevertheless quite monotonic during the optional phase with maximum gradient (day 60, 67.5 and 80). This is consistent with the temperature distributions during this period.

A number of observations can also be made by comparing the different predictions and the experimental results. There are generally two aspects that can be analyzed: the RH-distribution at steady-state, and the timescales to reach steady-state.

Steady-state was reached, at least closely, at day 40, 80 and 110. At the first two of these[1], the ClayTech and the UPC predictions were very similar, especially for day 40. Comparing with the experimental results, it is difficult to determine whether these predictions tend to over or underestimate the water redistribution. Later results, e.g. for day 110, indicate the latter. The similarity between the ClayTech and the UPC steady-state predictions is largely a consequence of similar ratios between the used flow coefficients.

The timescales during the transient periods differ to some extent between the ClayTech and the UPC predictions. At day 46 for instance, at the end of a two day isothermal period, the RH-distribution was heading toward a constant steady state level. At the time the UPC prediction was closest to this level, indicating the relatively fast response in this model. This difference reflects the different vapor diffusion coefficient values (τ) used in the models. This is further illustrated in Figure 7 in which model RH values are compared for the extreme sensor positions (HR1 and HR8). Comparisons with experimental results in this respect should be made with caution due to the uncertainties implied by the leakage of heat.

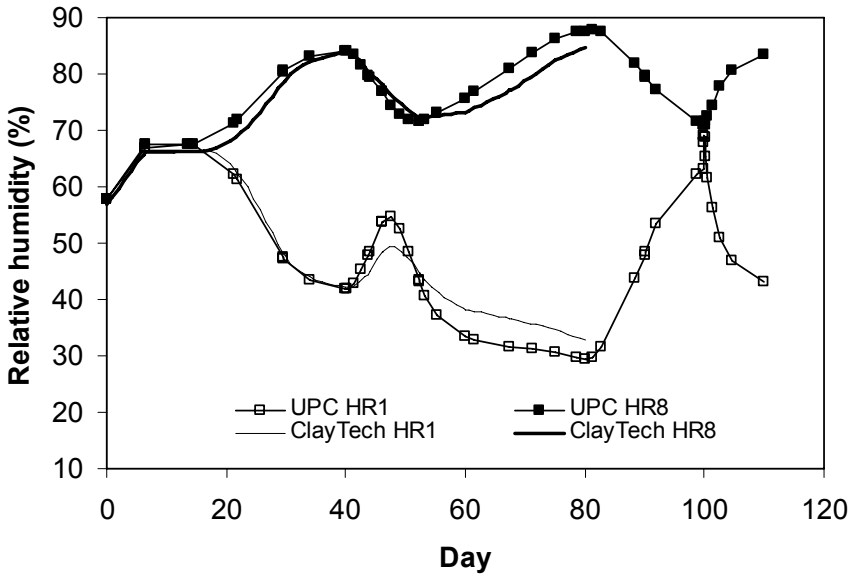

Figure 7. *Model RH results for HR1 and HR8.*

[1] The day 110 steady-state should be identical with the distribution at day 40, since the thermal conditions were the same and due to the used conceptual models (see Appendix III).

Predicted *radial stresses* are shown together with experimental results in Figure 8. Comparisons regarding *axial stresses* are shown in Figure 9. As can be noted, the predictions display very different results. For instance, the ClayTech model showed generally higher stress levels than the UPC model, both regarding radial and axial stresses. Both predictions displayed however higher radial stresses than axial stresses, at least in the uppermost part of the periphery. This relation is probably inevitable, if the volume is regarded as constant and if water redistributions and thereby the strains are symmetrical around the centre axis. The relation is however not apparent in the experimental data, for which the axial stresses are generally higher than the radial ones. The experimental radial stressed indicated actually most of the time tensile stresses. Best agreement between predictions and experiment was shown for the UPC model, in the case of radial stresses, and for the ClayTech model in the case of axial stresses.

3.3 Comments on experimental vapor pressures

The TBT_2 test can further illustrate one of the important questions regarding moisture transport in buffer materials. Vapor pressures can be calculated from the measured values of RH and temperature. Such a calculation is shown in Figure 10.

The annotated areas mark the end of the different phases. The converging lines illustrate that the gradients of vapor pressure and vapor mass fraction decrease with time. It can be noted that true steady-state conditions were not reached during the nominal equilibration phase, even though this period was extended to almost 40 days instead of 10 as prescribed in the protocol. An important goal for future tests is to see how far these lines will converge. If they converge to the same level, this would strongly support the notion that water only is transported in vapor form.

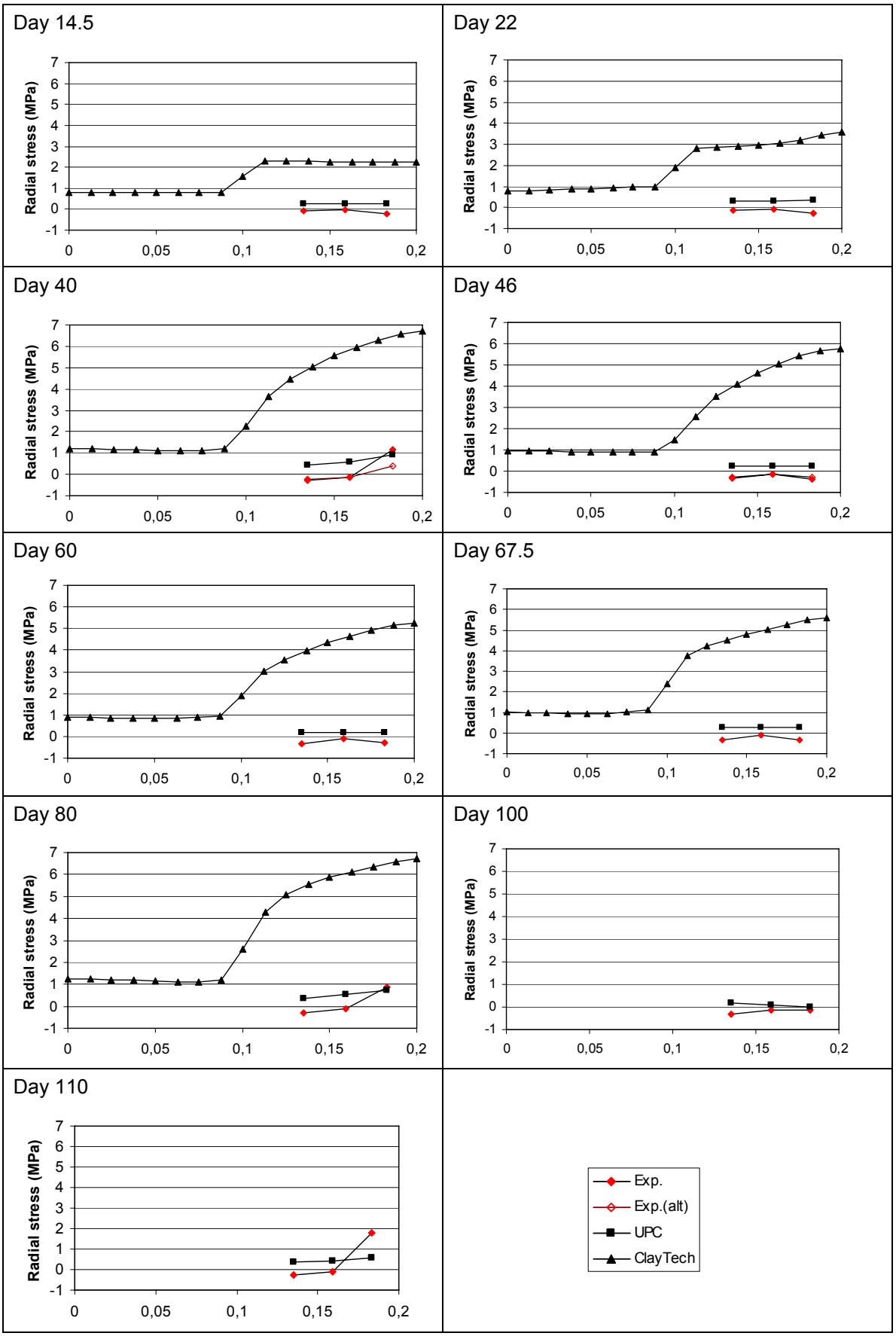

Figure 8. *Radial stress.*

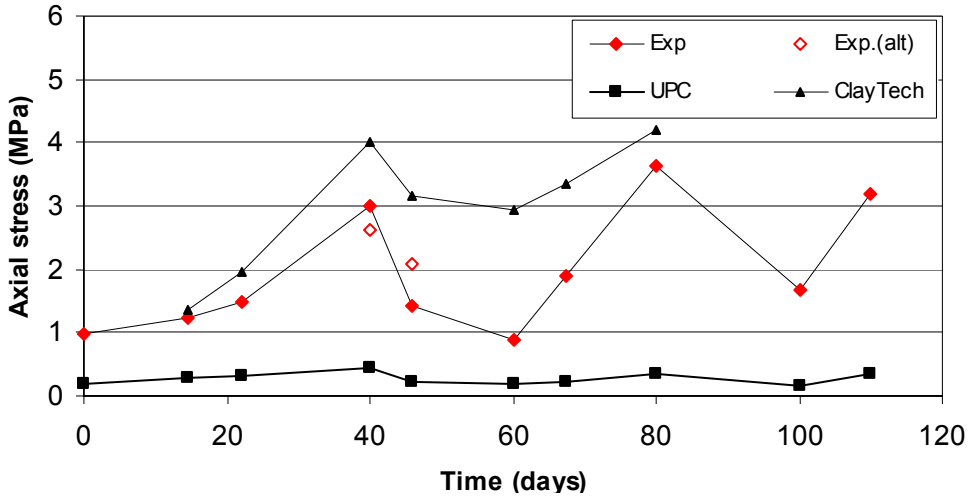

Figure 9. *Axial stress.*

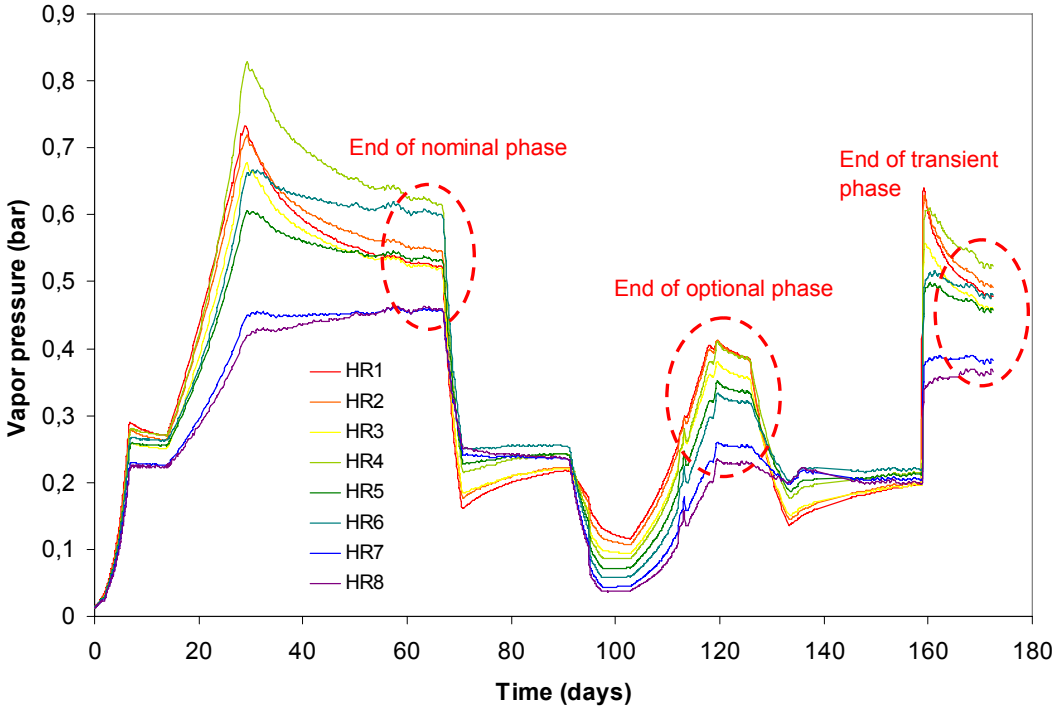

Figure 10. *Experimental vapor pressures. Saturated vapor pressure calculated according to /Sánchez, 2004/*[2].

[2] **Sánchez M., 2004.** Thermo-Hydro-Mechanical Coupled Analysis in Low Permeability Media. *PhD Thesis*, Geotechnical Engineering Department, Technical University of Catalunya, Spain.

Clay Technology AB

Ideon Research Center

Lund, Sweden

TBT_2 - Predictive modeling program

April, 2005

Mattias Åkesson

Harald Hökmark

Contents

1 TBT_2 Mockup experiment

1.1 Background

Within the framework of the TBT evaluation modeling task force, it has been decided to emphasize the initial thermo-hydraulic condition around the lower heater in the TBT test. The approach is two-parted, with a mockup test combined with a predictive modeling task, and addresses the phenomena of desaturation and the role of temperature gradients and temperature levels.

1.2 Time table

The mockup test is scheduled to start during the end of March 2005. The requested time frame for the predictive modeling is April 1st to June 30th , 2005. Comparisons and evaluations will be performed during September 2005 and the results will be presented in Barcelona on October 27th 2005.

1.3 Experimental setup

The used cell is illustrated in Figure 1 and is composed of:

- A stainless steel cylinder
- A 17 mm thick PTFE lining cylinder for thermal insulation.
- A stainless steel fixed base with temperature control
- A moving piston with temperature control
- The isostatic compacted ortho-cylindrical MX80 bentonite sample of 200 mm height and diameter.

The initial condition of the bentonite is described by following data:

Dry density: ≈ 1.75 g/cm^3

Initial water content: W = 12%

Initial saturation level: Sr = 62%

Initial temperature is equal to ambient temperature, approximately 20 °C.

The cell is instrumented with sensors for measurements of temperature, relative humidity, pore-water pressure, radial pressure and the axial vertical stress through the mobile piston.

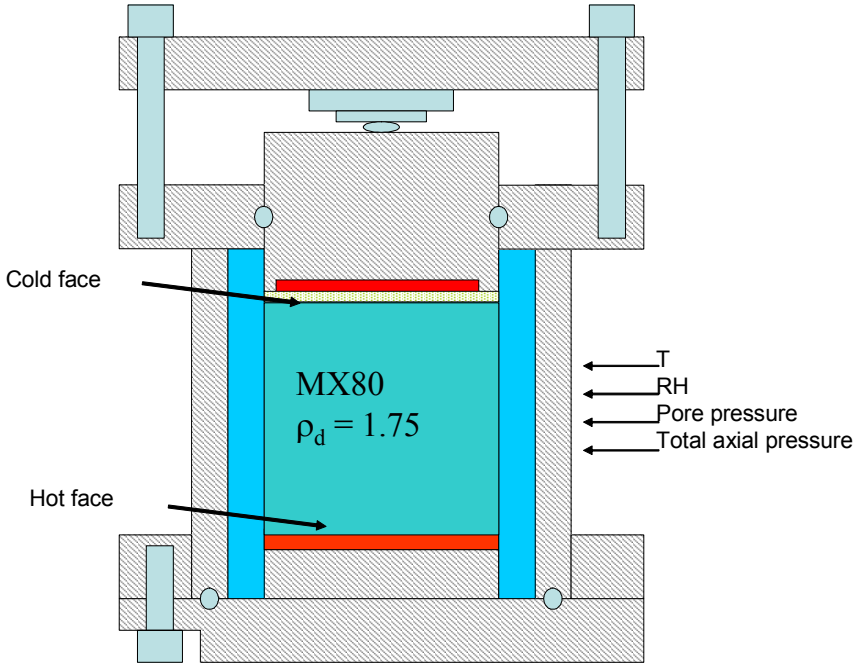

***Figure 1**. Diagram of the TBT_2 Mock-up*

1.4 Thermal protocol

The test is divided in three phases: a nominal, an optional and a transient phase. In the nominal phase, a thermal gradient is gradually increased from zero to maximum 1.8°C/cm. The protocol for the optional phase aims at establishing a 3°C/cm gradient in the sample, then at elevating temperature keeping the thermal gradient constant. Finally, in the transient phase, a gradient identical to the final gradient in the nominal phase is established momentarily (see Figure 2). If desaturation is detected during either one of the phase, the test is stopped at the end of that phase.

A detailed scheme is presented in Table 1. It should be noted though, that small protocol changes can be necessary due to practicalities, such as visual temperature control during certain cooling periods.

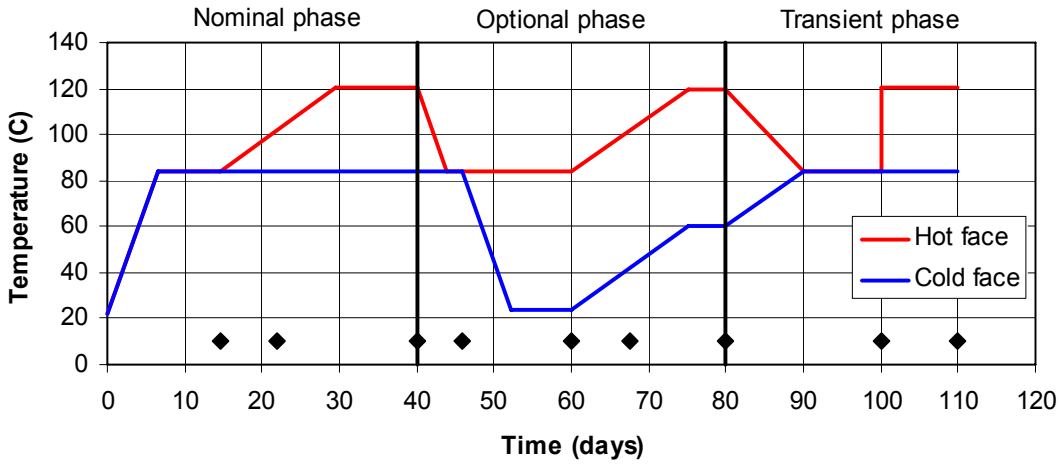

Figure 2. *Thermal protocol for planned phases. Modeling results are requested for events marked with ♦.*

Table 1. Details of thermal protocol.

Day	Temperature (Hot face)	Temperature (Cold face)	Requested Results
0	22	22	
6,5	84	84	
14,5	84	84	End-stabilization
22	102	84	Mid-heating
29,5	120	84	
40	120	84	End-stabilization
43,8	84	84	
46	84	84	End-stabilization
52,3	84	24	
60	84	24	End-stabilization
67,5	102	42	Mid-heating
75	120	60	
80	120	60	End-stabilization
90	84	84	
100	84	84	End-stabilization
100	120	84	
110	120	84	End-stabilization

1.5 Instrumentation

The clay core is fitted with 13 Pt-100-ohm temperature sensors (RTD), eight relative-humidity sensors and five pore-water-pressure sensors. Three total radial-pressure sensors are also installed in the cold section.

A force sensor (0-35 t) measures the axial vertical stress through a mobile piston. It is equipped with a device designed to maintain a constant temperature in the sensor in order to prevent any zero deviation due to temperature. The piston is fitted with two temperature sensors, one for regulating high temperatures and the second for measurement purposes.

All but one sensor are laid out perpendicularly to the vertical axis of the model, the sensitive part being located at the centre of the sand and of the clay core. One relative-humidity sensor, HR8, acts as peripheral sensor, its sensitive part being close to the cylindrical envelope.

The position of the sensors in the vertical axis is shown in Table 2. Reference levels are given in millimetres starting from level 0 located at the top face of the wafer heater.

Table 2. Sensors location for TBT_2.

Temperature		**Humidity****		**Pore-water pressure**		**Radial pressure**	
Sensor N°.	Y (mm)	Sensor N°.	Y (mm)	Sensor N°.	Y (mm)	Sensor N°.	Y (mm)
T 0	0	HR1	22.5	PI1	52	PT1	135
T 1	2.5	HR2	37.5	PI2	84	PT2	159
T 2	18.75	HR3	52.5	PI3	116	PT3	183
T 3	35.0	HR4	72.5	PI4	148		
T 4	51.25	HR5	92.5	PI5	180		
T 5	67.5	HR6	112.5				
T 6	83.75	HR7	132.5				
T 7	100	HR8***	152.5				
T 8	116.25						
T 9	132.5						
T 10	148.75						
T 11	181.25						
T 12	197.5						
Piston	206*						

** Taking into account a 3-mm stainless-steel plate.*

*** A temperature measurement is associated with each humidity measurement.*

**** Peripheral humidity sensor.*

2 Suggested scope and requested output

The mockup test emphasizes the thermo-hydraulic phenomena of desaturation. Ideally, the test can be described as a 1D problem. Modeling results regarding (i) temperature and (ii) relative humidity are to be presented for a vertical scan-line in the central axis of the mockup cell (Figure 3). Requested points in time for these results are the ends of each stabilization period (7 events) as well as the mid-points for the heating periods (2 events), see Table 1.

Due to the anticipated risk of the development of preferential paths along the envelope, a peripheral RH-sensor (HR8) is installed close to the cylinder at the uppermost level. An optional task is therefore to view the test as a 2D problem, and in this case results regarding temperature and relative humidity should in addition be presented for a radial scan-line at level y = 152.5 mm.

If the mechanical processes are included in the work, results from such calculations should be presented for the envelope surface (radial stresses) as well as for the top surface (axial stresses).

The experimental scheme, with three subsequent phases and the possible closure after either one of these phases, has implications for the modeling task and may necessitate the use of different modeling approaches. One alternative can be a complete "best guess" modeling exercise, covering all three experimental phases, disregarding the possible occurrence of desaturation in the model. A second approach can be applied if desaturation is observed during either one of the two first phases. In this case, the model is rerun with a modified parameter setting in order to suppress desaturation.

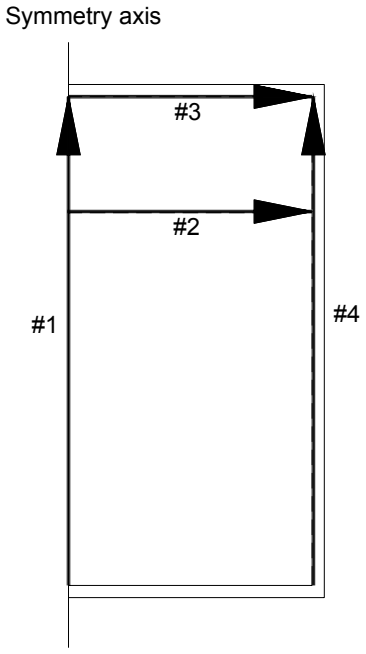

Scan-lines:

#1	#2	#3	#4
T, RH	T, RH	σ_A	σ_R

Figure 3. *Scan-lines requested for June 30th , 2005.*

Appendix Material properties MX80

Figure 4 shows suction values based on work being conducted at Clay Technology. The new experimental data indicate that the suction is considerably higher than the values proposed in the year 2003 predictive modeling program.

MX80 thermal conductivities for different void ratios versus saturation are shown in Figure 5. Figure 6 shows intrinsic permeability as function of void ratio. Figure 7 shows MX80 swelling pressure as function of void ratio.

Figures 8-10 show results from a temperature gradient test. In that test the initial void ratio was 1.0, the initial degree of saturation 0.70 and the temperature gradient 10 ºC/cm. The cold end was kept at room temperature. All boundaries were closed to water movement.

New experiments on MX-80 bentonite have been performed by C. Gatabin, CEA /Gatabin and Robinet, 2003/. Two cylindrical bentonite samples, 200 mm in height and 200 mm in diameter, were confined in steel cells with fixed 20°C temperature at the top and variable temperature (22°C to 150°C) at the base. The two samples, THM1G_Cell1 and THM1G_Cell2, had initial liquid saturations of 75.5% and 89.7%, respectively. Void ratios were 0.48 and 0.53. The cells were closed hydraulically, but not completely gas-tight. The temperature at the cell bases was increased from 22°C to 150°C in steps. Figure 11 shows the relative humidity as function of distance from the heated base.

The figures 12-14 give examples of results of hydro-mechanical tests performed on MX-80 bentonite. There is no complete or final set of test results that can be used to define a consistent material model that takes all the nuances of the behavior of unsaturated MX-80 bentonite into account.

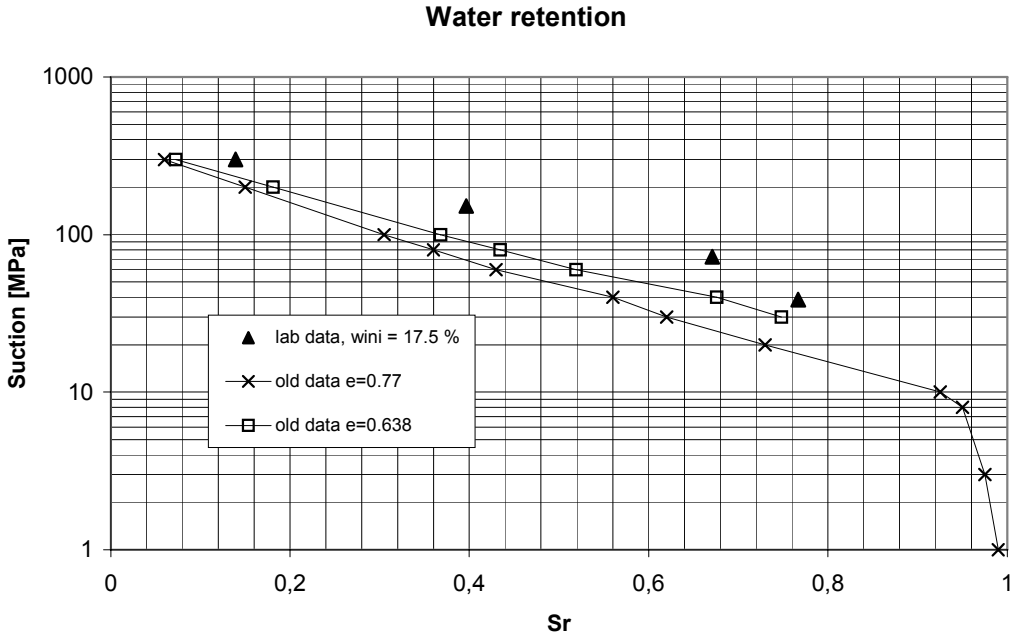

Figure 4: *Suction curves. "Old data e = 0.77" is the information given in the predictive modeling program for a void ratio of 0.77. "Old data e = 0.638" are these values translated to a relevant void ratio. Note that the translation is made only in saturation ranges where effects of swelling and confinement are small. The "lab data" are derived from measurements of suction as function of water ratio under un-confined conditions and have been converted here to apply for a void ratio of 0.638.*

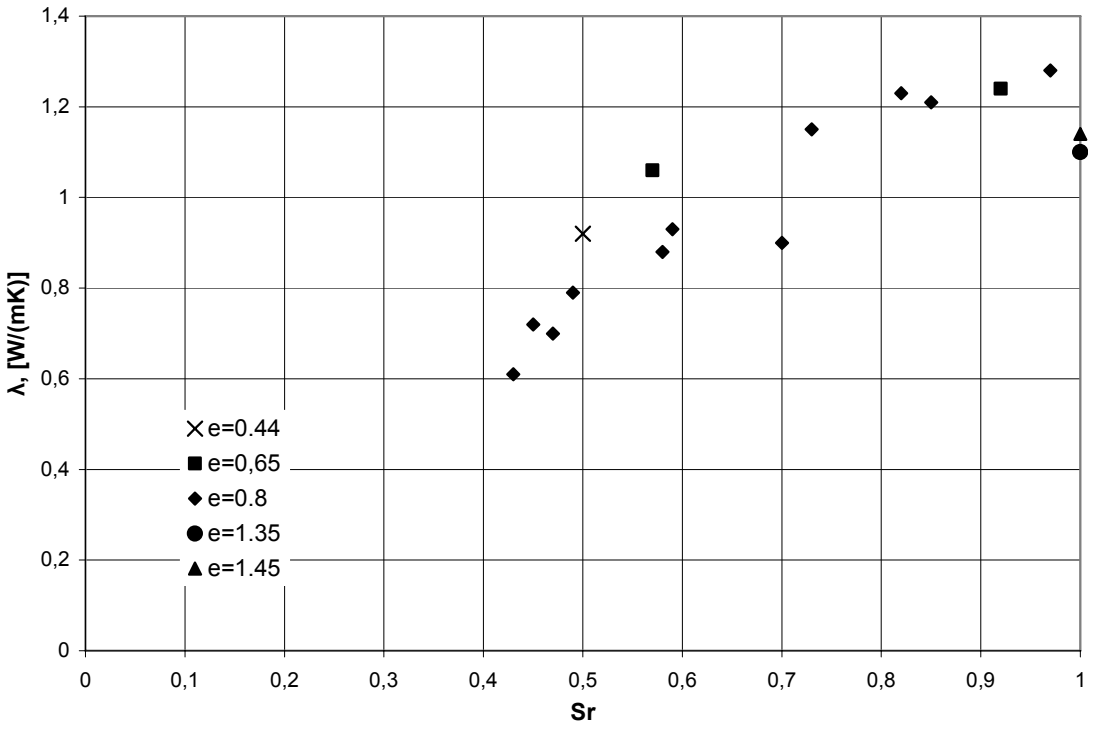

Figure 5. *MX 80 bentonite thermal conductivity, experimental values for different void ratios. From Börgesson et al (1995).*

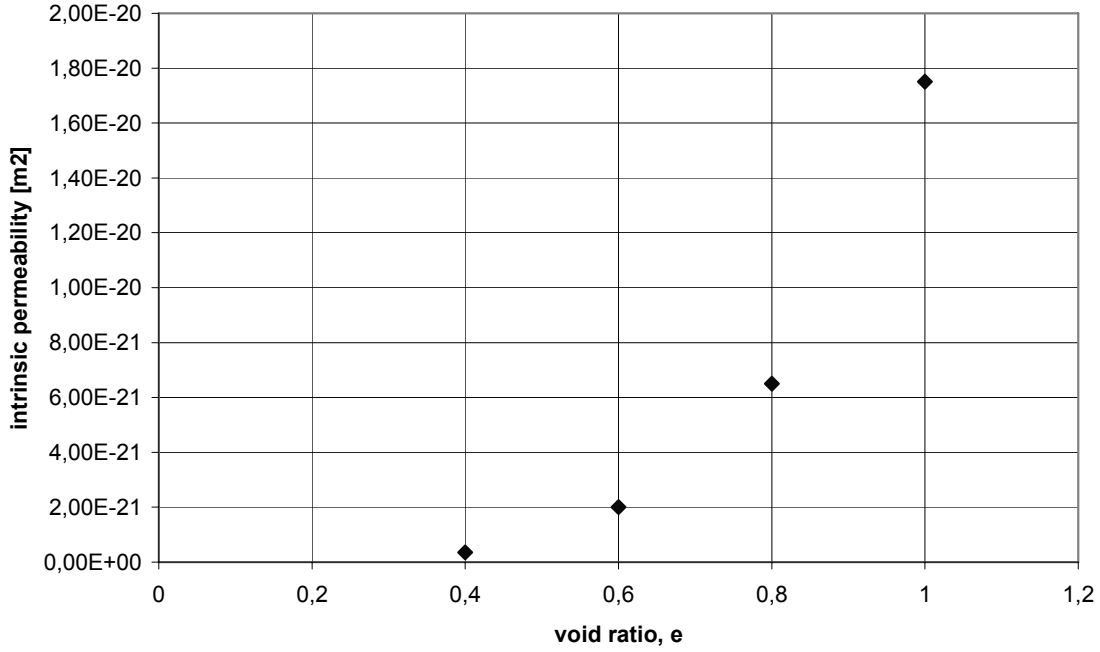

***Figure 6**. Intrinsic permeability for MX 80. From Börgesson et al (1999).*

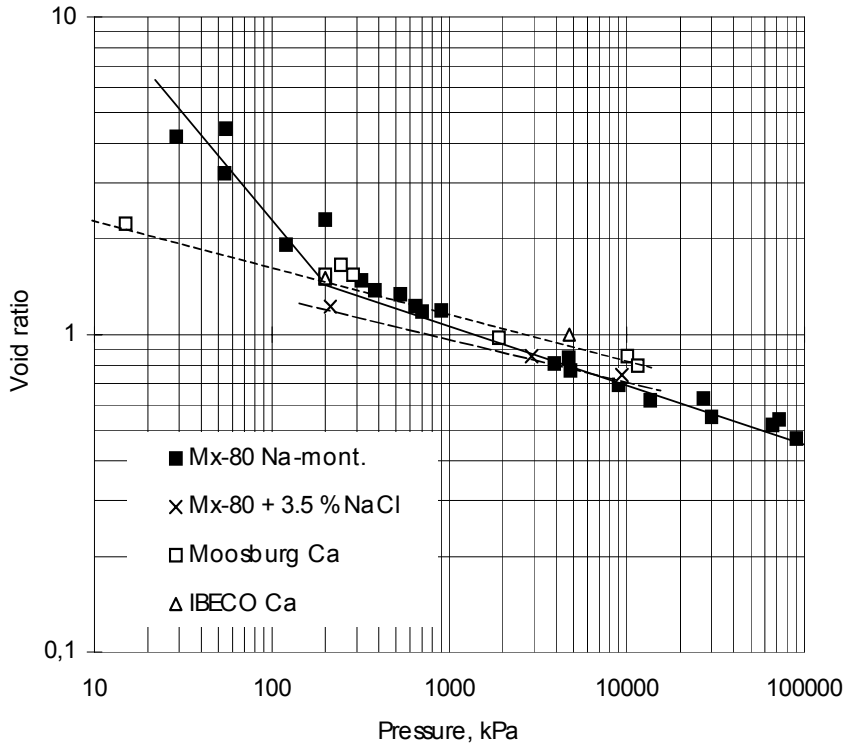

***Figure 7**. Swelling pressure as function of void ratio. From Börgesson et al (1995).*

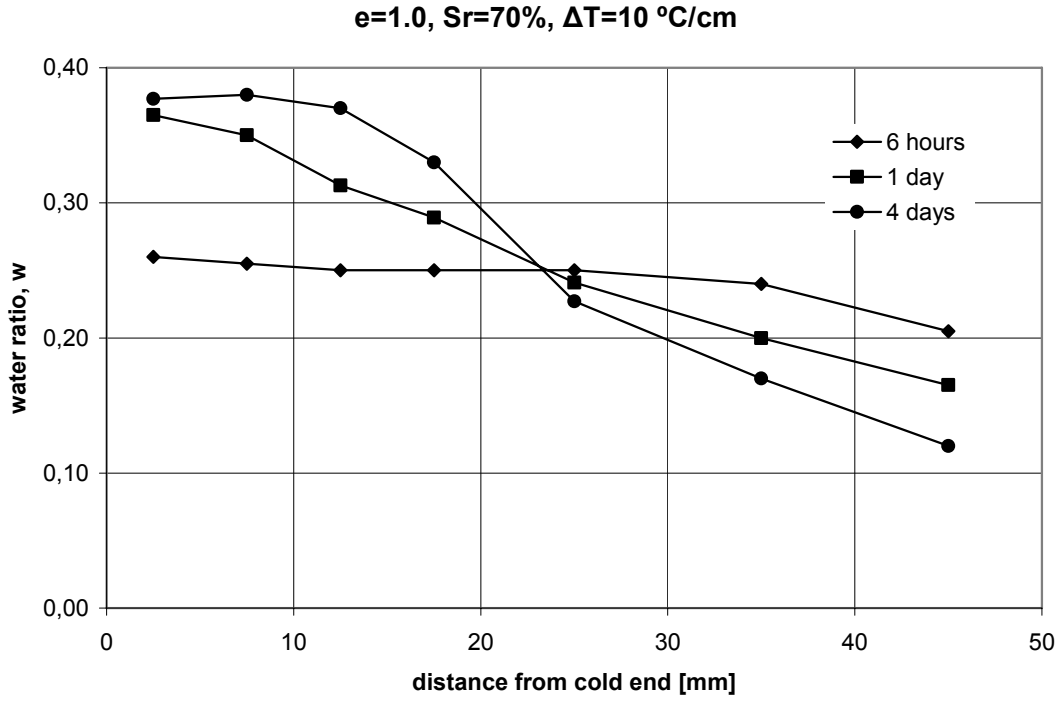

Figure 8. *Results from temperature gradient test. Water ratio as function of distance from cold end. From Börgesson (2001).*

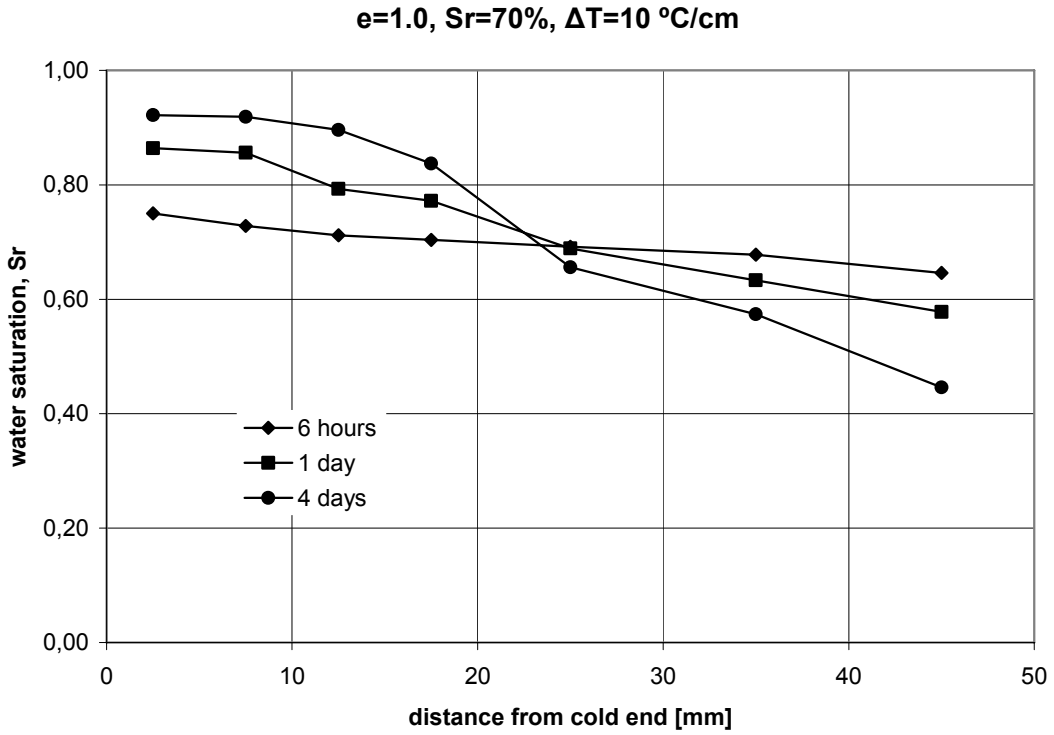

Figure 9. *Results from temperature gradient test. Degree of saturation S_r as function of distance from cold end. From Börgesson (2001).*

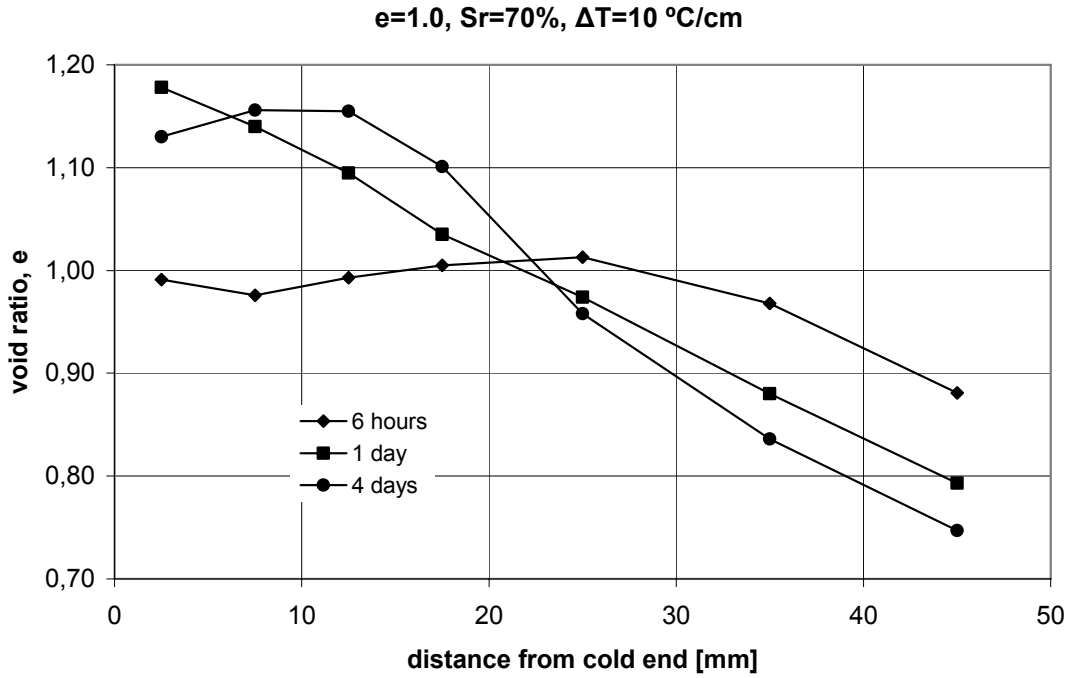

***Figure 10**. Results from temperature gradient test. Void ratio e as function of distance from cold end. From Börgesson (2001).*

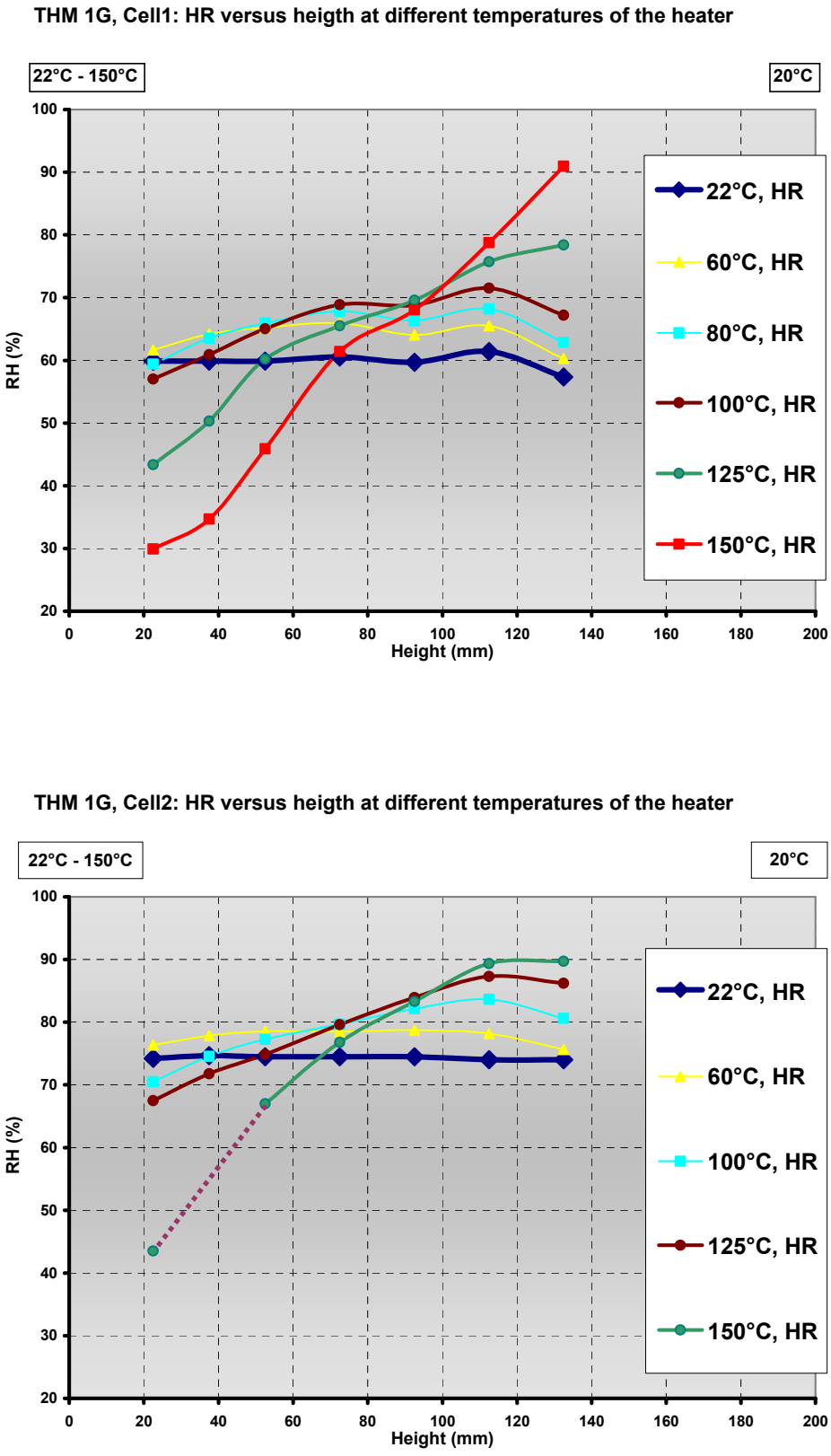

Figure 11: *Relative humidity as function of distance from the heated base. From /Gatabin and Robinet, 2003/.*

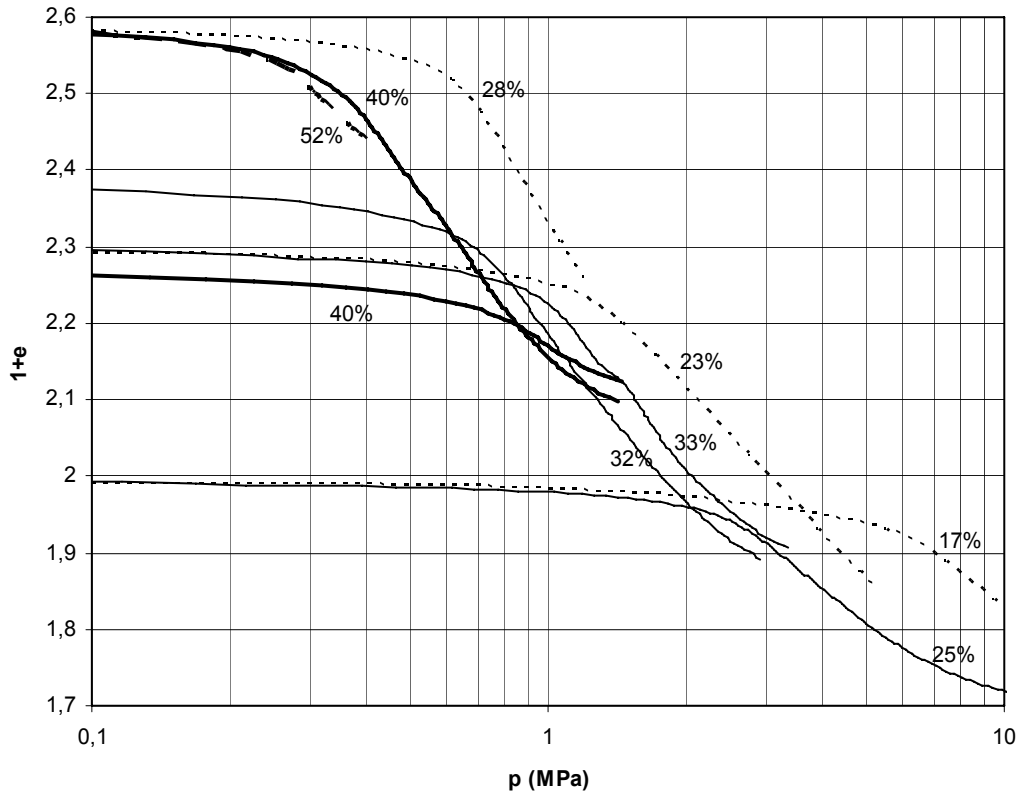

Figure 12. *Results from undrained constant (0.7mm/day) strain rate 1-D compression tests on unsaturated MX80. Specific volume (1+e) plotted vs. the load (p). The labels give the initial water contents. Derived from /Börgesson, 2001/.*

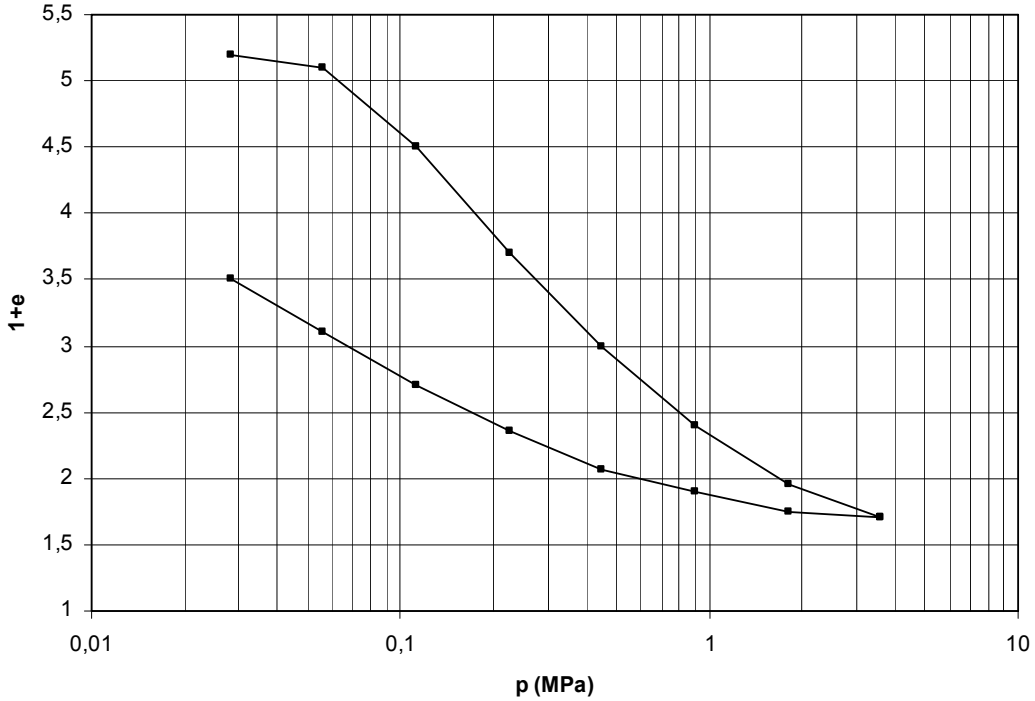

Figure 13. *Results from drained oedometer test with saturated MX80. Specific volume (1+e) plotted vs. the load (p). From /Börgesson et al., 1988/.*

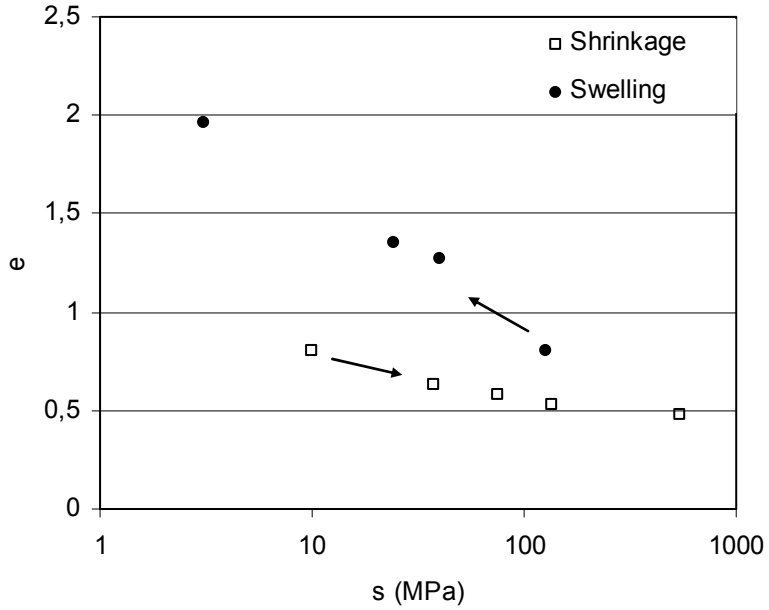

Figure 14. *Results from shrinkage and free swelling of MX80. Void ratio (e) plotted vs. suction (s). From Dueck (2004) and Börgesson (2001).*

References

Börgesson L.,Hökmark H. and Karnland O. 1988. Rheological properties of sodium smectite clay. SKB TR 88-30.

Börgesson L., Johannesson L-E, Sandén T. and Hernelind J., **1995**. Modeling of the physical behavior of water saturated clay barriers. Laboratory tests, material models and finite element application. SKB Technical Report TR-95-20.

Börgesson L., Hernelind J., 1999. Coupled thermo-hydro-mechanical calculations of the water saturation phase of a KBS-3 deposition hole. SKB Technical Report TR-99-41.

Börgesson L., 2001. Compilation of laboratory data for buffer and backfill materials in the Prototype Repository. SKB International Progress Report IPR-01-34.

Dueck, A. 2004. Hydro-mechanical properties of a water unsaturated sodium bentonite. Laboratory study and theoretical interpretation. Division of Soil Mechanics and Foundation Engineering, Lund Institute of Technology, Lund, Sweden.

Gatabin C., Robinet, J-C., 2003. Mock-up for studying THM behaviour of swelling clay MX80 at temperature >100°C. CEA/EuroGeomat.

TBT_2 – Predictive Modelling Program

Simulation of TBT_2 Mockup Experiment

ENRESA Contribution

July 2005

A. Ledesma, A. Jacinto, G. Chen
UPC, Barcelona, Spain

Contents

1 Introduction

This report presents the modelling work performed by the team coordinated by ENRESA (Spain) regarding the simulation of the "TBT_2 Mockup Experiment" performed at CEA (France). The guidelines considered in this simulation were defined in a document by M. Åkesson & H. Hökmark (Clay Technology, April 2005), entitled "TBT_2 Predicting Modeling Program". That report presented the protocol of the experiment and the variables expected from this modelling exercise.

As in previous simulation exercises, we have used the information provided in that report and in previous documents of the TBT project in order to define the parameters and the boundary conditions of the experiment. However, the complexity of this kind of experiment requires quite often the use of additional parameters or hypothesis that have not been defined in advance. In that case we have adopted reasonable values according to our experience, but that may become a source of discrepancy between predictions and field measurements. For instance, consideration or not of the gas tightness of the system may lead to different predictions. In those cases the hypothesis adopted in the analyses are clearly indicated in advance.

The Spanish participation in this project is coordinated by F. Huertas (ENRESA), and includes groups from UPC and from DM Iberia. In particular, the simulation work described in this report has been developed by the UPC group (A. Ledesma, A. Jacinto and G. Chen).

The code CODE_BRIGHT has been used in all cases, as in the previous simulations performed by the group. Up to 14 different models have been considered in the work, either assuming 1D or 3D (2D axisymmetric) conditions, TH or THM analyses, gas tightness or not, etc. The combination of all those factors required to develop different models in order to check the sensitivity of the required output to them. Not all the models are presented in this report. Only those cases that have been identified as relevant for understanding the behaviour of the test will be described.

Section two presents a brief explanation of the experiment and the material properties adopted in the simulations. Section three describes the initial attempts consisting of several 1D simulations of the test with TH analyses only. THM computations for 1D models are presented in section four. Section five refers to the 3D simulations which are adopted as the final proposal of the group. The report ends up with some concluding remarks about this simulation and the future work. Finally, an annex includes the output figures requested by the managers of the project.

2 Test description and input data

2.1 Experimental setup

Details of the experimental setup can be found in the report by Clay Technology already mentioned. For consistency figure 1 presents a sketch of the geometry obtained from that report.

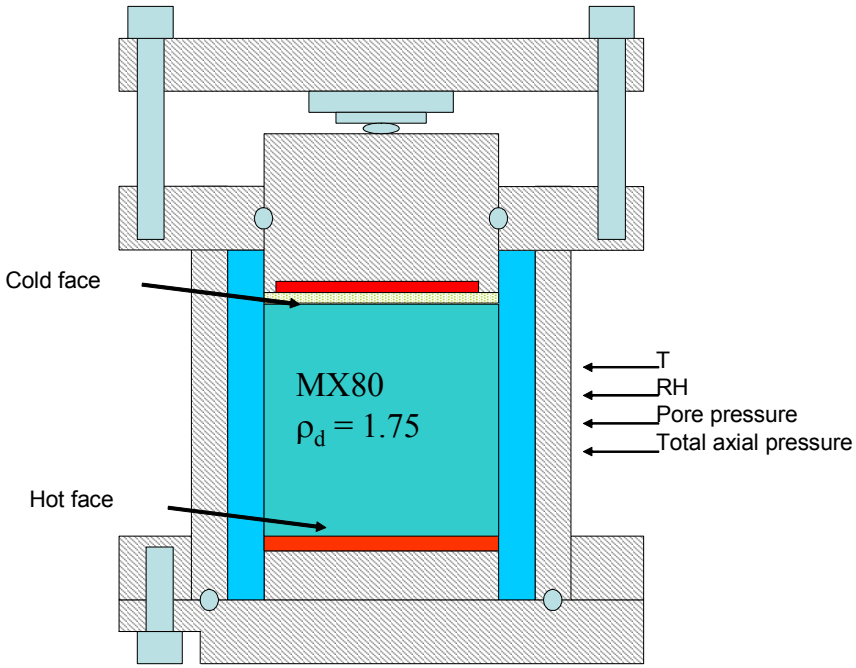

Figure 1. *Diagram of the TBT_2 Mock-up (from Clay Technology, 2005)*

The bentonite sample is a cylinder 20 cm height and 20 cm diameter subjected to a thermal gradient that follows the protocol described in figure 2. The MX-80 bentonite has the following basic properties:

- Dry density: 1.75 g/cm^3
- Initial water content: 12%
- Initial saturation level: 55% (this value has been changed with respect to the original value provided in the Clay Technology document, due to a different particle density adopted for the bentonite: 2.78 g/cm^3)
- Initial temperature: around 20ºC (22ºC)

The cell has been instrumented in order to measure the temporal evolution of temperature, RH, liquid pressure and stresses.

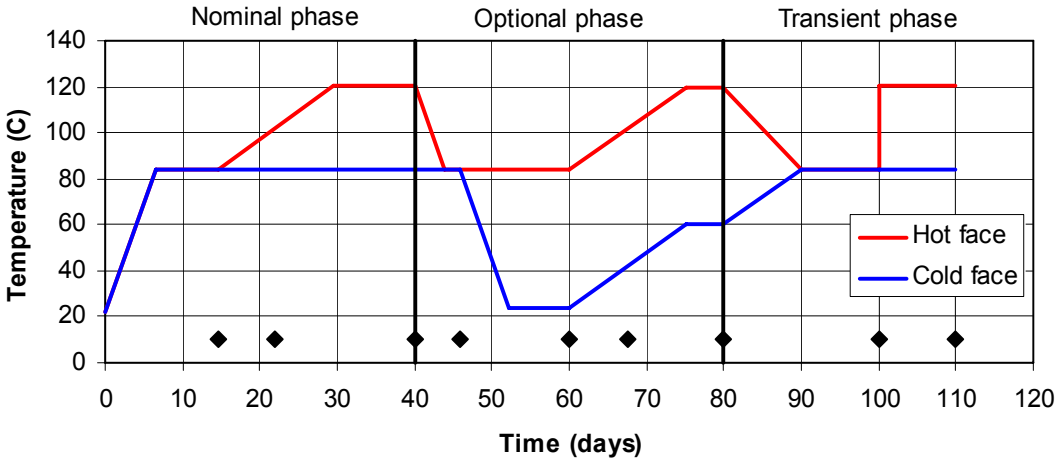

Figure 2. *Thermal protocol for planned phases. Modeling results are requested for events marked with ♦ (Clay Technology, 2005).*

2.2 Initial parameters considered

Material properties for the bentonite have been adopted from the previous experience in modelling THM behaviour of MX-80. Note that despite the amount of work already developed, the information available regarding the mechanical properties of MX-80 bentonite is still very limited. In this case we have adopted some parameters based on our previous experience. When other values have been used, it is clearly indicated in the text.

Thermal parameters

Thermal conductivity

λ (W/m·K) $\qquad \lambda = \lambda_{sat}^{S_l} \cdot \lambda_{dry}^{1-S_l} \qquad \lambda_{dry} = 0.3 \qquad \lambda_{sat} = 1.3$

Specific Heat

c (J/kg·K) $\qquad c = 1091$

Hydraulic parameters

Retention curve

$$S_e = \frac{S_l - S_{rl}}{S_{ls} - S_{rl}} = \left[1 + \left(\frac{P_g - P_l}{P_0}\right)^{\frac{1}{1-\beta}}\right]^{-\beta} \left(1 - \frac{P_g - P_l}{S_m}\right)^m$$

P_0 (MPa) = 60 $\qquad \beta = 0.3 \qquad S_m$ (MPa) = 800 $\qquad m = 1.1$

Intrinsic permeability

$$k = k_0 \frac{\phi^3}{(1-\phi)^2} \frac{(1-\phi_0)}{\phi_0^3} \qquad k_0 \text{ (m}^2\text{)} = 3.6\text{x}10^{-21} \qquad \phi_0 = 0.379$$

Liquid relative permeability

$k_{rl} = AS_e^{\lambda}$ $A = 1$ $\lambda = 3$

Gas relative permeability

$k_{rg} = AS_e^{\lambda}$ $A = 2.184\text{x}10^{7}$ $\lambda = 4.17$

Vapour molecular diffusion

$D_m^v = \tau D\left(\frac{(273.15+T)^n}{P_g}\right)$ $D = 5.9\text{x}10^{-6}$ $n = 2.3$ $\tau = 1$

Dissolved air molecular diffusion

$D_m^v = \tau D \exp\left(\frac{-Q}{R(273.15+T)}\right)$ $D = 1.1\text{x}10^{-4}$ $n = 24530$ $\tau = 1.0\text{x}10^{-5}$

Mechanical parameters

Barcelona Basic Model (BBM)

$\kappa_{i0} = 0.207$ $\kappa_{s0} = 0.1563$ $K_{\min} = 13.33$ MPa $\nu = 0.2$

$\lambda(0) = 0.621$ $r = 0.75$ $\beta = 0.05$ $p^c = 0.1$ MPa

$p_0 = 9.542$ MPa $M = 0.78$ $\alpha = 0.395$ $k = 0.1$

Initial conditions

The values considered as "default" follow:

$P_g = 0.1$ MPa $P_l = -124.9$ MPa $T = 22^{o}$C $e = 0.611$

This list refers to the parameters used in the initial simulations. Note that parameters corresponding to the "Final Base Case" may be different from those indicated here. Changes are explained in the text.

3 1D - TH Simulations

3.1 Case TBT2_1: Initial model

In this case a simple 1D mesh has been used. Only the thermo-hydraulic problem is considered, and the parameters refer to the list presented in previous section. Impervious boundary conditions are assumed for both, liquid and gas. Lateral wall of the cell is considered an adiabatic boundary, and the temperature has been imposed in both ends according to the protocol indicated in figure 2.

In order to summarize the results obtained, only a few figures are presented for this case. Figure 3 shows the temperature distribution in the bentonite at different times. Note that temperature inside the sample follows almost a linear relationship, typical of steady state conditions and constant thermal conductivity.

Figure 4 presents suction versus sample height for different times, whereas in figure 5, suction is depicted against time for some of the sensor locations indicated in the protocol. Note that at the beginning of the test, when both ends have the same temperature, suction decreases, basically because relative humidity increases from 40% to 51% due to water evaporation. When there is a temperature gradient, the hot face exhibits higher suction than the cold one. Cycles of heating and cooling are reproduced in the computed values of suction, as indicated in figure 5.

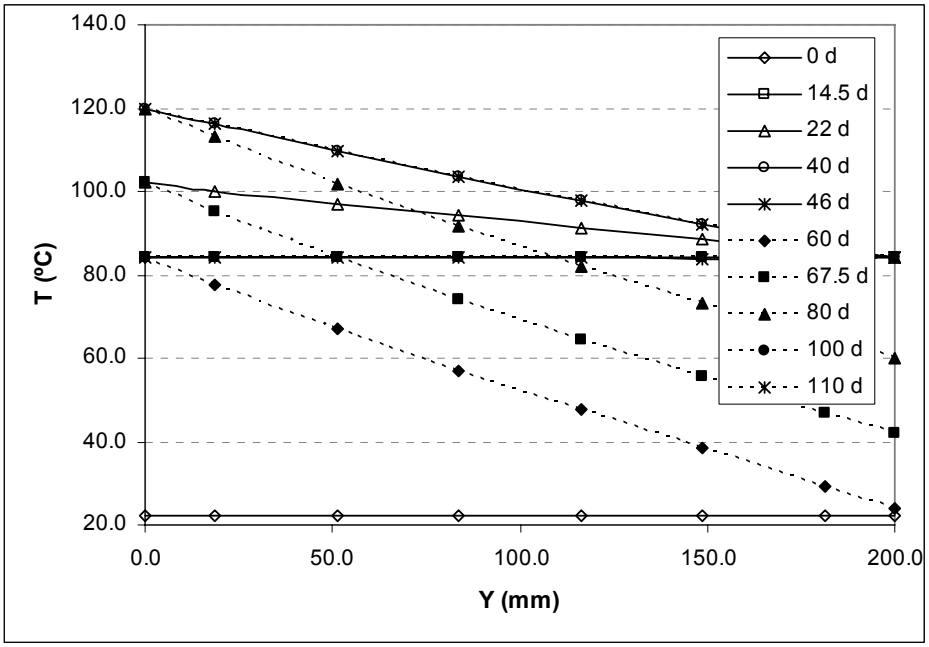

Figure 3. *Suction versus sample height in case TBT2_1*

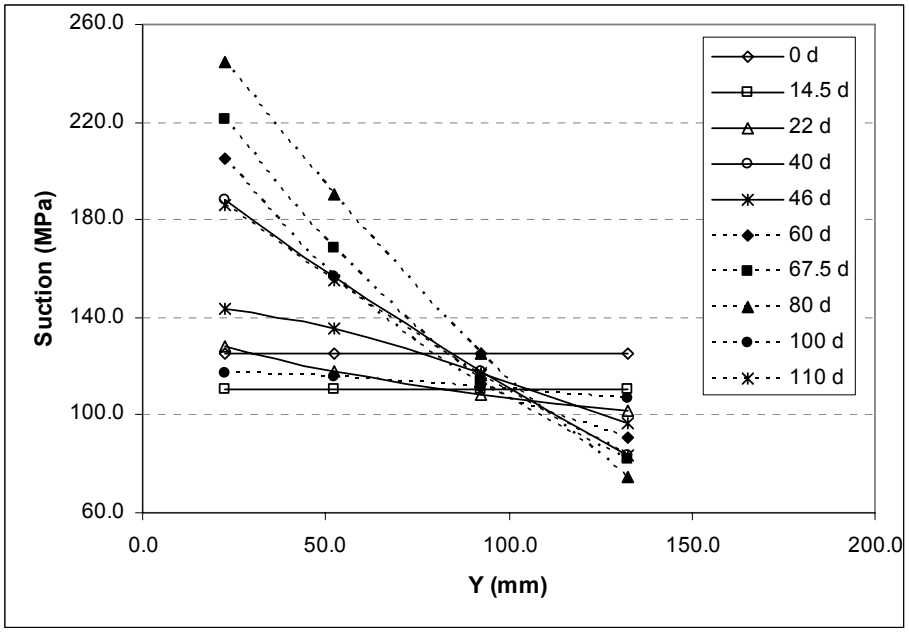

Figure 4. *Suction profiles for different times. Case TBT2_1*

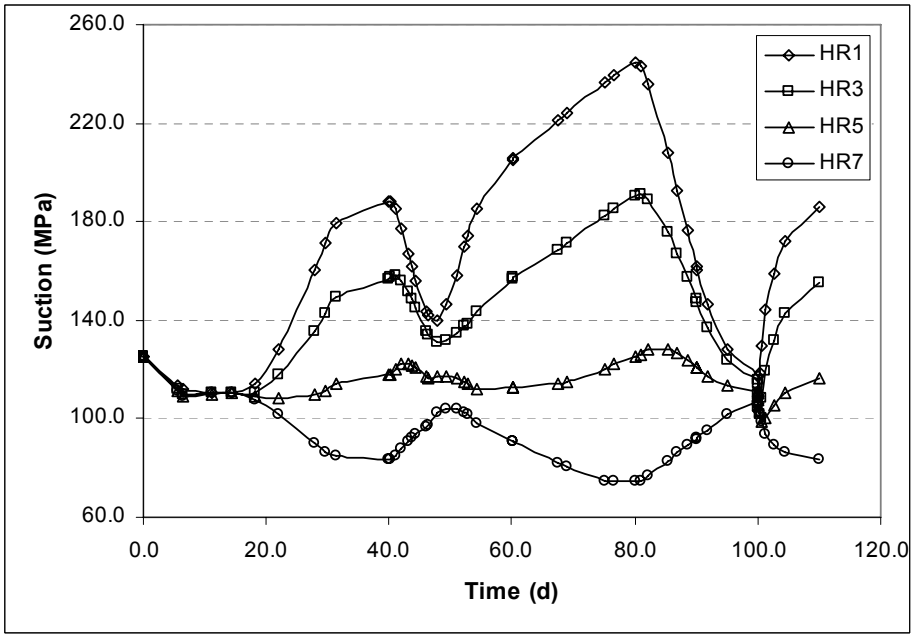

Figure 5. *Suction versus time for different sensor locations. Case TBT2_1*

3.2 Case TBT2_2: Influence of retention curve

Retention curve is a basic hydraulic property that has much influence on TH calculations, due to the log-scale in the suction axis. Small changes in that curve may cause important differences in the final simulations. Because of that, an analysis of the experimental data available was carried out. Figure 6 presents several measurements of that curve for MX-80 bentonite obtained from different authors: Ciemat (Villar, 2005), Andra (Dang & Robinet, 2004) and Clay Technology (TBT2 proposal, 2005). All values correspond in practice to the same dry density.

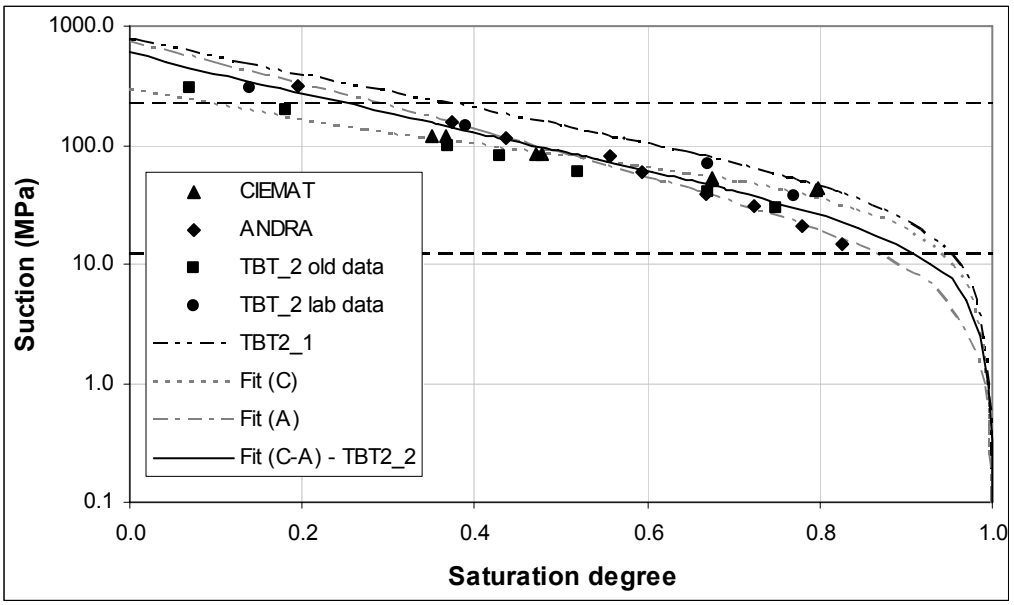

Figure 6. *Retention curves for MX-80 bentonite.*

In that figure, the curve used in this example (TBT2_2) has been depicted as well. It is considered to be more appropriate than the curve used in the previous case. Now the parameters corresponding to this new fit are:

$$P_0 = 30.6 \text{ MPa} \qquad \beta = 0.30 \qquad S_m = 600.0 \text{ MPa} \qquad m = 1.1$$

Note that they differ from the values presented in section 2.2. This new values will be adopted in all the cases that follow.

The initial degree of saturation of the bentonite (55%), corresponds now to a liquid pressure of -74.9 MPa, when the new retention curve is used.

Figures 7 and 8 present the comparison between models TBT2_1 and TBT2_2 in terms of suction for different times and points. Note that tendencies are the same in both models, although case TBT2_2 shows lower suction values in general.

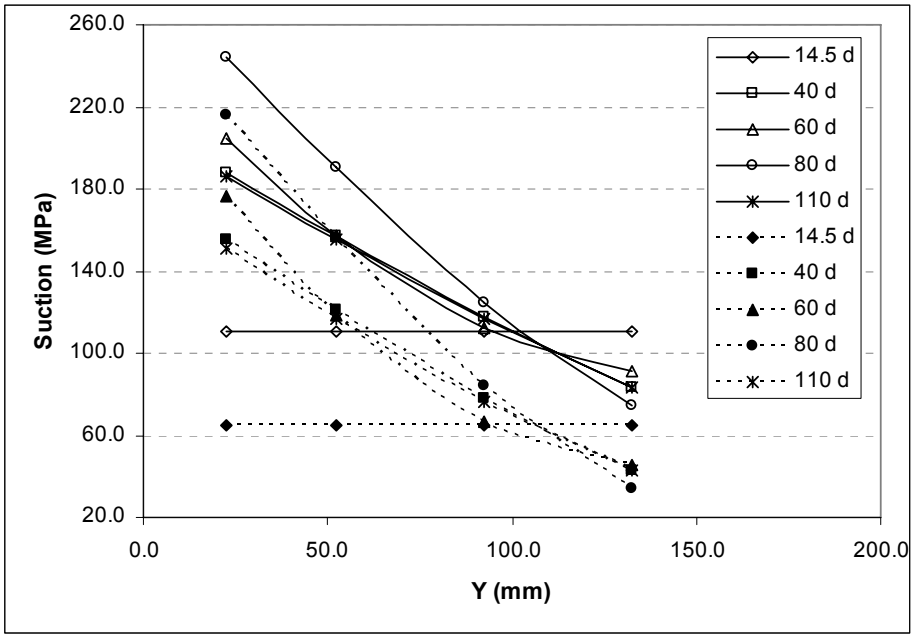

Figure 7. *Suction vs sample height. TBT2_1 (continuous line) & TBT2_2 (dashed line)*

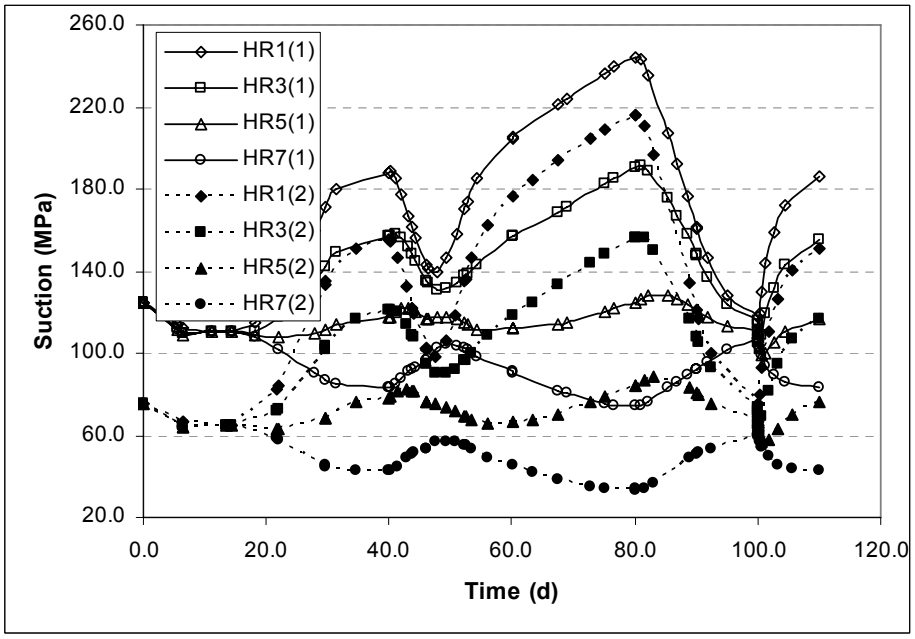

Figure 8. *Suction vs time. TBT2_1 (continuous line) & TBT2_2 (dashed line)*

3.3 Case TBT2_3: Influence of intrinsic permeability

There are some measurements of the MX-80 intrinsic permeability, but as expected, they present some scatter. Figure 9 shows some data compiled from Ciemat (Villar, 2005), Börgesson & Hernelind (1999), and Pusch (2001, cited in the report by Dang & Robinet, 2004).

Figure 9. *Intrinsic permeability versus porosity for MX-80 bentonite*

Measurements have been fitted using Kozeny's law. The results from Villar (2005) provide with an intrinsic permeability: $k_o = 1 \cdot 10^{-20}$ m^2 (value used in TBT2_3), whereas the results from Börgesson (1999) and Pusch (2001) give $k_o = 3.6 \cdot 10^{-21}$ m^2 (value used in model TBT2_1).

Figures 10 and 11 present the suction profiles for different times and the suction evolution for particular points within the sample, respectively. Curves for this model (TBT2_3) and model TBT2_1 are compared in those figures.

The range of porosities in the bentonite sample is 0.34 – 0.44. For that range, the measurements performed by Börgesson et al (1999) and by Pusch (2001) seem more appropriate, and therefore, the value of intrinsic permeability used in model TBT2_1 has been finally adopted for further analyses.

A combined influence of the water retention curve and intrinsic permeability was also analysed in a different model (TBT2_4). When both effects are considered, the differences with respect case TBT2_1 become more evident, although the patterns and tendencies are quite similar in all cases. As a result of these previous exercises, it was decided to use the water retention curve from case TBT2_2 and the intrinsic permeability from case TBT2_1 in further analyses.

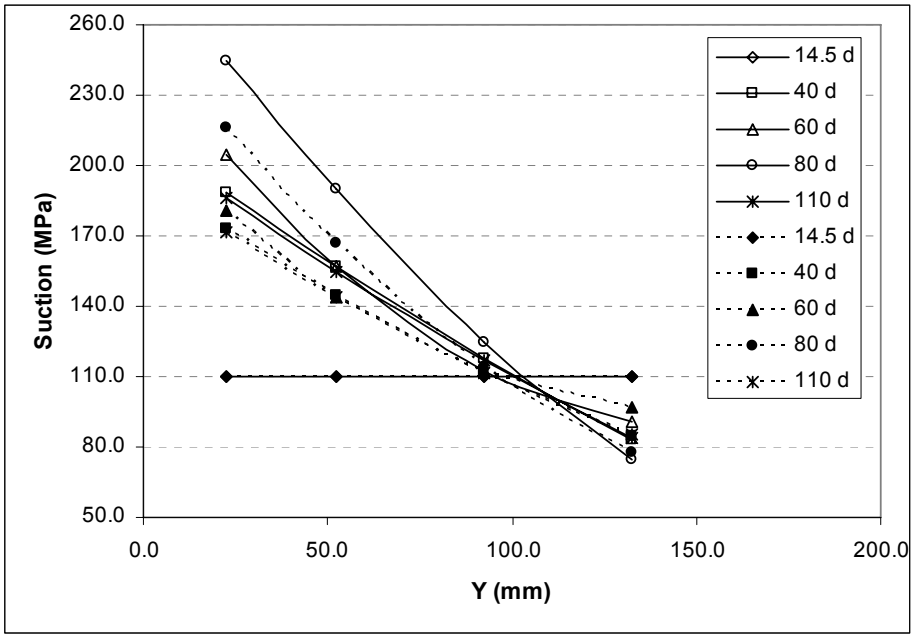

Figure 10. *Suction – sample height for two models: TBT2_1 (continuous line) & TBT2_3 (dashed line)*

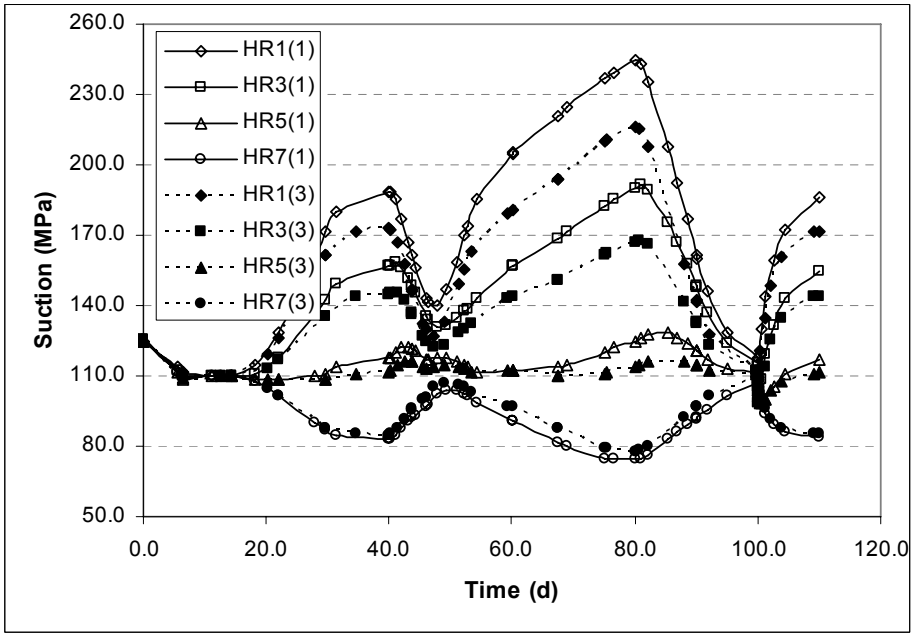

Figure 11. *Suction against time for two models: TBT2_1 (continuous line) & TBT2_3 (dashed line)*

4 1D - THM Simulations

4.1 Case TBT2_5: Basic mechanical model

When considering the mechanical behaviour, the "Barcelona Basic Model" was adopted in all analyses. Parameters for this base case were indicated in section 2 already. In addition to them, a value of 0.2 MPa (isotropic) was assumed for the initial stress in the bentonite. Both ends of the sample were considered fixed (zero displacement), and only a vertical displacement was allowed (1D conditions).

Figure 12 presents the suction profiles obtained in this case, compared with the results from model TBT2_2 corresponding to a TH analysis. It can be seen that both models give similar results in terms of suction, which suggests that this experiment is mainly a thermo-hydraulic test, and that the mechanical behaviour has probably little influence on the TH variables. Despite that, some variations of stresses and porosity within the sample have been computed, and they are presented in figures 13 and 14. Stresses are considered isotropic and, due to equilibrium conditions and the restrictions of a 1D analysis, the model computes the same value in all points of the bentonite. Changes in stresses are due to the development of swelling pressure in the cold zone of the sample, where suction decreases, as it can be seen in the porosity evolution plot (figure 14).

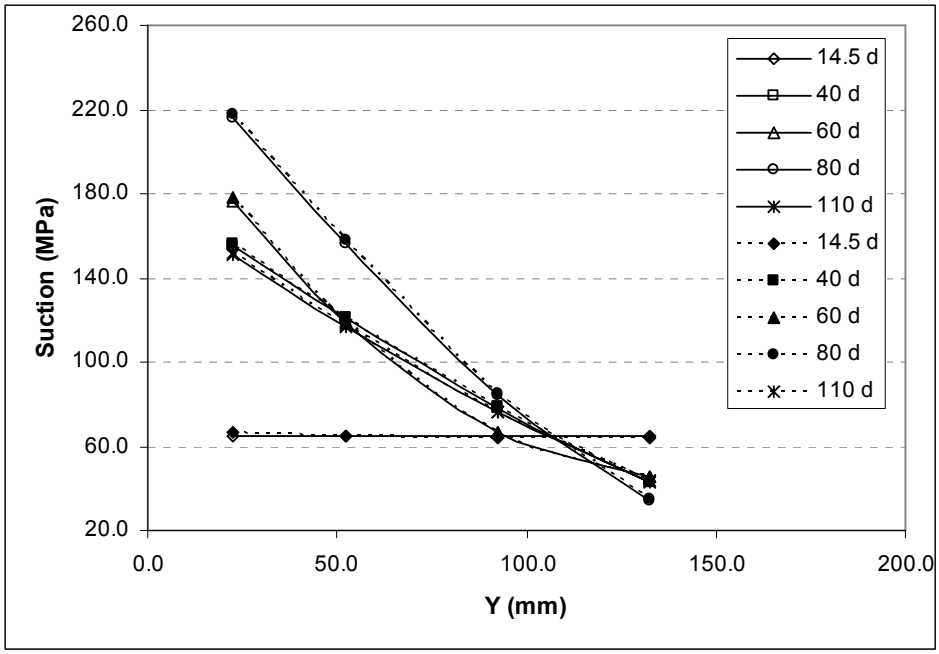

Figure 12. *Suction versus height sample for different times and case TBT2_2 (continuous line) and TBT2_5 (dashed line)*

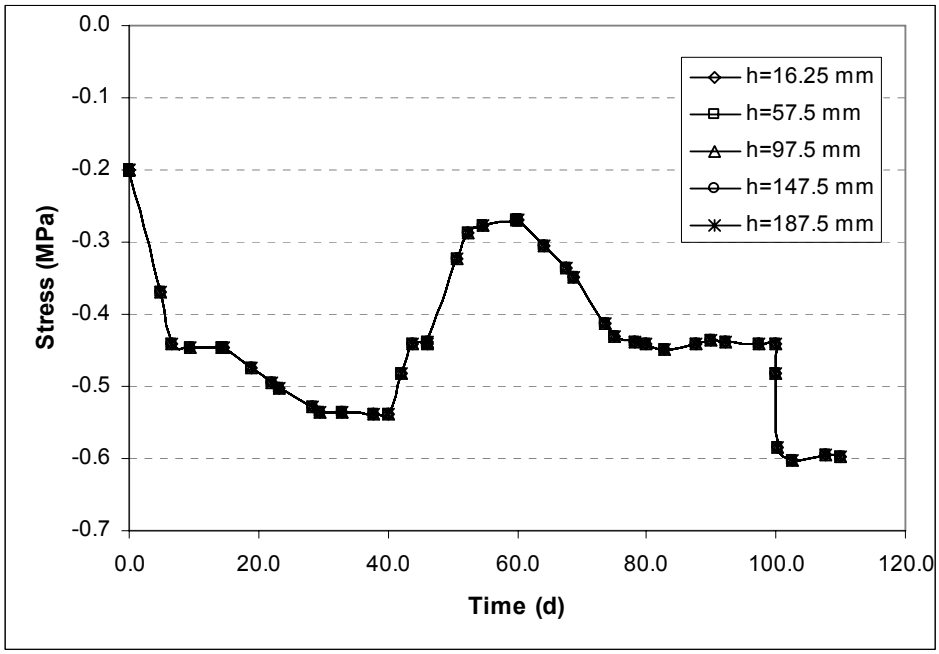

Figure 13. *Stress evolution, case TBT2_5 (negative indicates compression).*

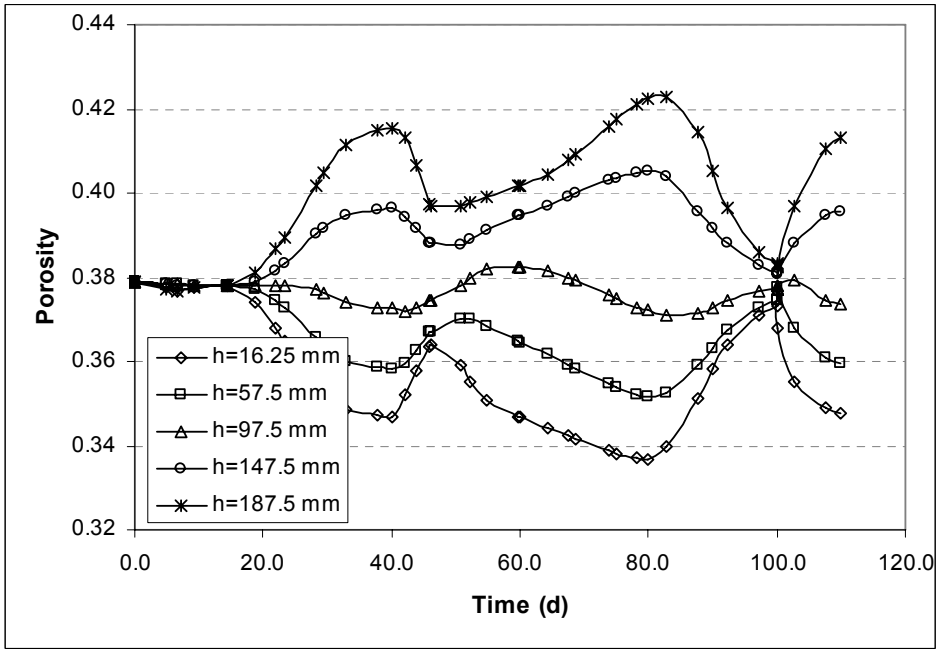

Figure 14. *Evolution of porosity. Model TBT2_5.*

4.2 Cases TBT2_6 & TBT2_7: Influence of mechanical parameters

The information on the mechanical properties of MX-80 is surprisingly scarce. It should be pointed out, however, that the tests required for that are difficult and time consuming. Mechanical parameters used in the previous case TBT2_5 came from the experience and they have been used during the development of TBT project so far. We have found, nevertheless, some discrepancies between those parameters and the results of some oedometer tests with suction control performed recently by Ciemat (Villar, 2005). Figure 15 presents the void ratio – vertical stress plot corresponding to these experiments. From that plot, the following parameters can be updated:

$$\kappa_{i0} = 0.032 \qquad \lambda(0) = 0.244$$

These values differ from those used in case TBT2_5, and therefore they were used in a new model (TBT2_6). Figure 16 presents the comparison between both cases in terms of suction profiles. Note that both models give similar results, which suggests that κ_{i0} and $\lambda(0)$ do not have influence on the Thermo-Hydraulic problem. Obviously the mechanical response is different in each case, as it can be observed in figure 17. Parameters of TBT2_6 correspond to a stiffer material and the resulting total stress is therefore bigger than in case TBT2_5, for an imposed displacement.

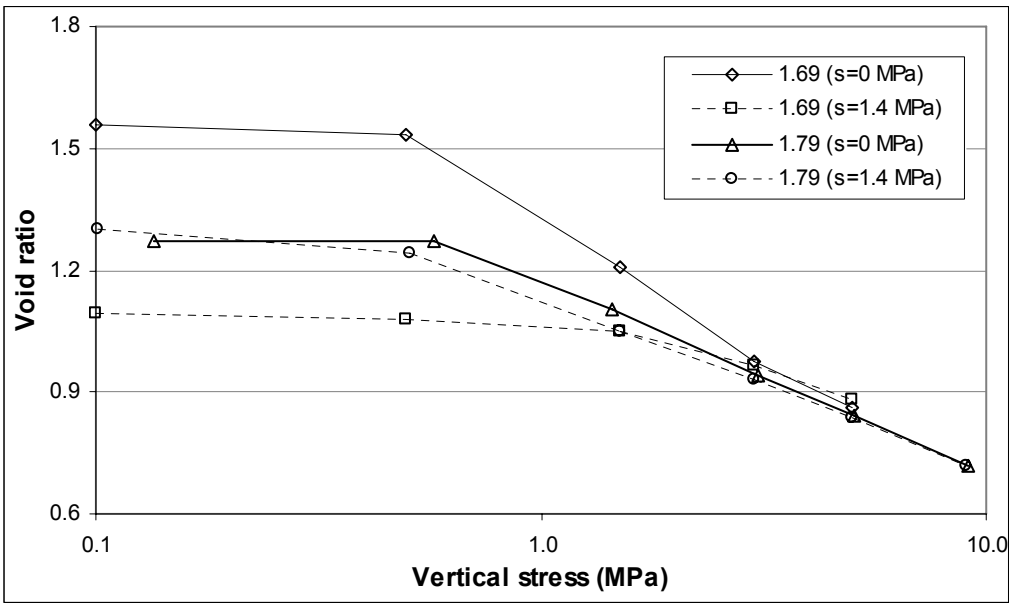

Figure 15. *Void ratio against vertical stress for different dry densities (in g/cm^3) and constant suctions (Villar, 2005).*

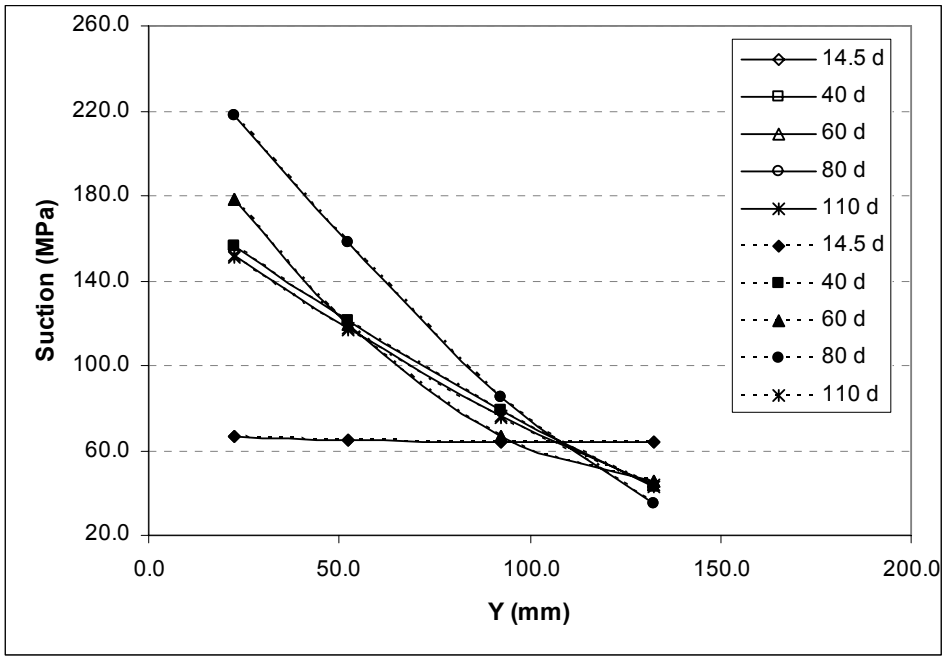

Figure 16. *Suction profiles for different times: case TBT2_5 (continuous line) & TBT2_6 (dashed line)*

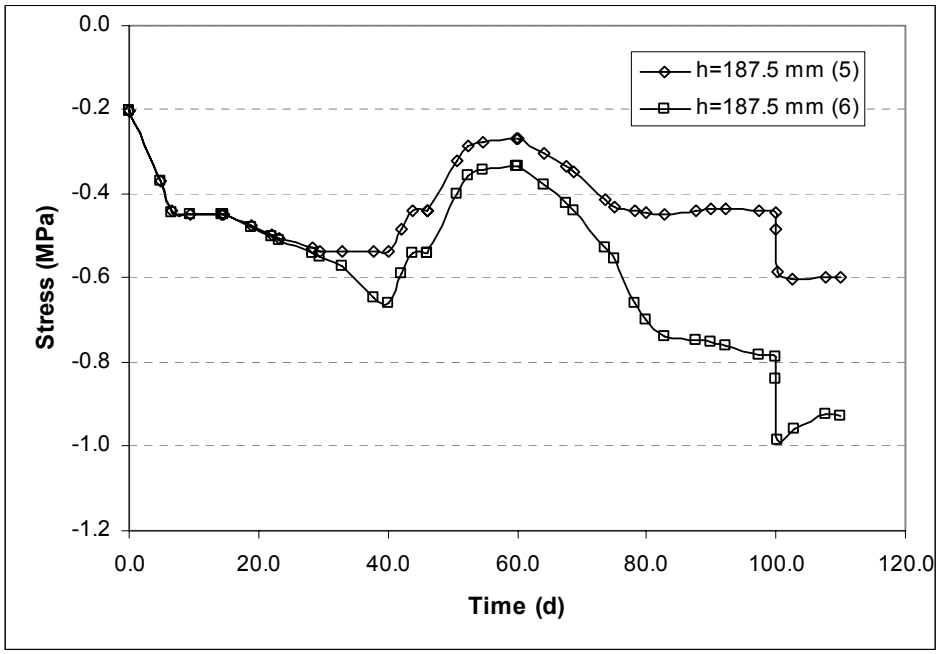

Figure 17. *Stress evolution for case TBT2_5 and TBT2_6 (negative indicates compression).*

There are other mechanical parameters that may affect the computed stresses. Among them, the value of κ_s may play an important role, particularly on the computed swelling pressure. Although in this experiment the stresses are limited, a new model (TBT2_7) was developed in order to explore the effect of this parameter. From recent experiments on MX-80 performed at Ciemat (Villar 2005), the following law was considered for that parameter (figure 18):

$$\kappa_s = \kappa_{s0} \exp(\alpha_{ss} s)$$

For TBT2_7 the values adopted correspond to the curve depicted in figure 18:

κ_{s0} = 0.1563 (as used in TBT2_6, assuming κ_s constant)

α_{ss} = -0.04 MPa^{-1} (it was nil in TBT2_6)

Vertical lines in figure 18 indicate the range of suction involved in this simulation. Note that the experimental information is rather limited to low values of suction and the exponential law considered is based more on assumptions than in experiments. However, it is expected that model TBT2_7 will provide with a better representation of the mechanical behaviour of the bentonite.

Figure 19 shows the suction profiles obtained for models TBT2_6 and TBT2_7. Note that both give similar profiles, which indicates that κ_s does not have influence on the TH behaviour of the sample (either assuming a constant value or a function of suction). Regarding stresses, however, some differences become evident and case TBT2_6 with a constant value of that parameter results in bigger axial stresses (figure 20).

An additional model (TBT2_8) was also considered, assuming a constant value of κ_s = 0.05, which is an average value in the range of suctions considered. For this analysis the results were similar to those obtained in case TBT2_7. Therefore, the exponential law assumed in model TBT2_7 was used in further models.

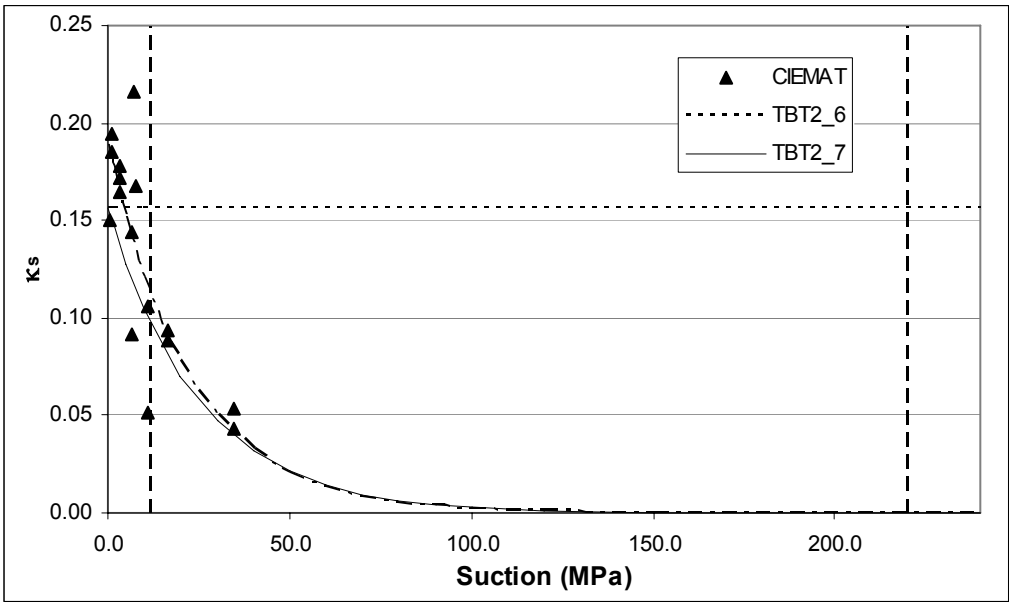

Figure 18. *Variation of parameter κ_s with suction*

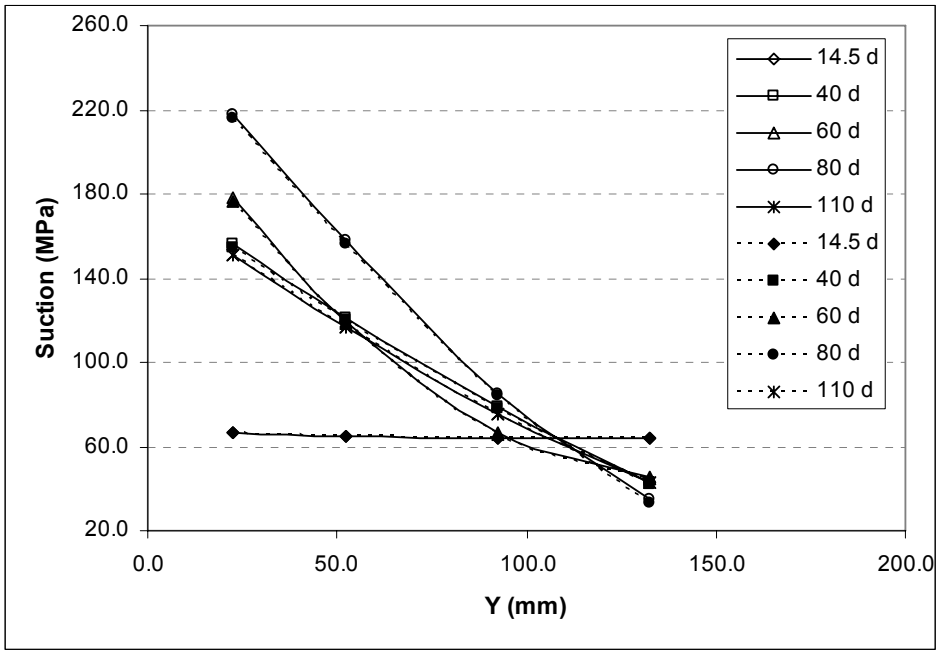

Figure 19. *Suction profiles for different times: case TBT2_6 (continuous line) & case TBT2_7 (dashed line).*

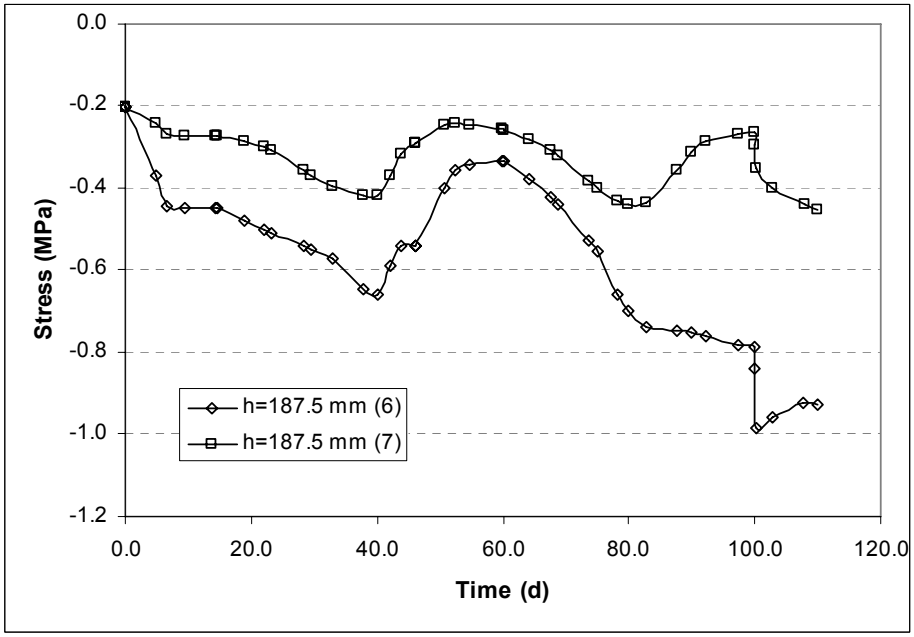

Figure 20. *Stress evolution for case TBT2_6 and TBT2_7 (Negative means compression).*

4.3 Cell tightness: Case TBT2_9

A 1D case analysing the effect of loss of gas through the cell has been considered as well. In order to simulate that, the node of the finite element 1D mesh corresponding to the cold end has been assumed with a constant gas pressure of 0.1 MPa. That corresponds to the value of atmospheric pressure assumed in Code_Bright. In this manner, if there is an increment of gas pressure inside the sample, there will be a loss of vapour in the bentonite. Obviously this is a limit case, because in practice the loss of gas could be more difficult (that is, instead of a direct contact of the sample with atmosphere, the gas may escape through a non direct path in the cell walls).

Figure 21 shows the computed suction profiles of this model, compared with the previous case TBT2_7. Note that now suction values are higher, due to the water loss (vapour form) in the bentonite.

Regarding stresses, figure 22 presents the evolution for both models, TBT2_9 and TBT2_7. Differences are not significant, as it occurs in the suction profile graph. It can be concluded, that the effect of cell tightness does not play a fundamental role in this experiment, although the 3D models should be also analysed to confirm that.

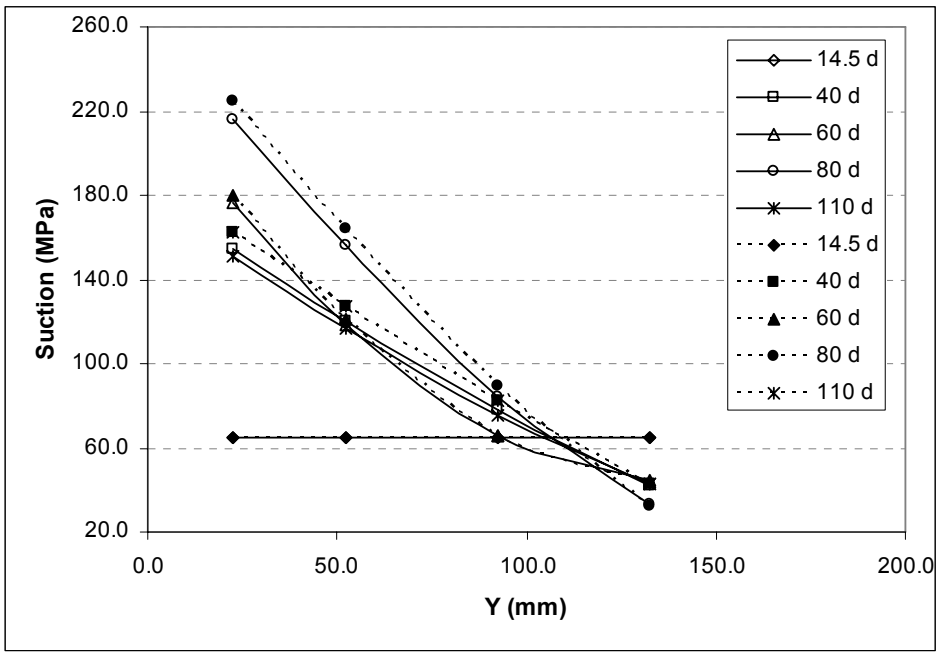

Figure 21. *Suction profiles for different times. Case TBT2_7 (continuous line) and Case TBT2_9 (dashed line).*

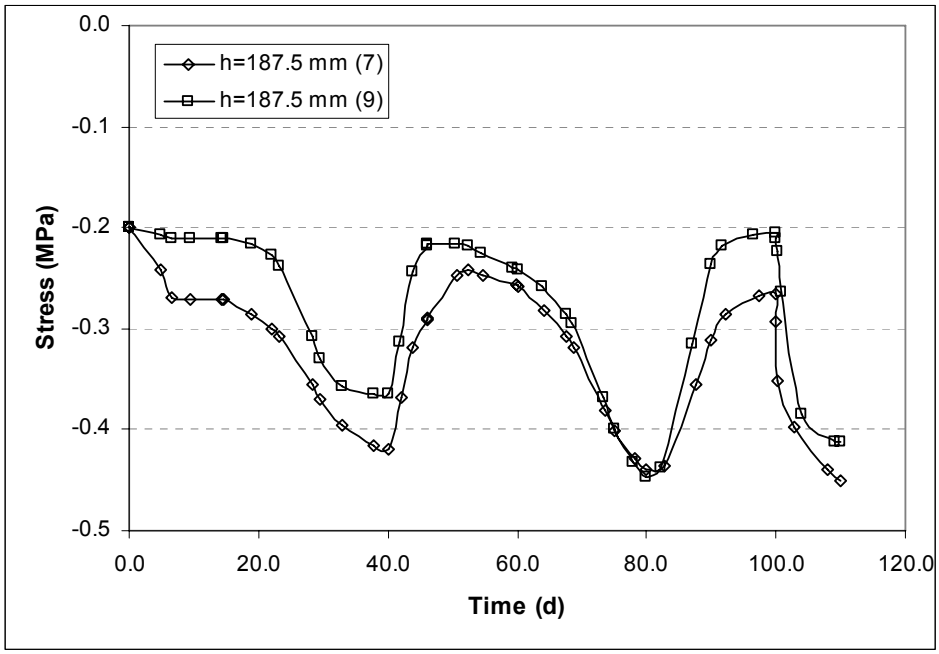

Figure 22. *Stress evolution for Case TBT2_7 and Case TBT2_9 (Negative means compression).*

5 Q3D - THM Simulations

In this section a few models based on a 2D axi-symmetric ("Quasi3D") geometry are presented. Despite the 1D symmetry of the whole setup, the proposal from Clay Technology suggested to perform 2D or 3D analyses as well, in order to evaluate the effect of potential preferential flow paths in the contact bentonite – cell walls. The following model, case TBT2_10, was finally assumed as the "Base Case" and it has been considered as the most likely scenario for the experiment.

5.1 Base case: TBT2_10

A 2D – axisymmetric mesh was considered for this model, imposing the boundary conditions described in previous sections:

- Zero displacements in the contact bentonite-cell and in the sample axis (the effect of temperature on the cell walls was assumed negligible)

- Fixed temperature at both ends of the sample, and adiabatic boundary condition on the lateral wall.

- Impervious boundary condition at all boundaries.

Current parameters are those of case TBT2_7. The results in terms of thermo-hydraulic variables are quite similar. As an example, figure 23 presents the suction profiles corresponding to this analysis, which are comparable to those presented for case TBT2_7 in figure 19.

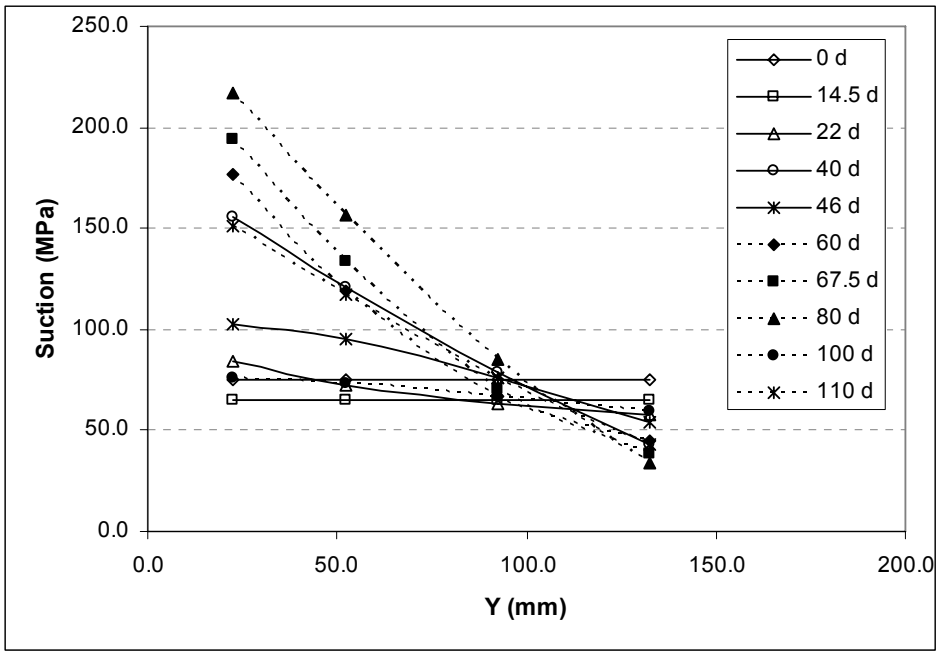

Figure 23. *Suction profiles for different times. Case TBT2_10.*

With respect to stresses, however, this model provides with different values than the 1D case. This is a consequence of the geometry considered. In the Q3D model, radial and circumferential stresses develop, and they depend on the height considered. They tend to be higher where bentonite expands. Axial stresses are constant due to equilibrium conditions, but they are affected by the rest of the components of the stress field. In the 1D analysis, the stress conditions were isotropic, and equilibrium restrictions became in a constant axial stress for the whole sample as well.

Figure 24 compares axial stresses for both models, 1D and Q3D, against time. Other stresses for the Q3D case are indicated in the following figures:

- Radial stress in figure 25
- Circumferential stresses in figure 26
- Tangential r-y stresses in figure 27

Note that tangential stresses θ-y are nil due to symmetry.

The parameters and the conditions used in this case TBT2_10 are assumed to be representative of the experiment, after taking into account the experience gained from the previous models and the information available. Therefore, a set of plots corresponding to the expected output from the group are presented in the annex enclosed at the end of the document. They present the simulation results in several figures with a one page format, to facilitate the comparison with measurements.

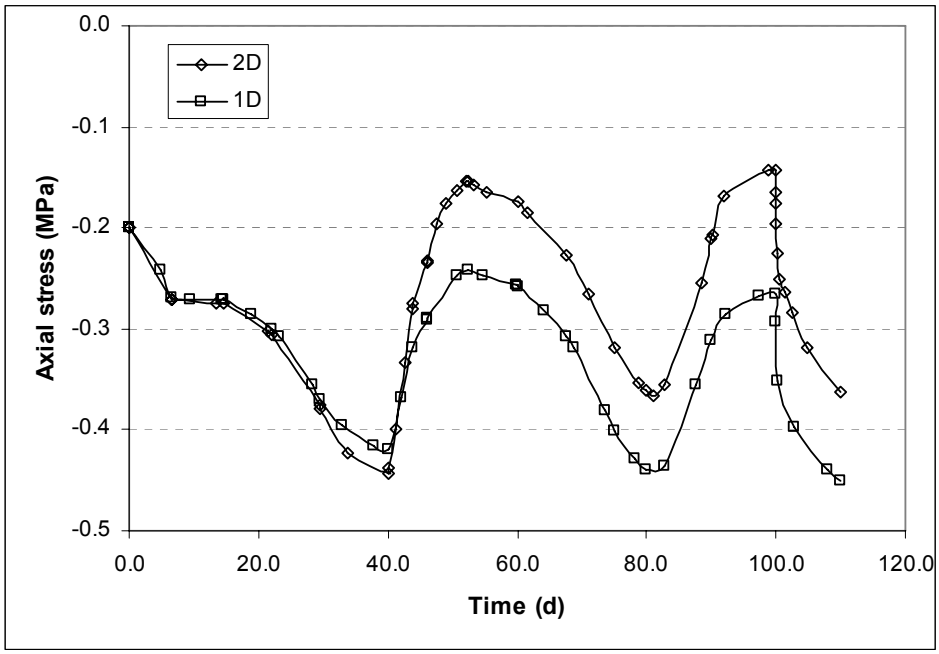

Figure 24. *Axial stress versus time for model TBT2_10 (2D) and model TBT2_7 (1D). Axial stress is constant at a particular time for all heights in the sample (Negative means compression).*

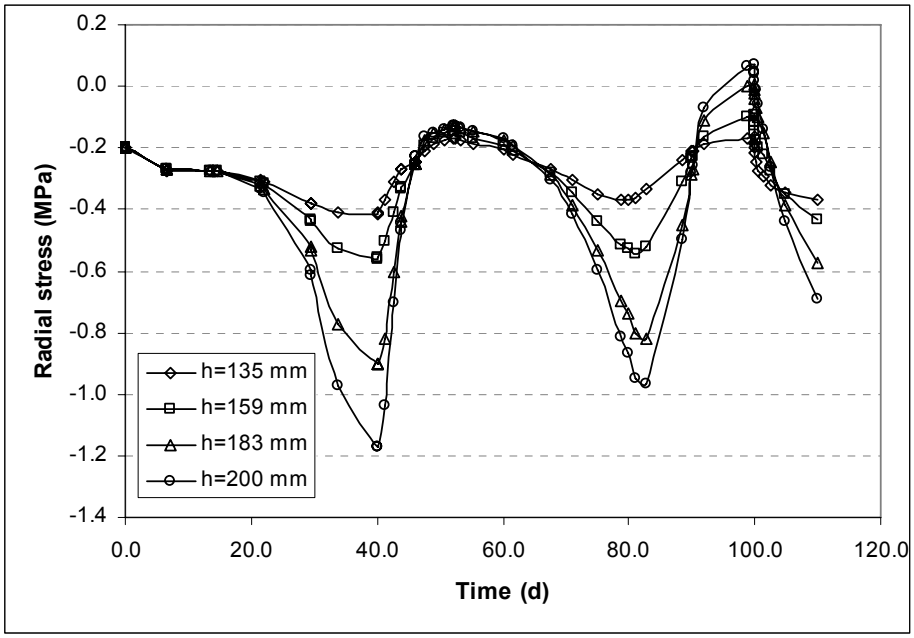

Figure 25. *Radial stress evolution for case TBT2_10 (Negative means compression).*

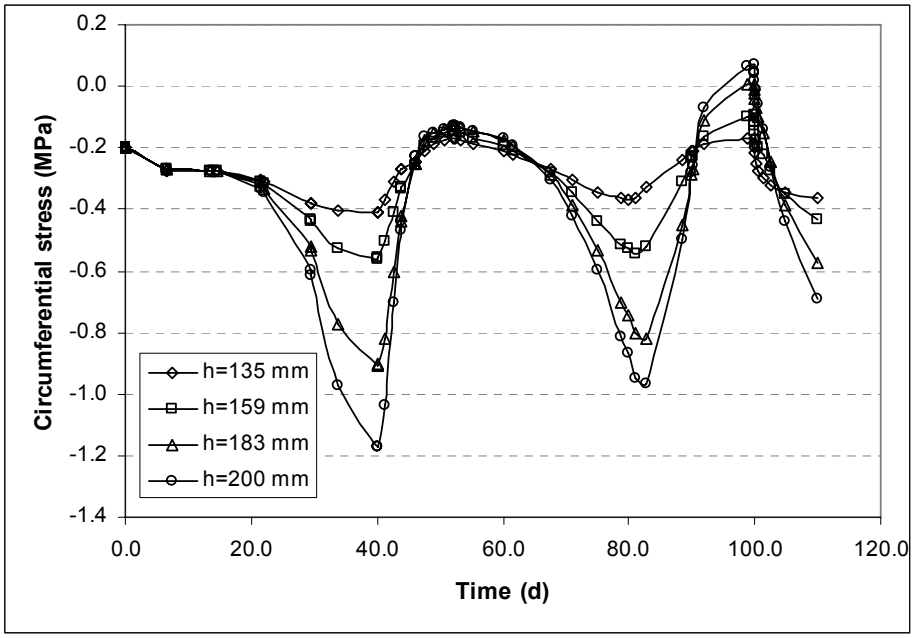

Figure 26. *Circumferential stress evolution for case TBT2_10 (Negative means compression).*

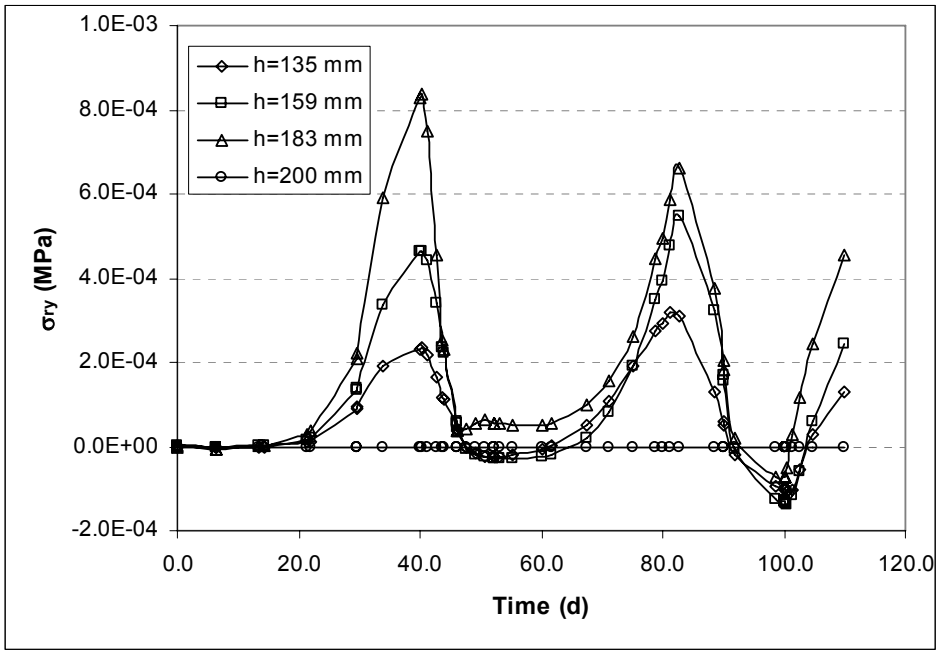

Figure 27. *Tangential stress (r-y) evolution for case TBT2_10 (Negative means compression).*

Apart from stresses and the variables already depicted (either in previous figures or in the Annex), the variation of porosity within the sample gives an interesting picture of the evolution of the experiment. Figure 28 presents the distribution of porosity in the bentonite for different times, whereas figure 29 shows the porosity evolution for different points. It becomes evident that cold zones in the sample receive water from the hot areas and therefore they swell and increase porosity following the cycles of temperature applied.

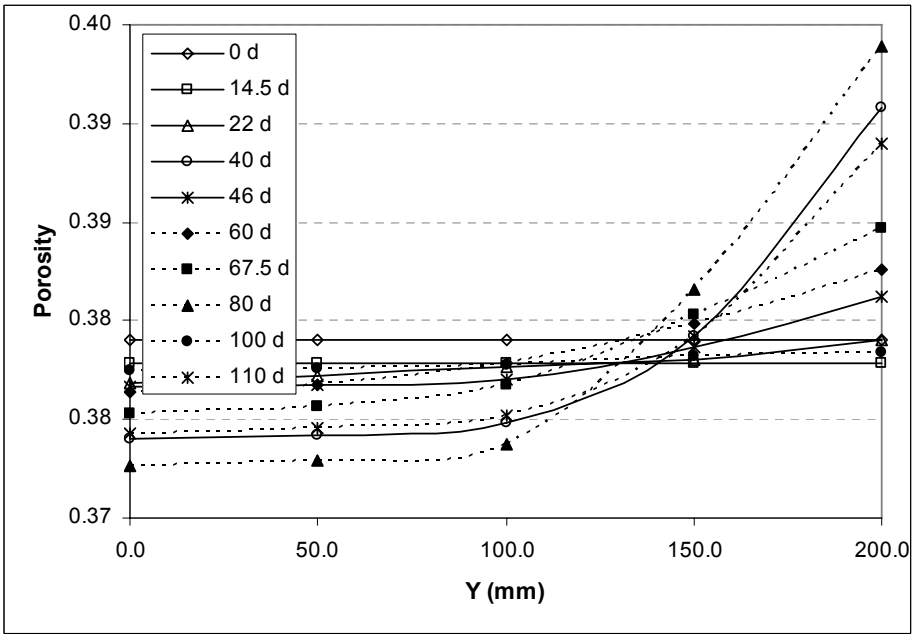

Figure 28. *Porosity profiles for different times. Case TBT2_10.*

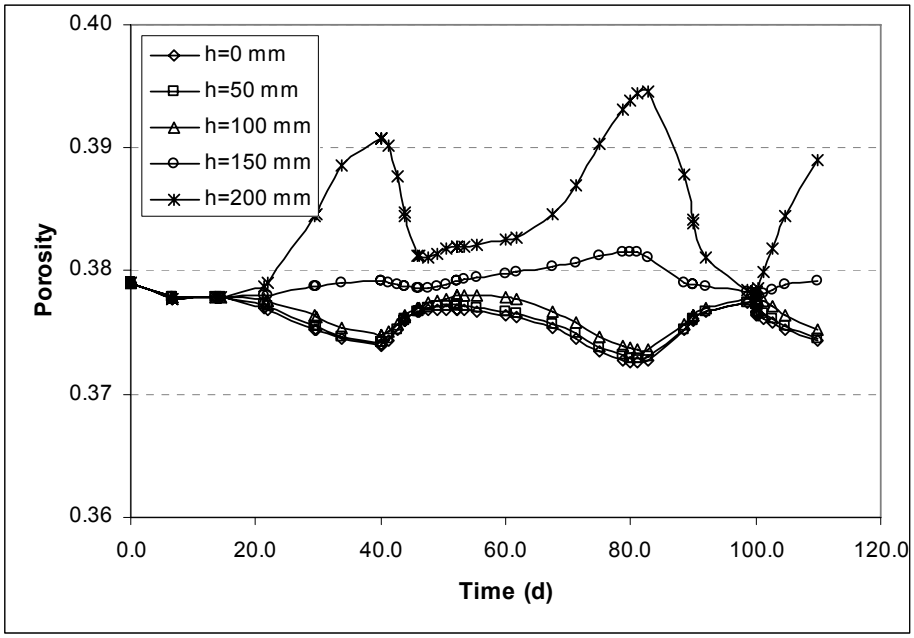

Figure 29. *Porosity evolution for different points. Case TBT2_10.*

5.2 Considering preferential flow paths & cell tightness

In order to fulfil the work program objectives, a few additional models have been considered. They are based on previous case TBT2_10, but they incorporate other features that may be important in the experiment:

- Case TBT2_11 included a gas boundary condition of 0.1 MPa at the upper end of the sample, in order to simulate a gas escape assumption. The results indicate that this effect is not very significant, because gas pressures inside the sample do not reach high values. Suction profiles are slightly higher (around 5%-10%) than in case TBT2_10.

- Case TBT2_13 is similar to base model TBT2_10, except for a column of elements in the contact bentonite – cell walls that have higher permeability than the standard bentonite elements. That column represents a preferential flow path for the water and vapour flow. The results are in general very similar to the base case TBT2_10.

- Case TBT2_14 combines the effect of a preferential flow path in the contact bentonite sample – cell wall with the condition of atmospheric gas pressure at two nodes of the top of that contact. In this case, that preferential path plays certain role in the development of the experiment, because it allows the gas to escape in a more rapid manner. That is, only when there is a preferential flow path, cell tightness seems to be somehow important. Some results follow.

Figure 30 presents the suction profiles obtained for model TBT2_14 compared with the corresponding profiles of base case TBT2_10. As it could be expected, the gas escape generates an increase of suction, although not very significant. The effect in terms of suction is similar than in case TBT_11 and case TBT_9. Finally, figure 31 presents suction as a function of time for different points in the sample. A comparison with base case TBT2_10 is also included.

In the Annex, some figures corresponding to model TBT2_14 have been included. They have a one page format, so they can be used for comparison with measurements if necessary. It is expected that case TBT2_10 will be more appropriate for comparison with laboratory data, but in case of a vapour loss in the sample, TBT2_14 would give probably better predictions than the base case.

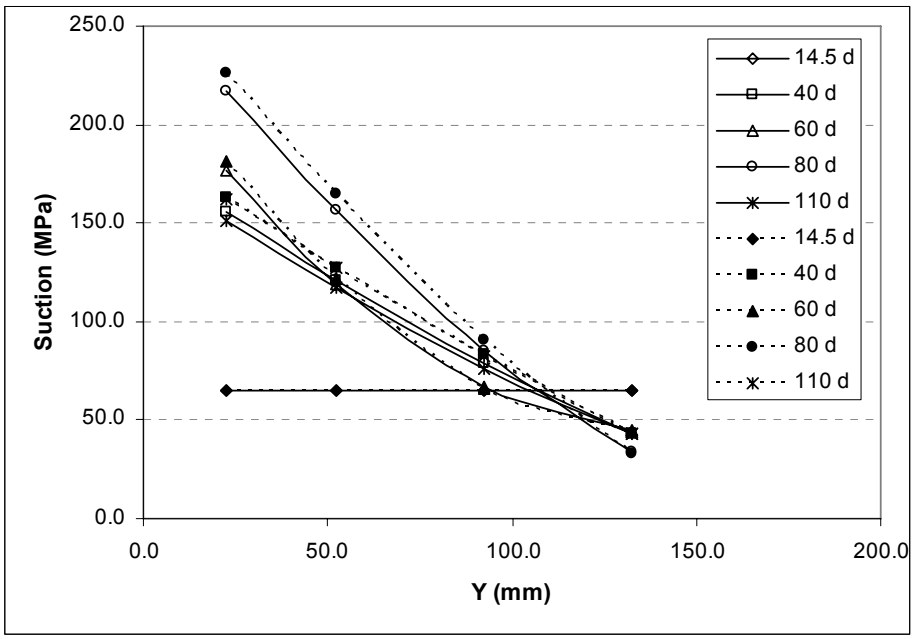

Figure 30. *Suction profiles at different times. Case TBT2_10 (continuous line) & Case TBT2_14 (dashed line).*

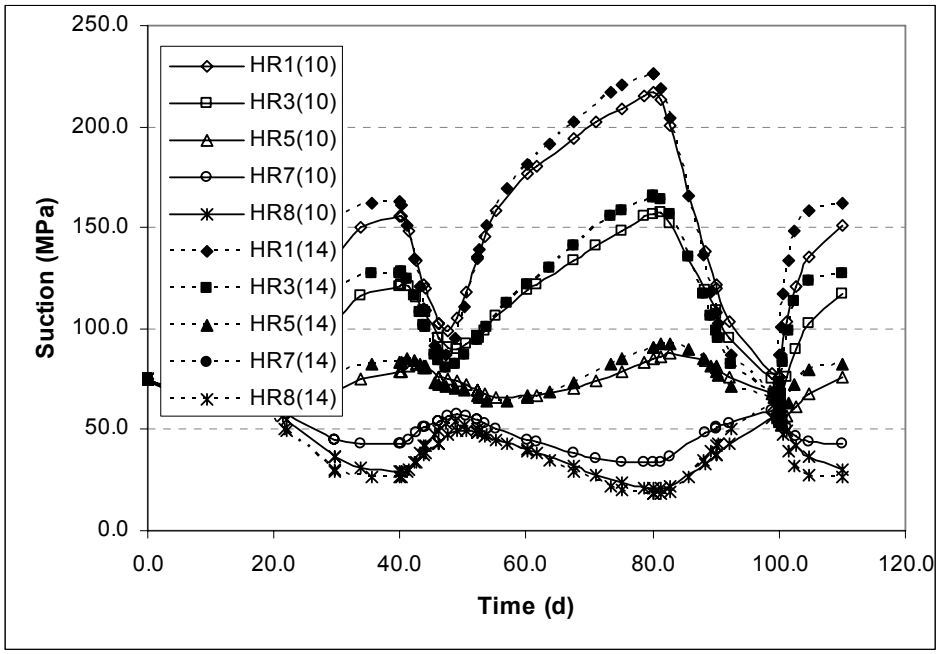

Figure 31. *Suction evolution for different points. Case TBT2_10 and TBT2_14.*

6 Concluding Remarks

This report includes the results of the predictive modelling programme of the TBT_2 experiment performed by the group coordinated by ENRESA. The definition of the models and the parameters used in the computations follow the guidelines of the document by Clay Technology (2005).

The modelling work has followed three basic steps:

- Initial TH models in a 1D geometry
- THM models in a 1D geometry
- THM models in a Quasi3D geometry

All steps have been described in this report and they are useful to understand the evolution of the analyses performed. It should be pointed out that the final "base case" (TBT2_10) is a consequence of many previous analyses that have been carried out to understand the behaviour of the system. Please note that the parameters and conditions used in that base model may differ from the initial values indicated in section 2.2. The sensitivity analyses performed with simpler 1D models were useful in order to obtain a final set of parameters more likely for this MX-80 bentonite. Despite that work, there is still some degree of uncertainty regarding the values of the parameters (i.e., mechanical information from MX-80 is indeed scarce).

The attached annex presents the required output regarding the THM variables of the experiment for the final case TBT2_10. Some figures including a comparison with case TBT2_14 have been included as well, just in case there is a problem with the cell tightness and some water loss. Please refer to the Annex figures for a direct comparison with experiments.

References

Börgesson, L. & Hernelind, J. (1999). Coupled thermo-hydro-mechanical calculations of the water saturation phase of a KBS-3 deposition hole. SKB Technical Report TR-99-41.

Clay Technology (2005) – (M. Åkesson, H. Hökmark). TBT_2 – Predictive Modeling Program, April 2005.

Dang K.D., Robinet J.C. (2004). Thermo-hydro-mechanical behavior of MX80 bentonite for temperature ≥ 100ºC. Final Report. C.RP.0EUG.02.008. ANDRA.

Villar M.V. (2005). MX-80 Bentonite. Thermo-Hydro-Mechanical Characterisation Performed at CIEMAT in the Context of the Prototype Project. Informes Técnicos Ciemat. 1053. Febrero, 2005.

ANNEX
Case TBT2_10 – “Final Base Case”

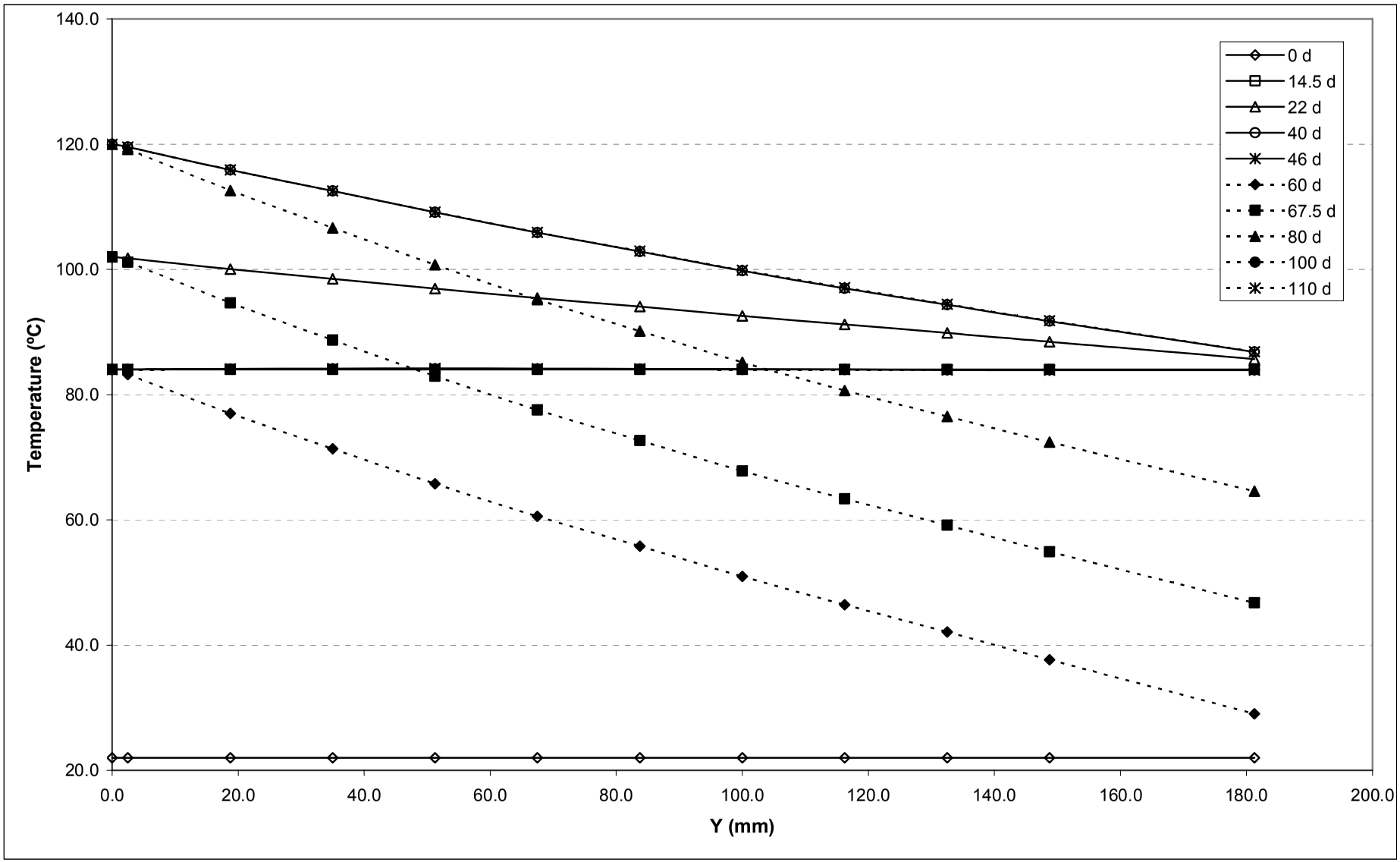
140.0
120.0
100.0
80.0
60.0
40.0
20.0
Temperature (ºC)
0.0
20.0
40.0
60.0
80.0
100.0
120.0
140.0
160.0
180.0
200.0
Y (mm)
0 d
14.5 d
22 d
40 d
46 d
60 d
67.5 d
80 d
100 d
110 d

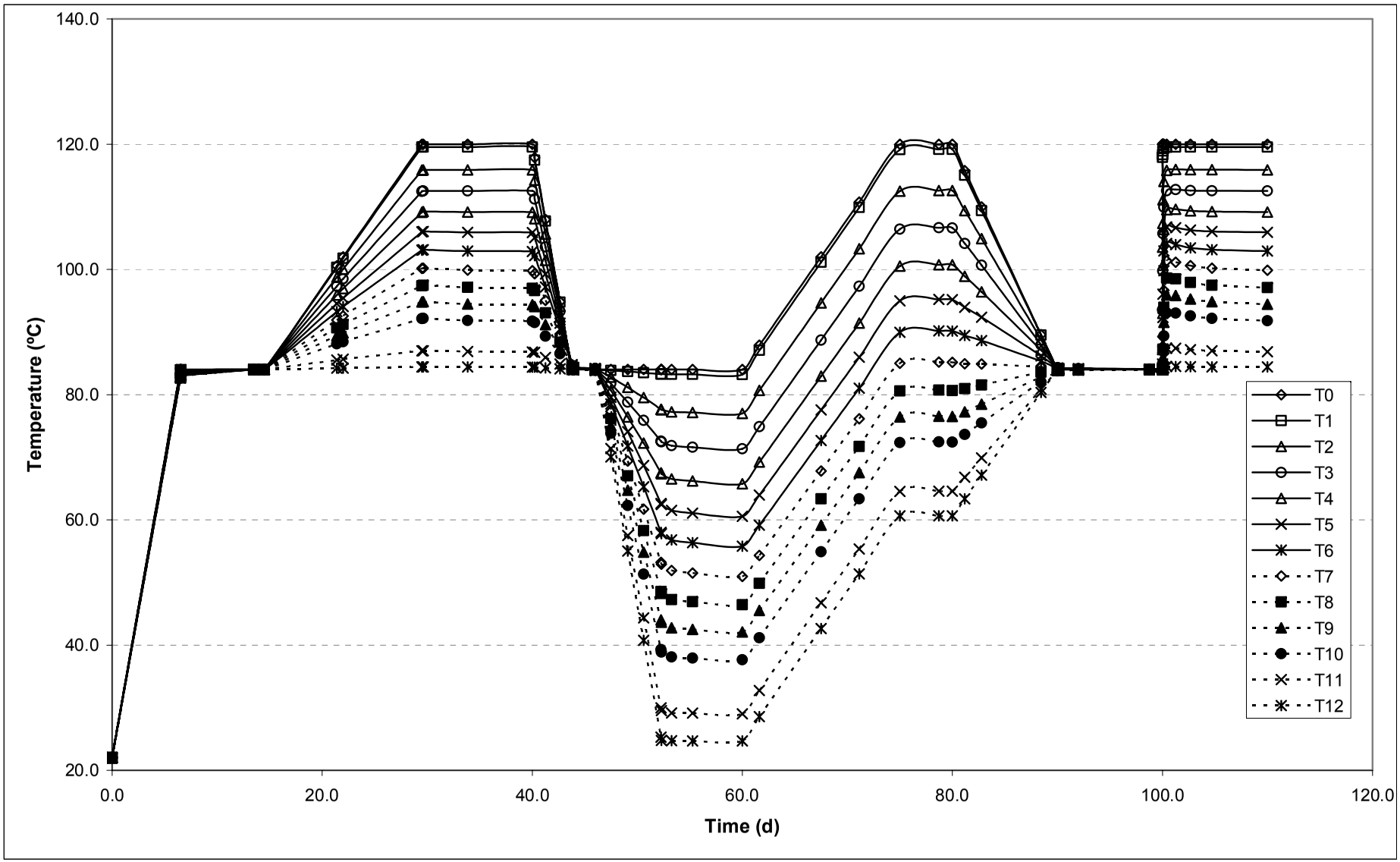
140.0
120.0
100.0
80.0
60.0
40.0
20.0
Temperature (ºC)
0.0
20.0
40.0
60.0
80.0
100.0
120.0
Time (d)
T0
T1
T2
T3
T4
T5
T6
T7
T8
T9
T10
T11
T12

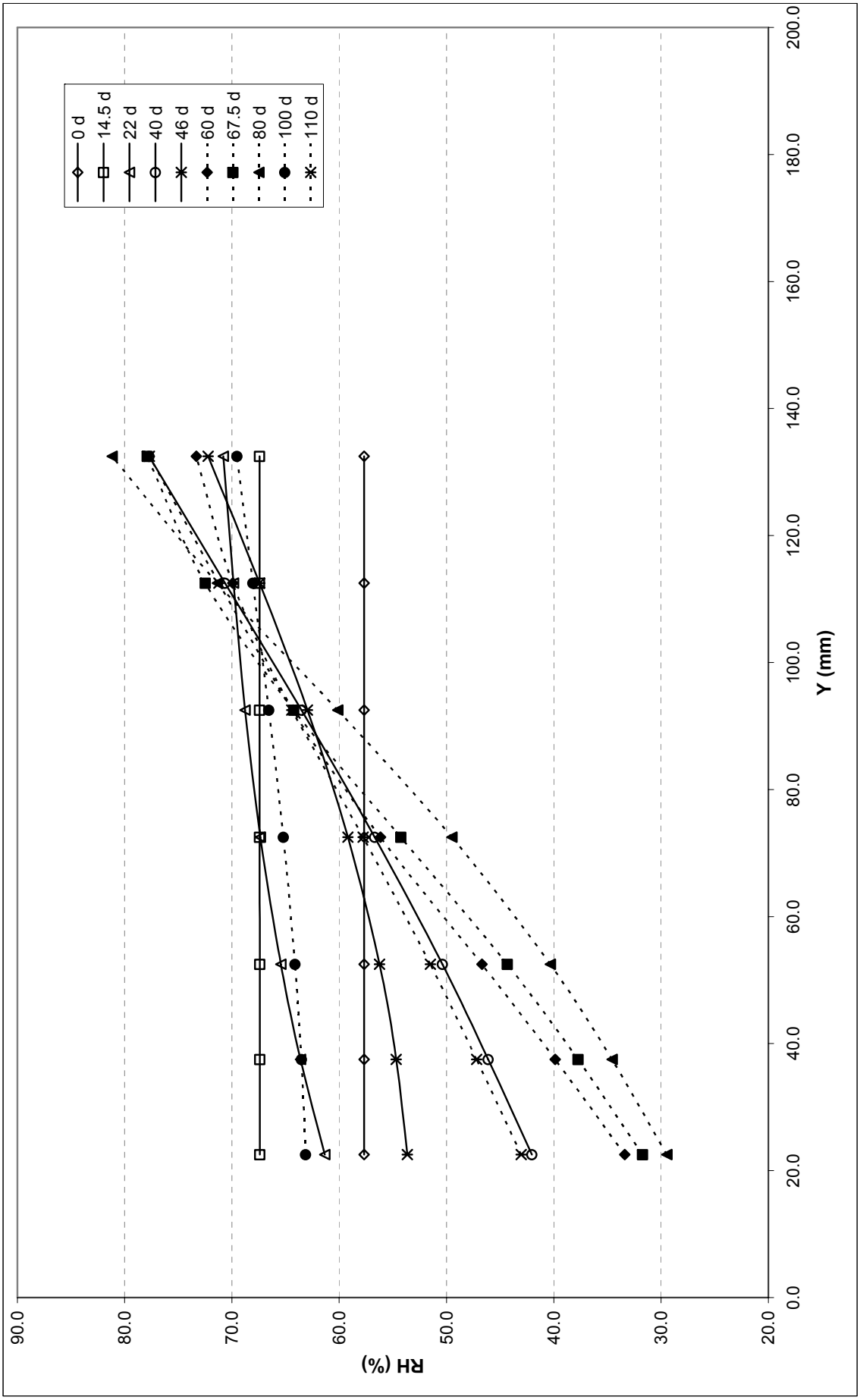
0 d
14.5 d
22 d
40 d
46 d
60 d
67.5 d
80 d
100 d
110 d
RH (%)
Y (mm)
90.0
80.0
70.0
60.0
50.0
40.0
30.0
20.0
0.0
20.0
40.0
60.0
80.0
100.0
120.0
140.0
160.0
180.0
200.0

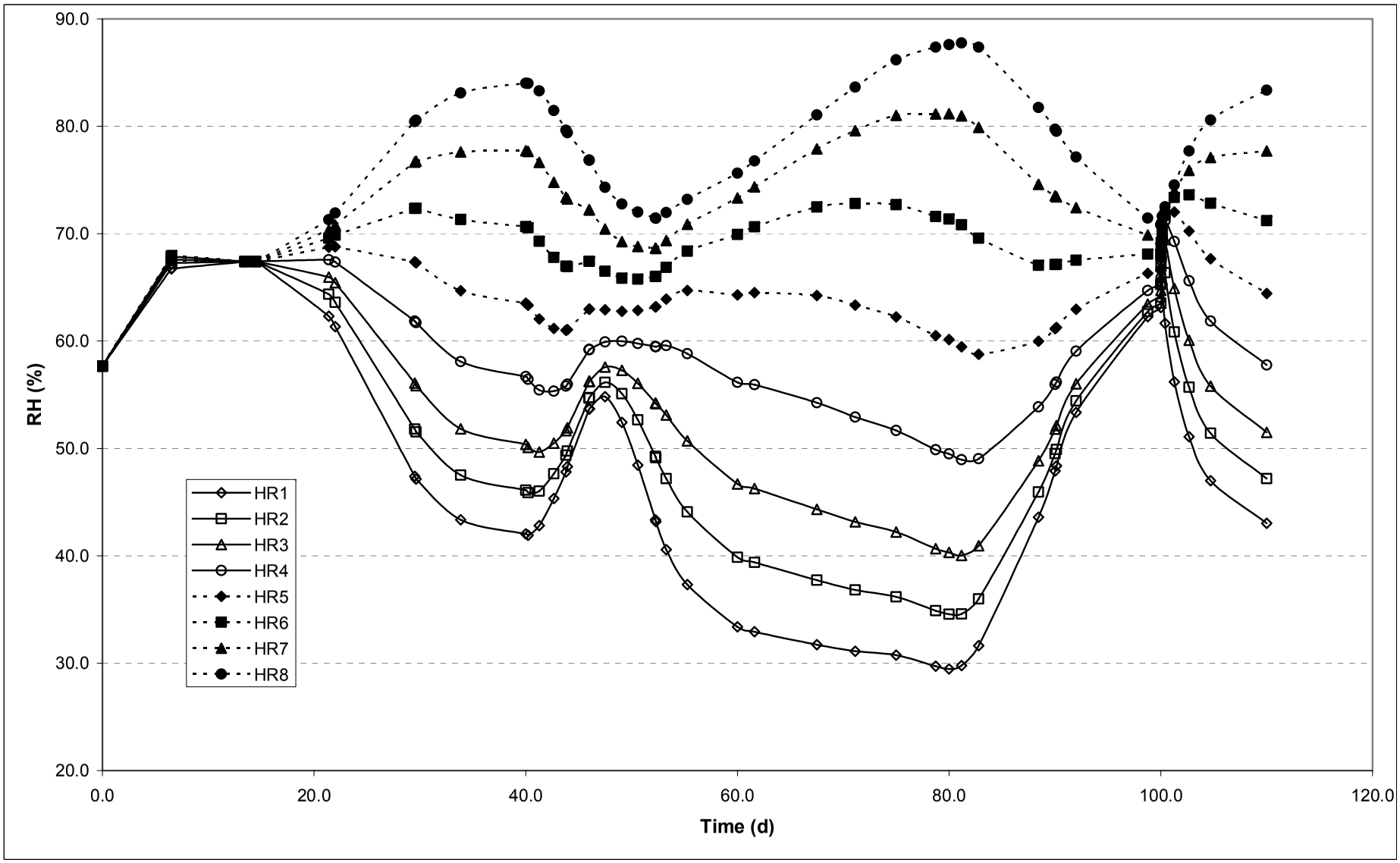
90.0
80.0
70.0
60.0
50.0
40.0
30.0
20.0
RH (%)
0.0
20.0
40.0
60.0
80.0
100.0
120.0
Time (d)
HR1
HR2
HR3
HR4
HR5
HR6
HR7
HR8

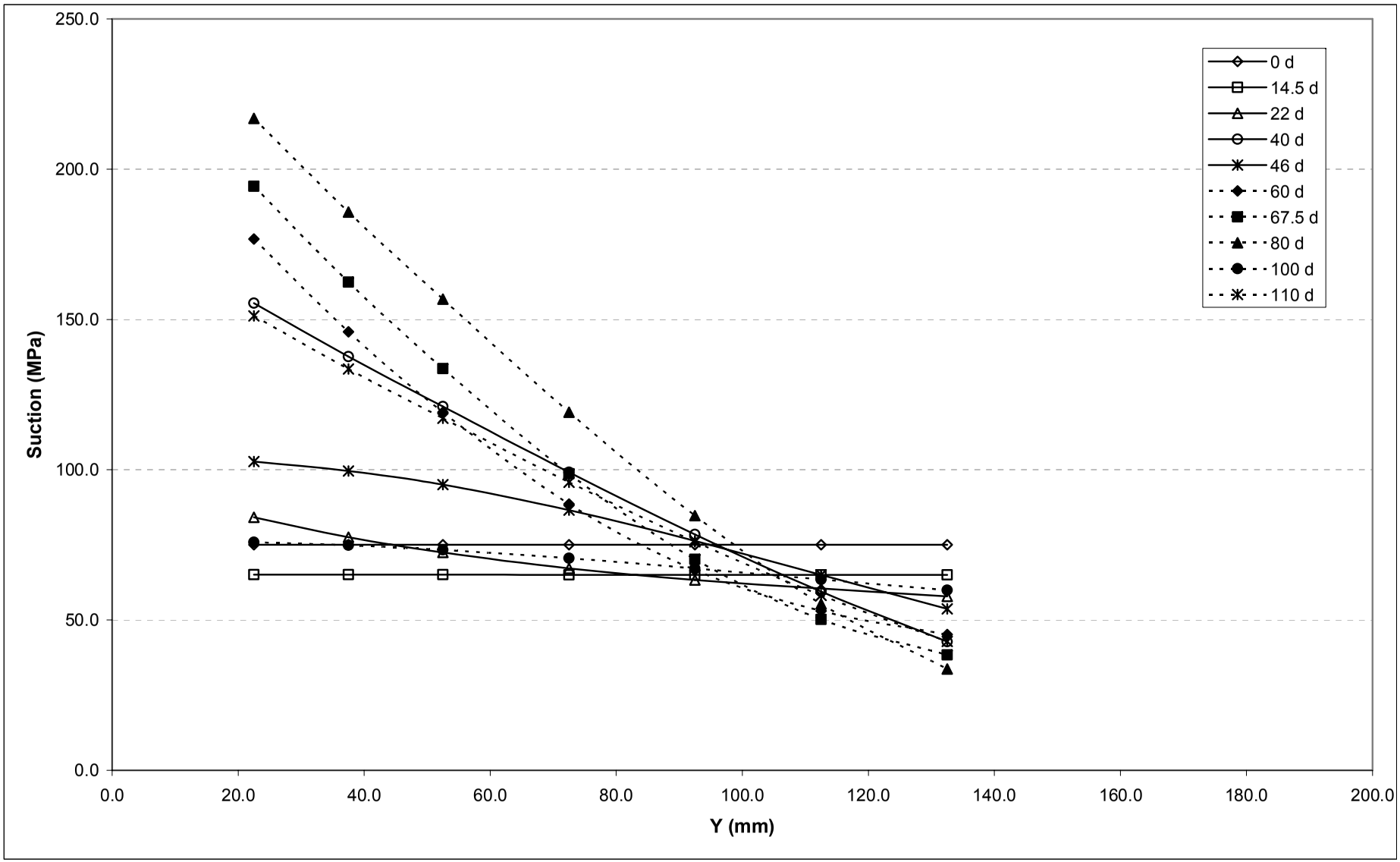
250.0
200.0
150.0
100.0
50.0
0.0
Suction (MPa)
0.0
20.0
40.0
60.0
80.0
100.0
120.0
140.0
160.0
180.0
200.0
Y (mm)
0 d
14.5 d
22 d
40 d
46 d
60 d
67.5 d
80 d
100 d
110 d

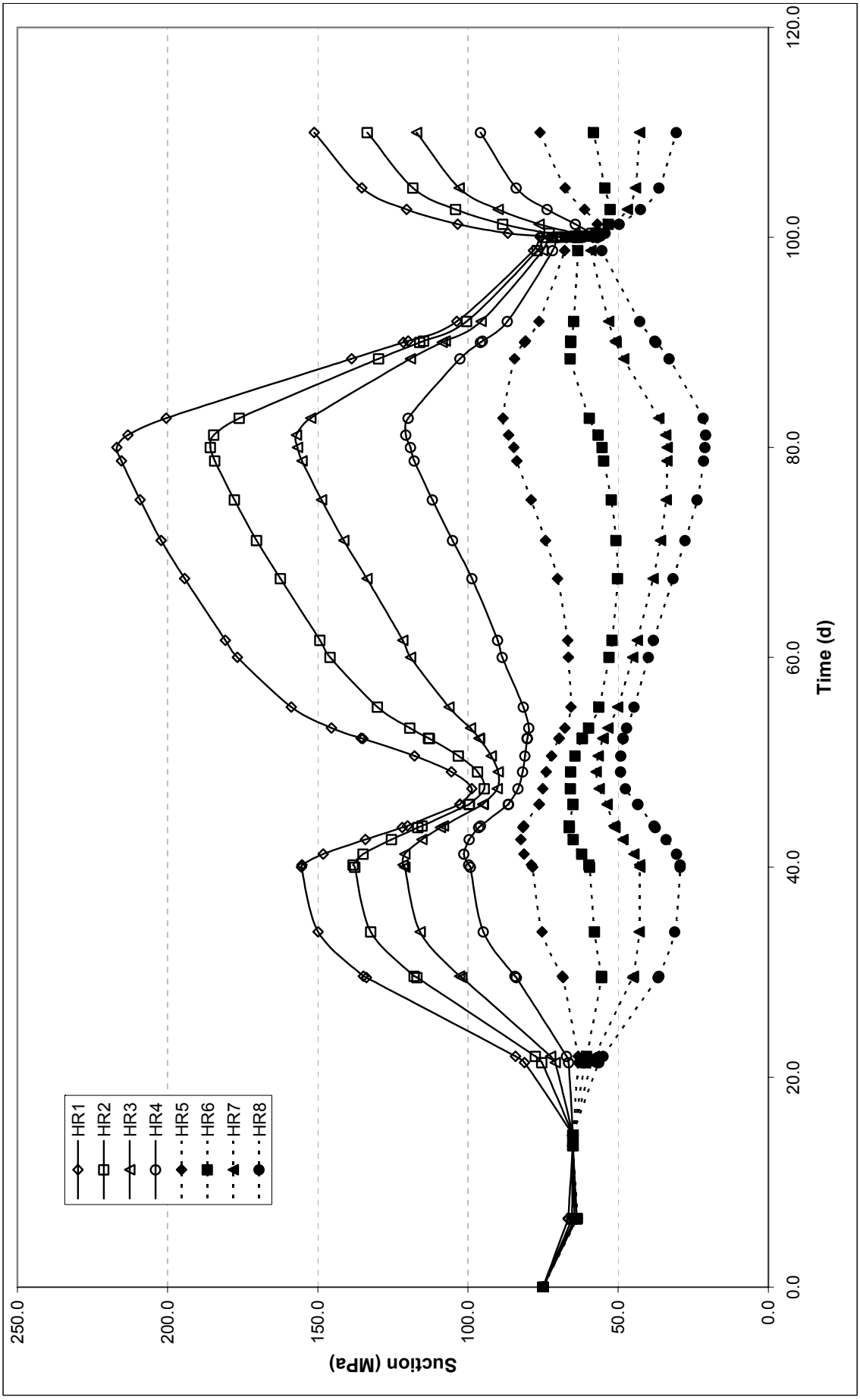
Suction (MPa)
250.0
200.0
150.0
100.0
50.0
0.0
Time (d)
0.0
20.0
40.0
60.0
80.0
100.0
120.0
HR1
HR2
HR3
HR4
HR5
HR6
HR7
HR8

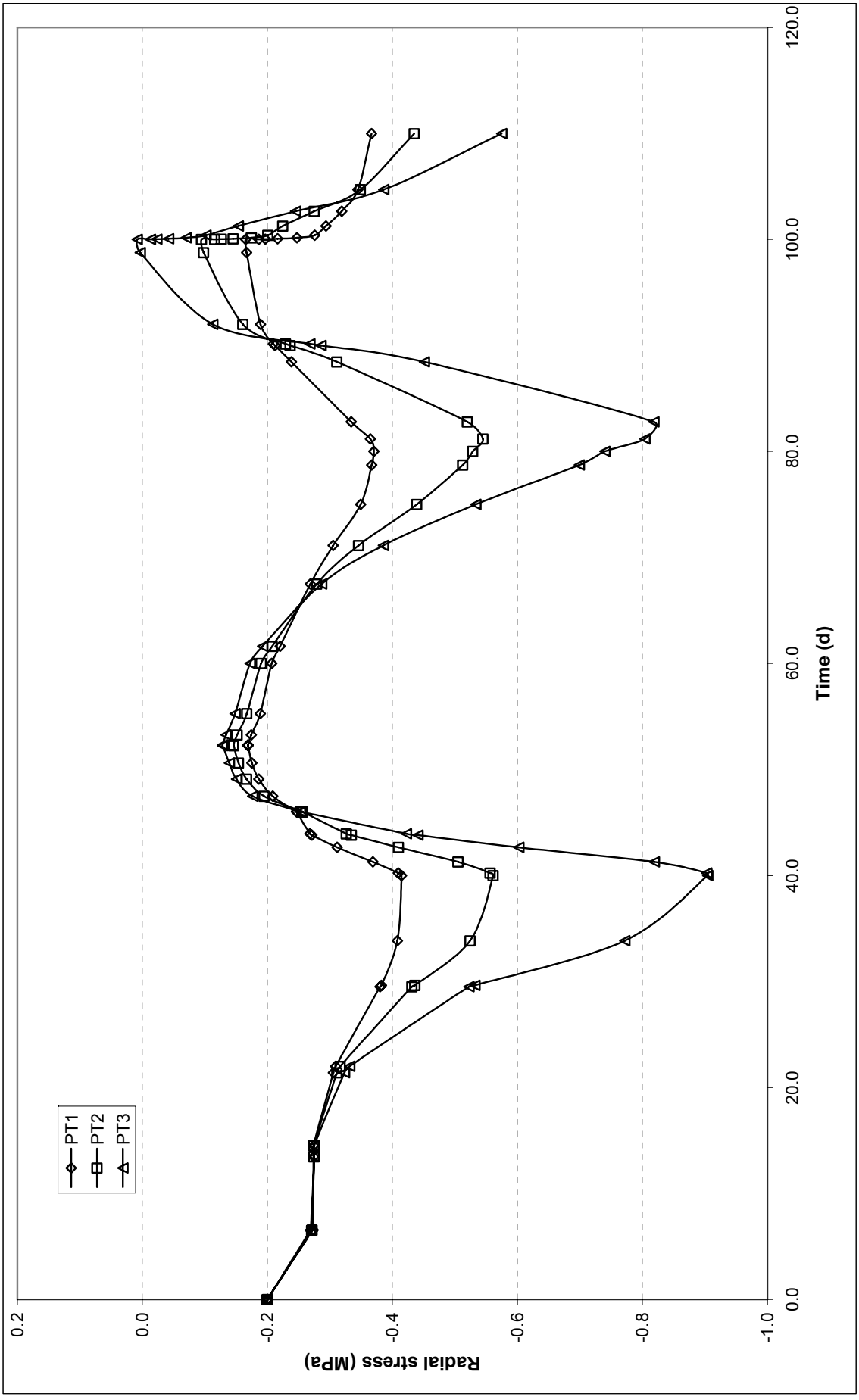
PT1
PT2
PT3
Radial stress (MPa)
0.2
0.0
-0.2
-0.4
-0.6
-0.8
-1.0
0.0
20.0
40.0
60.0
80.0
100.0
120.0
Time (d)

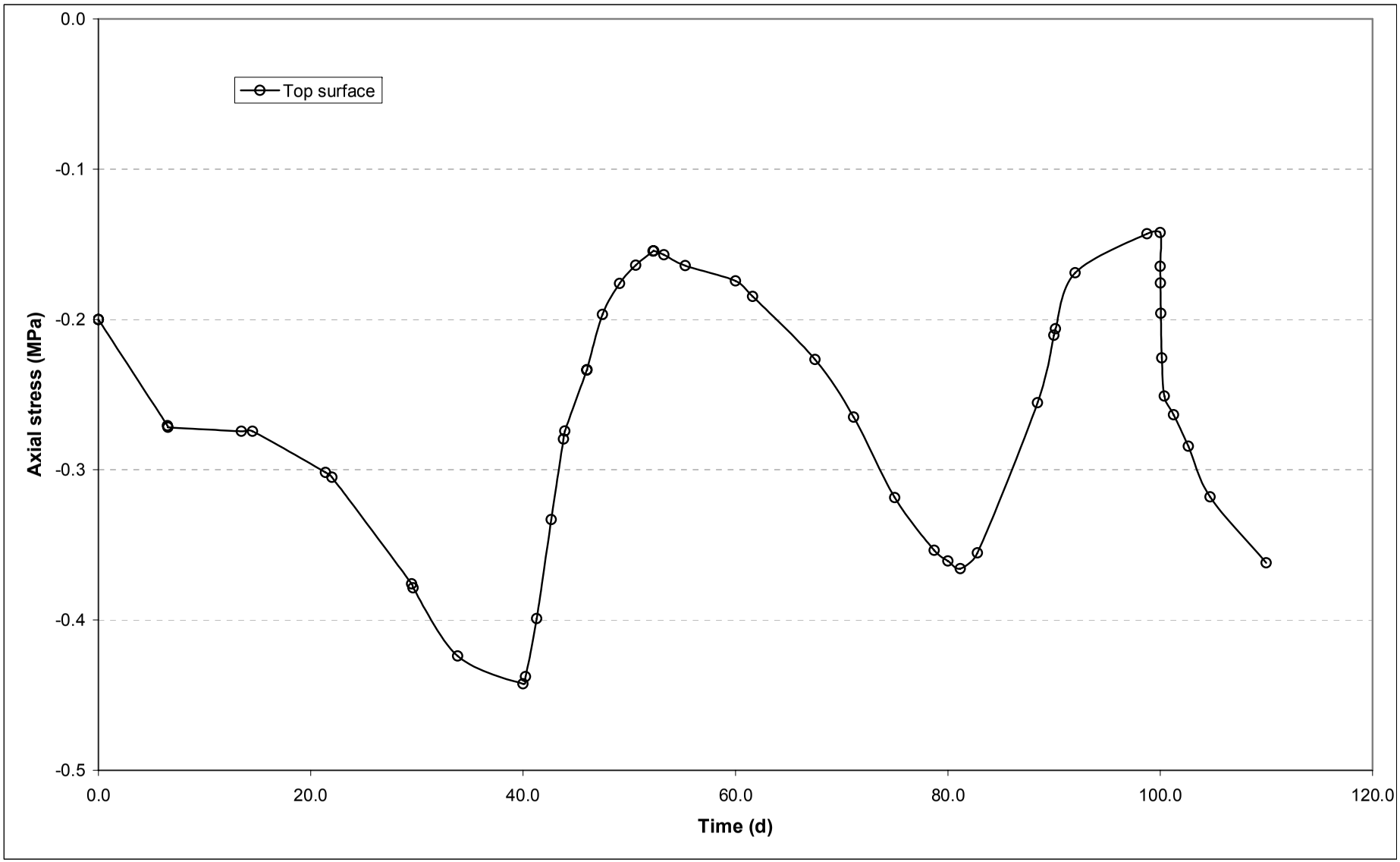
Top surface
Axial stress (MPa)
0.0
-0.1
-0.2
-0.3
-0.4
-0.5
0.0
20.0
40.0
60.0
80.0
100.0
120.0
Time (d)

TBT2_10 vs. TBT2_14

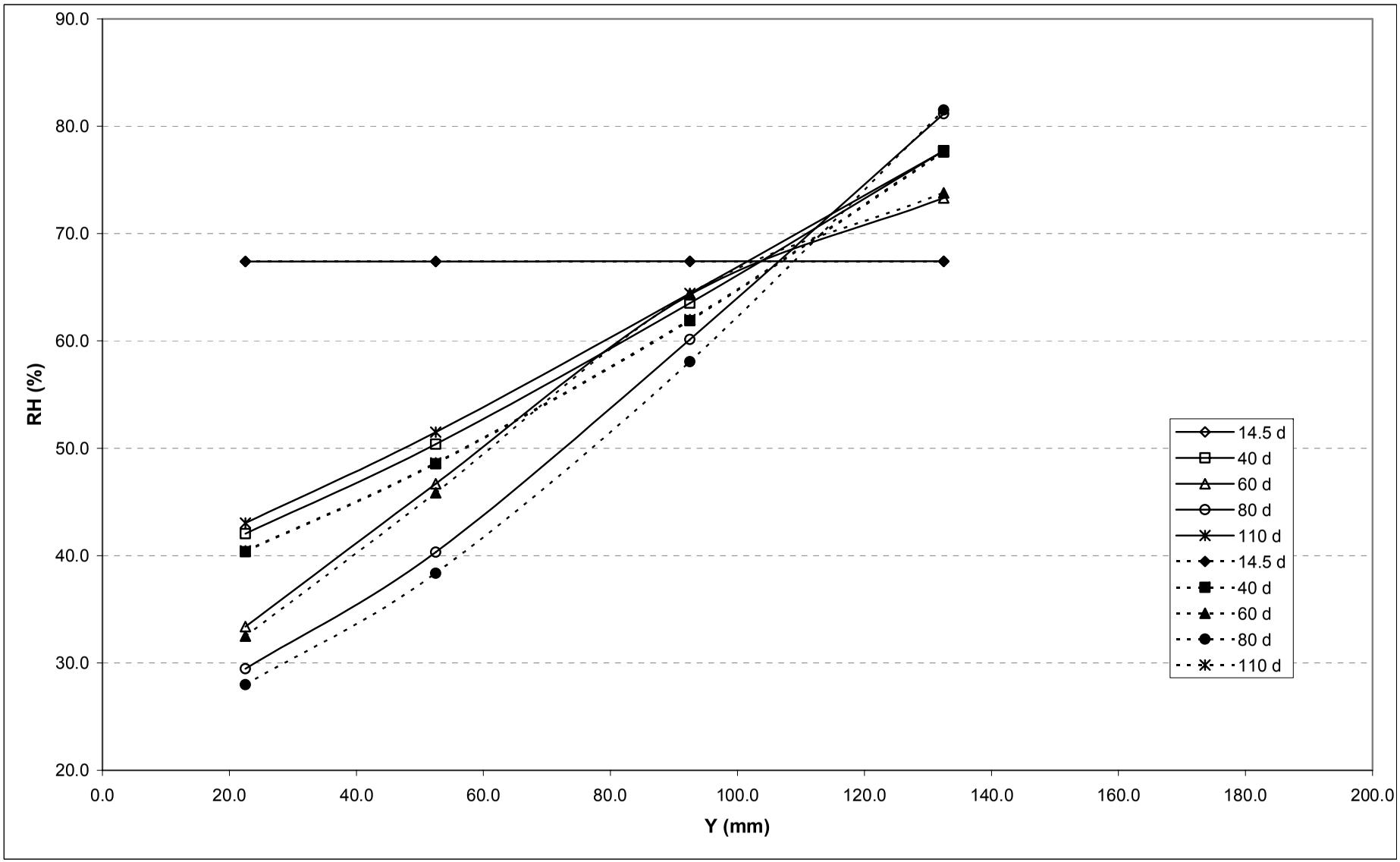
90.0
80.0
70.0
60.0
50.0
40.0
30.0
20.0
RH (%)
0.0
20.0
40.0
60.0
80.0
100.0
120.0
140.0
160.0
180.0
200.0
Y (mm)
14.5 d
40 d
60 d
80 d
110 d
14.5 d
40 d
60 d
80 d
110 d

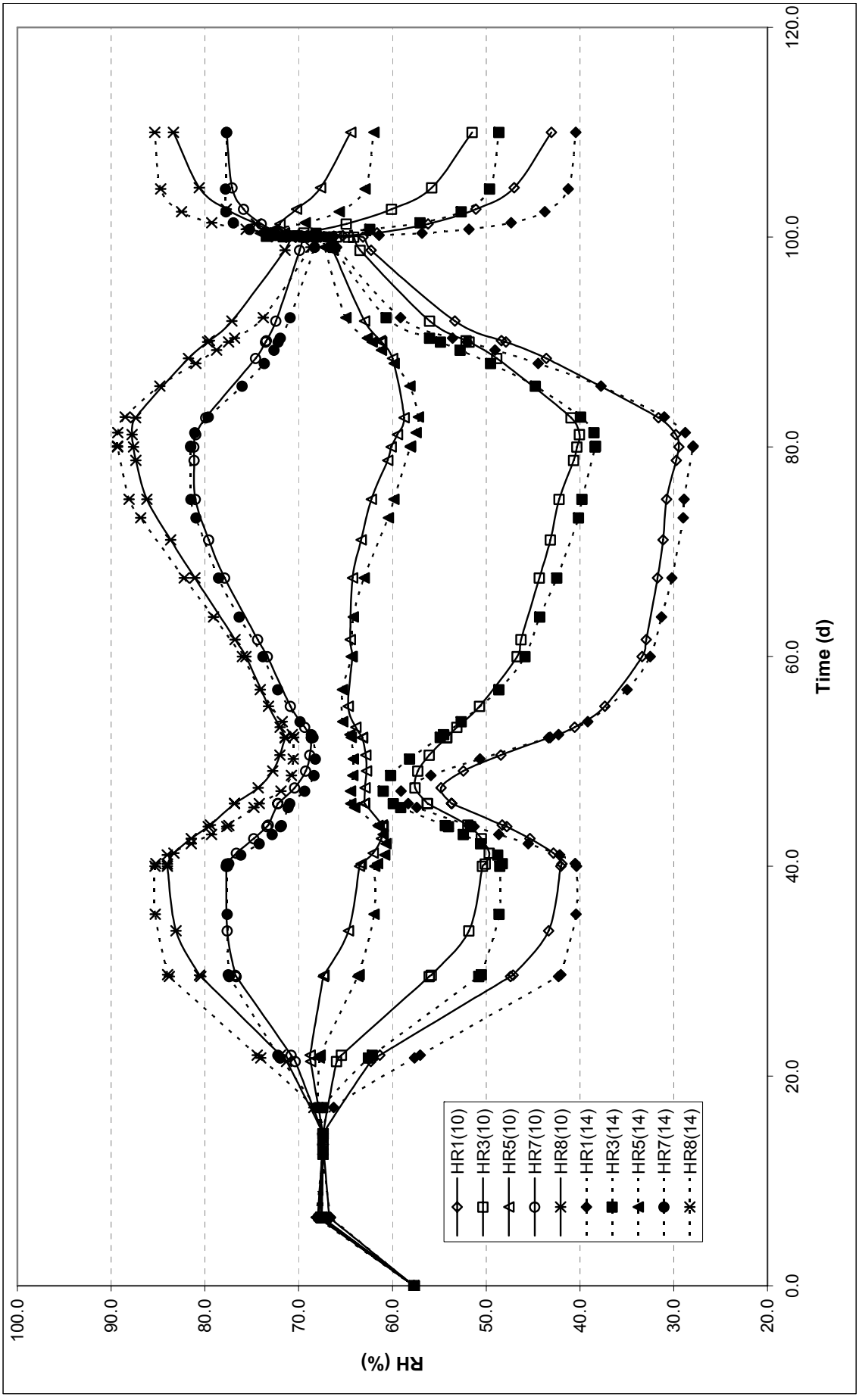
RH (%)
100.0
90.0
80.0
70.0
60.0
50.0
40.0
30.0
20.0
0.0
20.0
40.0
60.0
80.0
100.0
120.0
Time (d)
HR1(10)
HR3(10)
HR5(10)
HR7(10)
HR8(10)
HR1(14)
HR3(14)
HR5(14)
HR7(14)
HR8(14)

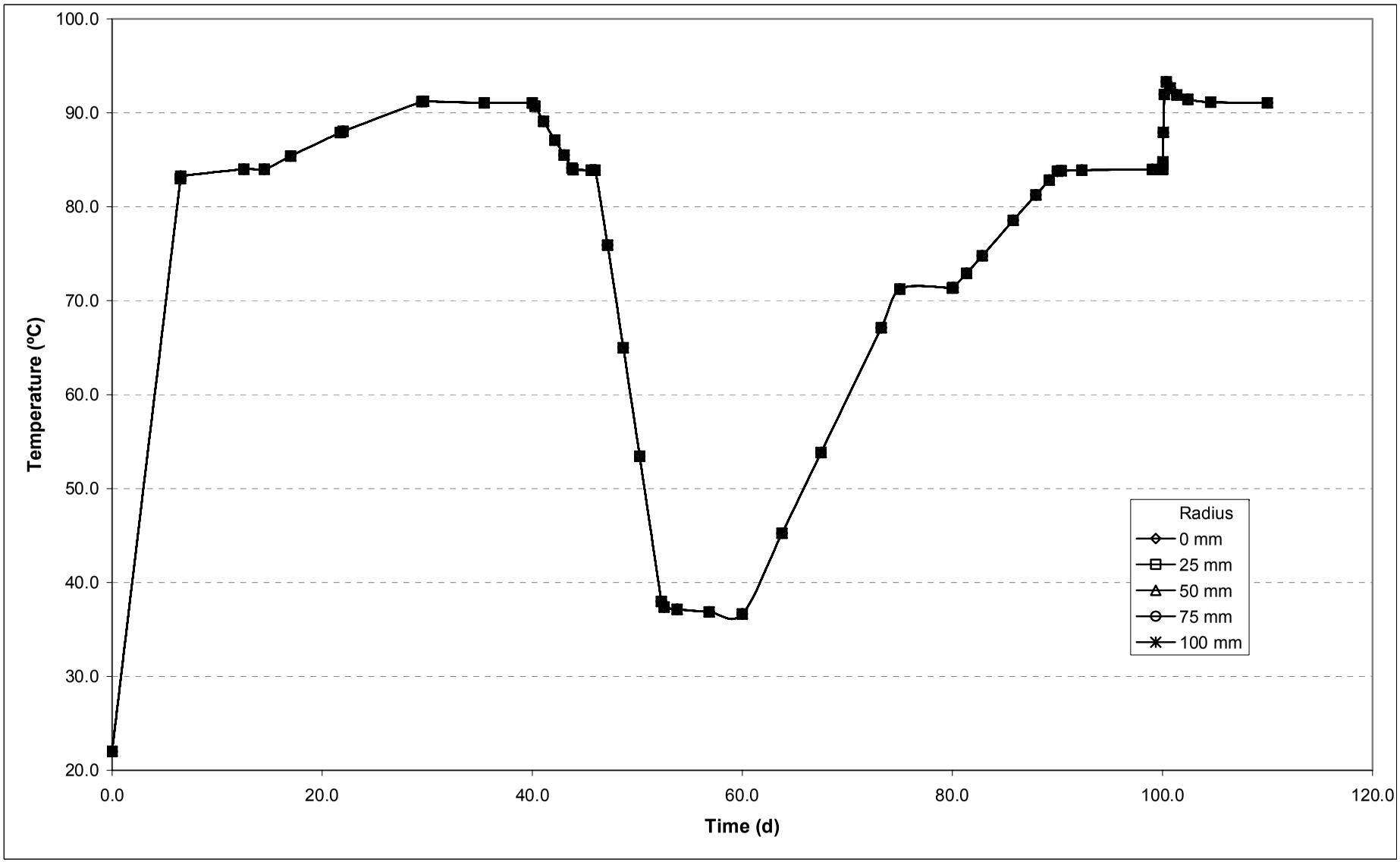
100.0
90.0
80.0
70.0
60.0
50.0
40.0
30.0
20.0
Temperature (ºC)
0.0
20.0
40.0
60.0
80.0
100.0
120.0
Time (d)
Radius
0 mm
25 mm
50 mm
75 mm
100 mm

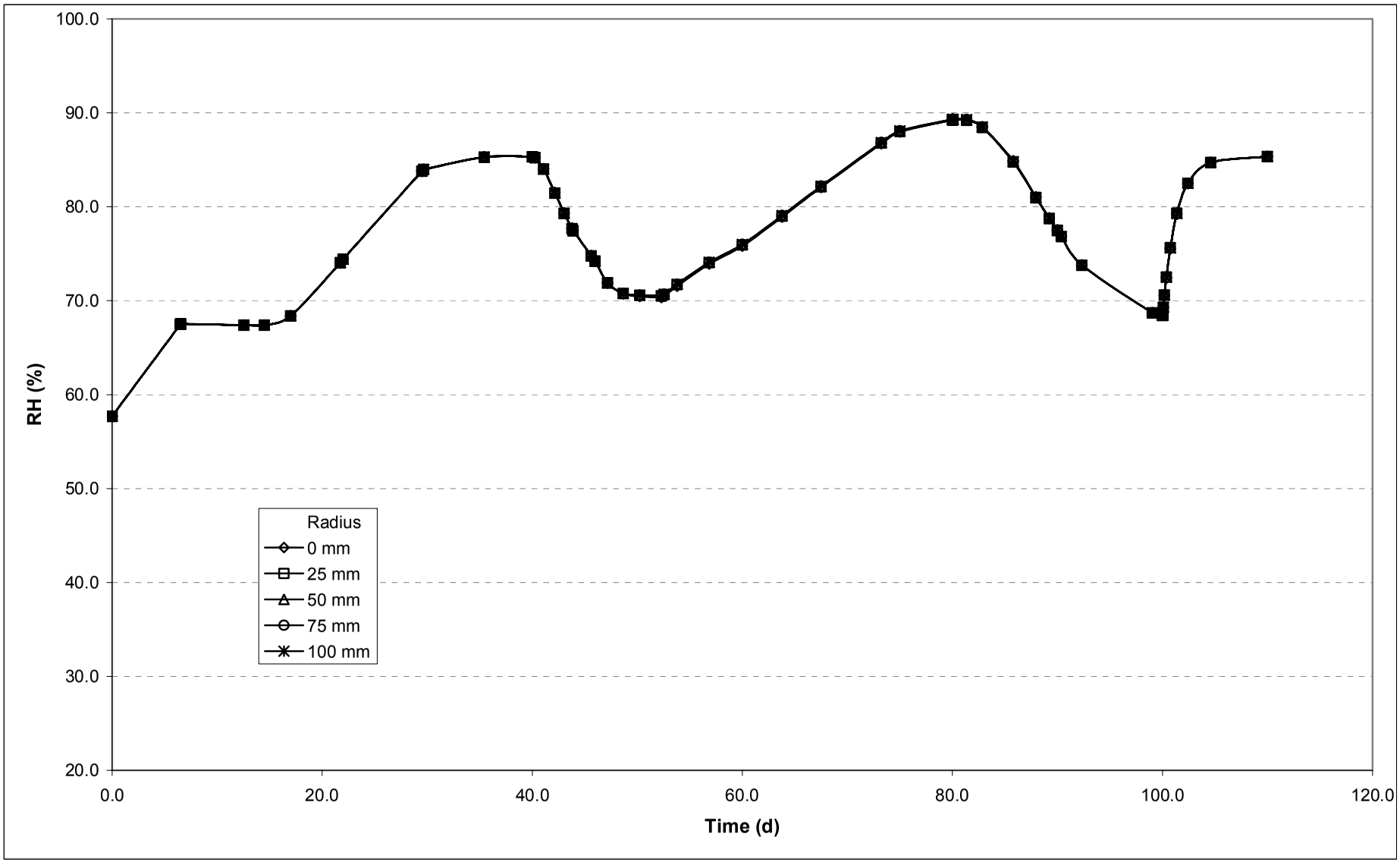
100.0
90.0
80.0
70.0
60.0
50.0
40.0
30.0
20.0
RH (%)
0.0
20.0
40.0
60.0
80.0
100.0
120.0
Time (d)
Radius
0 mm
25 mm
50 mm
75 mm
100 mm

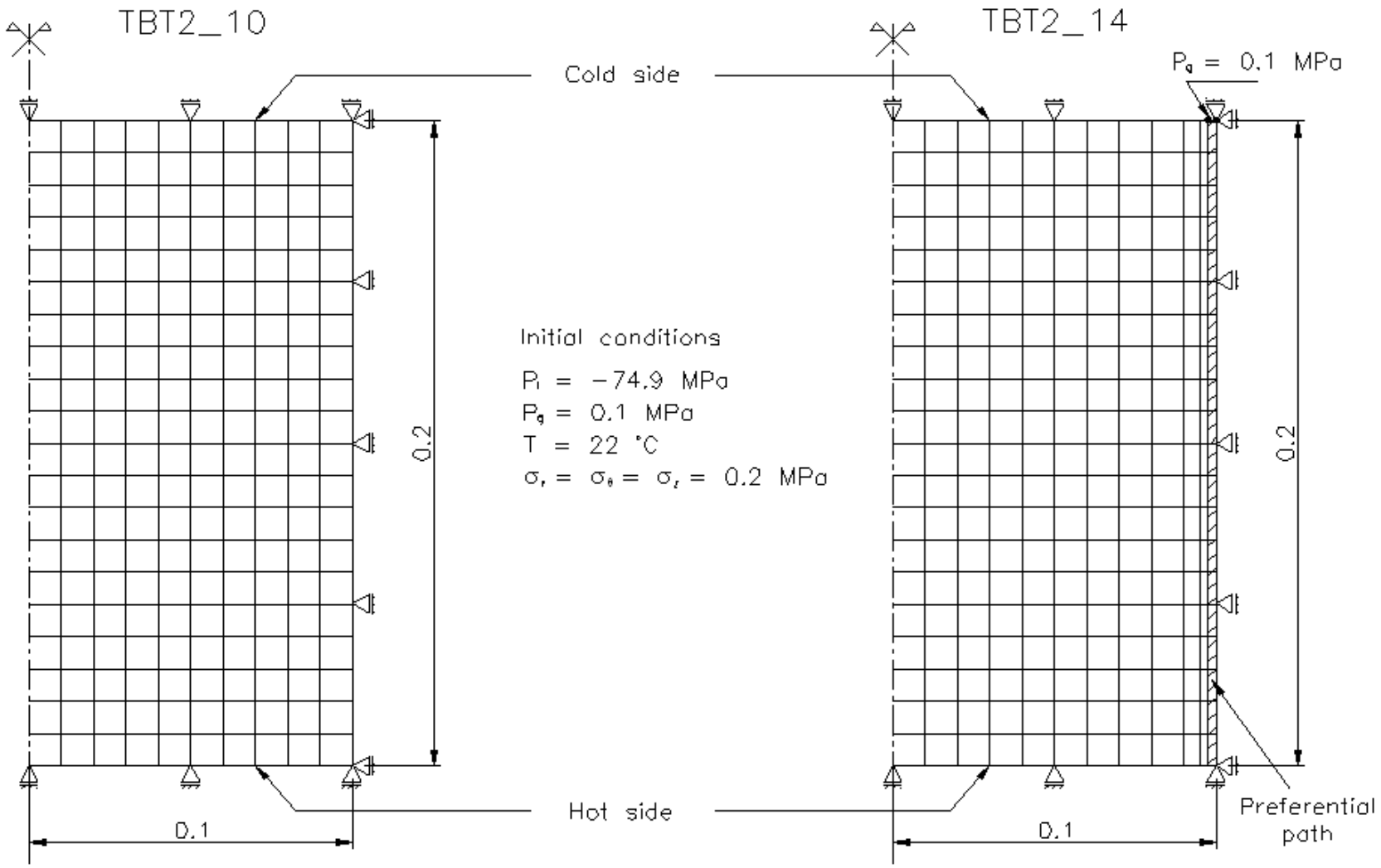
TBT2_10
TBT2_14
Cold side
Hot side
Initial conditions
P_l = −74.9 MPa
P_g = 0.1 MPa
T = 22 °C
$\sigma_r = \sigma_\theta = \sigma_z$ = 0.2 MPa
P_g = 0.1 MPa
0.2
0.2
0.1
0.1
Preferential path

Clay Technology AB

Ideon Research Center

Lund, Sweden

TBT_2 Mock-up predictions

June, 2005

Mattias Åkesson

Martin Birgersson

Harald Hökmark

Contents

1 Background

Within the framework of the TBT modeling task force, it has been decided to consider particularly the thermo-hydraulic conditions around the lower heater in the TBT test. In the field experiment, there was a significant and fast dehydration in an approximately 0.15 m wide annular zone around the heater /Goudarzi et al., 2005/. The temperature increased to just below 130 °C during the first 20 days. The temperature gradients were almost 4.5 °C/cm in the region where desaturation appeared to have taken place. Figure 1 shows measured temperatures and calculated thermal gradients at different distances from the heater axis.

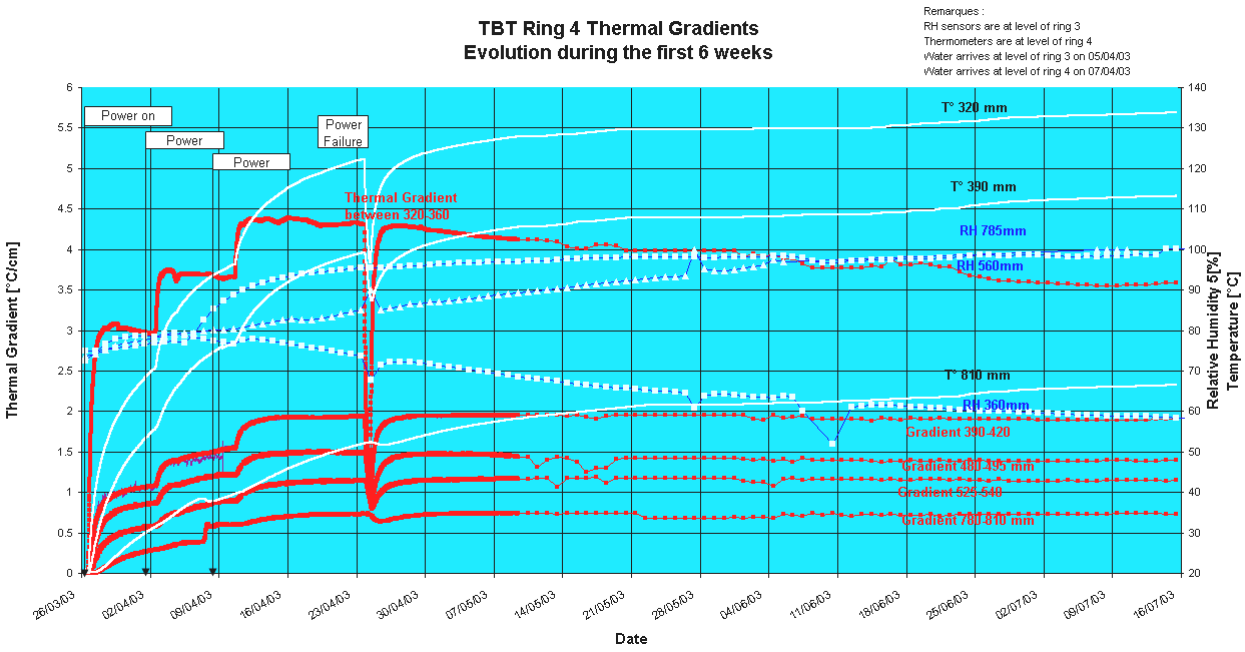

***Figure 1**. Temperatures and thermal gradients at different distances from the lower heater axis.*

The pattern of desaturation and the desaturation time-scale has raised the question whether the thermal gradient alone or the combination of high temperatures and high thermal gradients is responsible for the process. However, it is not possible to infer any such information directly from Figure 1. The high gradient close to the heater is partly an effect of the drying, and not the clear-cut cause of it. At some distance from the heater, there is no drying. This may well be an effect of moisture moving in from the regions close to the heater, rather than an indication of insufficient thermal gradients.

The approach decided by ANDRA and the TBT modeling teams is two-fold, with a lab-scale mock-up test combined with a predictive modeling task, and addresses the phenomenon of desaturation and the relative importance of temperature gradients and temperature levels.

2 TBT_2 Mock-up experiment

2.1 General

The mock-up test was planned and designed at the CEA laboratory in Paris, France. The basic idea is to subject a confined sample of MX80 bentonite material to thermal gradients similar to those around the lower heater in the TBT field experiment, and to monitor the development of temperatures, relative humidities and stresses during a well-defined sequence of thermal loading.

2.2 Experimental setup

The used cell is illustrated in Figure 2 and is composed of:

- A stainless steel cylinder
- A 17 mm thick PTFE lining cylinder for thermal insulation.
- A stainless steel fixed base with temperature control
- A moving piston with temperature control
- An isostatically compacted ortho-cylindrical MX80 bentonite sample of 200 mm height and diameter.

The initial cell temperature is equal to ambient temperature, approximately 20 °C.

The cell is instrumented with sensors for measurements of temperature, relative humidity, pore-water pressure, radial pressure and the axial vertical stress.

2.3 Thermal protocol

The thermal loading is divided in three phases: a nominal, an optional and a transient phase. In the nominal phase, a thermal gradient is gradually increased from zero to a maximum of 1.8°C/cm. The protocol for the optional phase aims at establishing a 3°C/cm gradient in the sample, then at elevating temperature keeping the thermal gradient constant. Finally, in the transient phase, a gradient identical to the final gradient in the nominal phase is established momentarily (see Figure 3). If desaturation is detected during either one of the phases, the test is stopped at the end of that phase.

A detailed scheme is presented in Figure 3. It should be noted though, that small protocol changes may be necessary due to practicalities, such as visual temperature control during certain cooling periods.

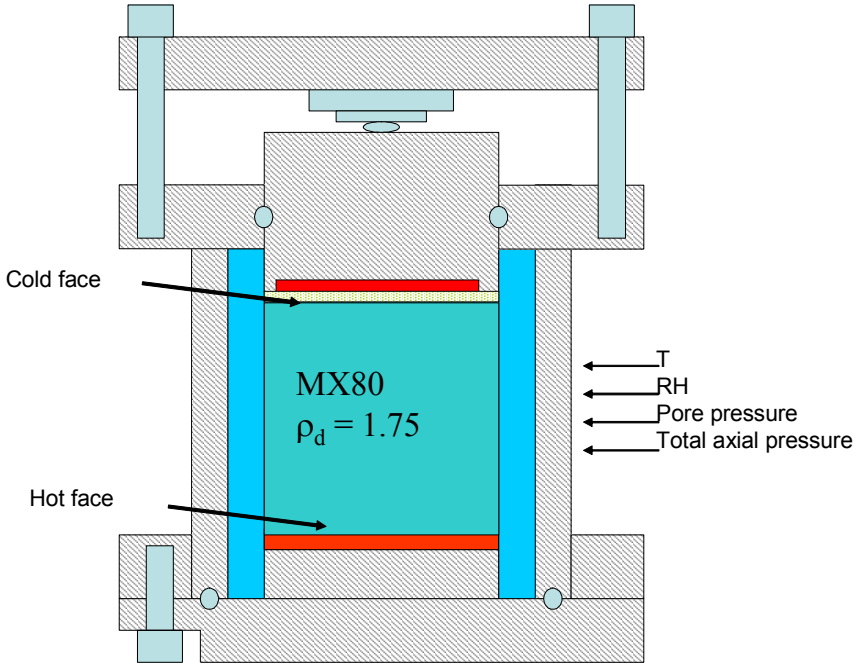

***Figure 2**. Diagram of the TBT_2 Mock-up*

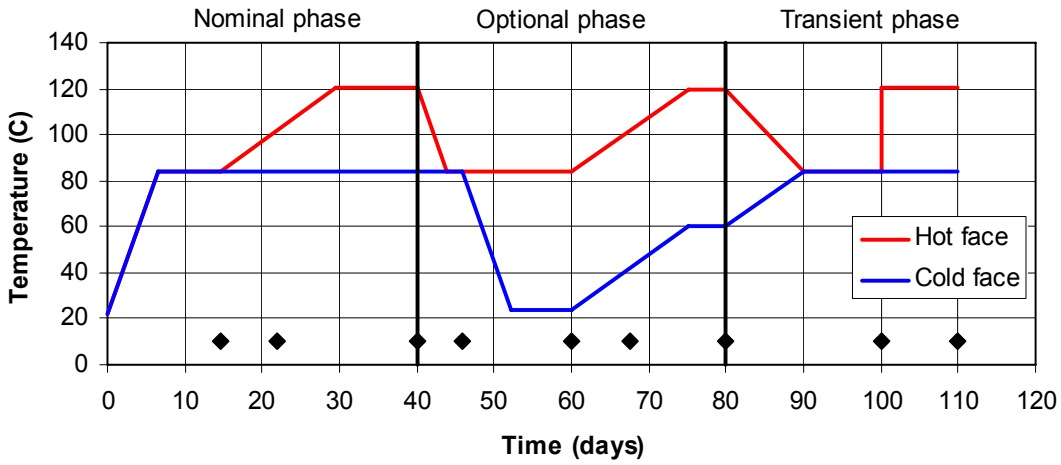

***Figure 3.** Thermal protocol for planned phases. Modeling results are requested for events marked with ♦.*

3 Predictive modeling

3.1 Introductory remarks

The current modeling task is focused on the phenomenon of desaturation and on the thermo-hydrodynamic processes, and follows the modeling guidelines issued April 2005 /Åkesson and Hökmark, 2005/. One important mechanical feature described below is the special description of MX80 during shrinkage. Otherwise no attempts have been made to modify the description of the mechanical properties given in the guidelines.

During the course of the work, an analytical solution of steady-state conditions has come to our attention. This solution provides new insights into the current problem regarding the role of temperature gradients and temperature levels. The approach and its implication for the current problem are described in the final chapter of this report.

It should also be mentioned that attempts were made to improve the material model through evaluation of a previous mock-up test, reported by Gatabin and Billaud /2005/. This work will be included in the final version of this report.

3.2 Model description

The approach chosen for the current task is a "best guess" modeling exercise, as suggested in the modeling program. The modeling work was performed with the finite element program Code_Bright version 2.2.

Table 1. Parameters and constitutive laws defining the problem.

Initial Saturation level	S_{ini} = 57	%
Initial water ratio	w_{ini} = 12	%
Dry density	ρ_{dry} = 1.75	g/cm^3
Solid phase density	ρ_s = 2.78	g/cm^3
Porosity	ϕ = 0.37	-
Void ratio	e = 0.59	-
Intrinsic permeability (isotropic)	k = 1.6 10^{-21}	m^2
Liquid relative permeability	$k_r = S_r^3$	-
Gas phase relative permeability	$k_{rg} = 10^8(1-S_r)^4$	-
Solid state specific heat	C_s = 800	J/(kg·K)
Heat conductivity	$\lambda = 0.3\cdot(1-S_r) + 1.2\cdot S_r$	W/(m·K)
Tortuosity for vapor diffusion	τ = 0.3	-
Extended van Genuchten model:		
P_0	42 MPa	MPa
λ	0.3	-
P_m	402	MPa
λ_m (not fitted)	1	-
σ_0 (not fitted)	0.072	N/m

Since all models considered here have appeared to predict substantial desaturation already during the nominal phase, we have only covered the first two phases (nominal and optional). The relevant (hydrodynamic and thermal) model parameters and constitutive laws are summarized in Table 1.

The following comments can be made regarding the chosen parameter values.

3.2.1 Solid phase density

The parameter values describing the experimental setup presume a density of the solid phase of 2.64 g/cm^3. We have chosen to adjust this value to the commonly used ρ_s =2.78 g/cm^3 (/Hökmark and Fälth, 2002/, Table 1) by allowing the initial saturation level to change accordingly (from 62% to 57%).

3.2.2 Retention curve parameters

Parameters for the extended van Genuchten model /CIMNE, 2000/ of the retention curve were estimated from experimental RH vs. water mass ratio data /Dueck, 2004/. These data series, corresponding respectively to an initial water mass ratio of 8 and 17.5%, were linearly interpolated to the present value of w=12%. Furthermore, a non-linear least square fit of the model parameters was made to this data giving the estimates presented in Table 1. The retention curve is shown in Figure 4 together with the experimental data.

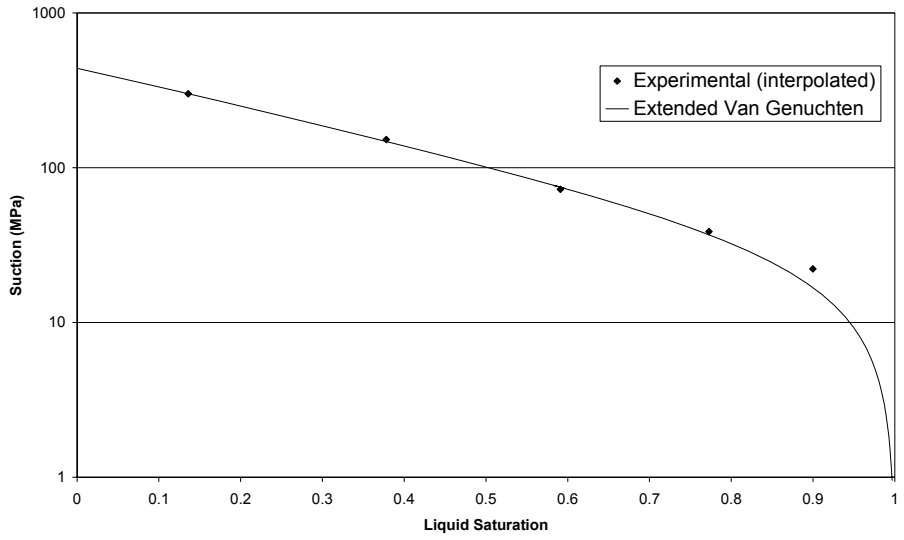

Figure 4. *The fitted extended Van Genuchten retention curve and experimental points interpolated to an initial water ratio of 12%. The experimental point with the highest saturation value was not included in the fitting procedure.*

3.2.3 Vapor diffusion

The Code_Bright default expressions was used for the vapor diffusion coefficient:

$$D = (1-S_r)\, D_{vapor}, \quad (3\text{-}1)$$

where

$$D_{vapor} = \tau \cdot 5.9 \cdot 10^{-6} \cdot (T+273)^{2.3} / P_g, \quad (3\text{-}2)$$

P_g is the gas pressure and T the temperature. The tortuosity factor, τ, was determined by calibration calculations using experimental data by Gatabin and Billaud /2005/.

3.2.4 Intrinsic permeabilities

The intrinsic permeability was set in accordance to experimental data relating it to porosity, as described in the modeling program.

3.2.5 Other parameters

The rest of the parameters and constitutive laws describing the bentonite were taken to be identical with those found in the evaluation modeling of the TBT experiment /Fälth and Hökmark, 2004/.

3.2.6 Model geometry

The only material explicitly considered in the model is the bentonite, with mechanical confinement being handled by mechanical boundary conditions. The calculations are performed in a 2-dimensional radial symmetric cylindrical system as displayed in figure 5a. The model is divided into a lower and an upper part where the mechanical material properties differ due to the fact that the clay is losing water (shrinking) in the lower part and gaining water in the upper during the course of the thermal protocol execution. In order to model cases where possible preferential escape paths are formed at the circumference of the cylinder during the progression of the experiment, additional systems were considered where the material properties was altered in the outermost 5 mm shell of the cylinder. The motive for these attempts is described in section 3.4.2.

3.2.7 Boundary conditions

Modeling was performed both with a completely isolated effectively 1-dimensional system (no gas or liquid was allowed to escape) as well as with a system where gas was allowed to escape at the top of the cylinder. The latter system was accomplished by imposing a boundary condition of atmospheric gas pressure (0.1 MPa) at a 5 mm circumference on top of the cylinder (figure 5b). On the remaining boundaries (the vertical boundaries and the lower base) gas flux was completely prohibited in all models considered. Hydraulically, all boundaries were closed.

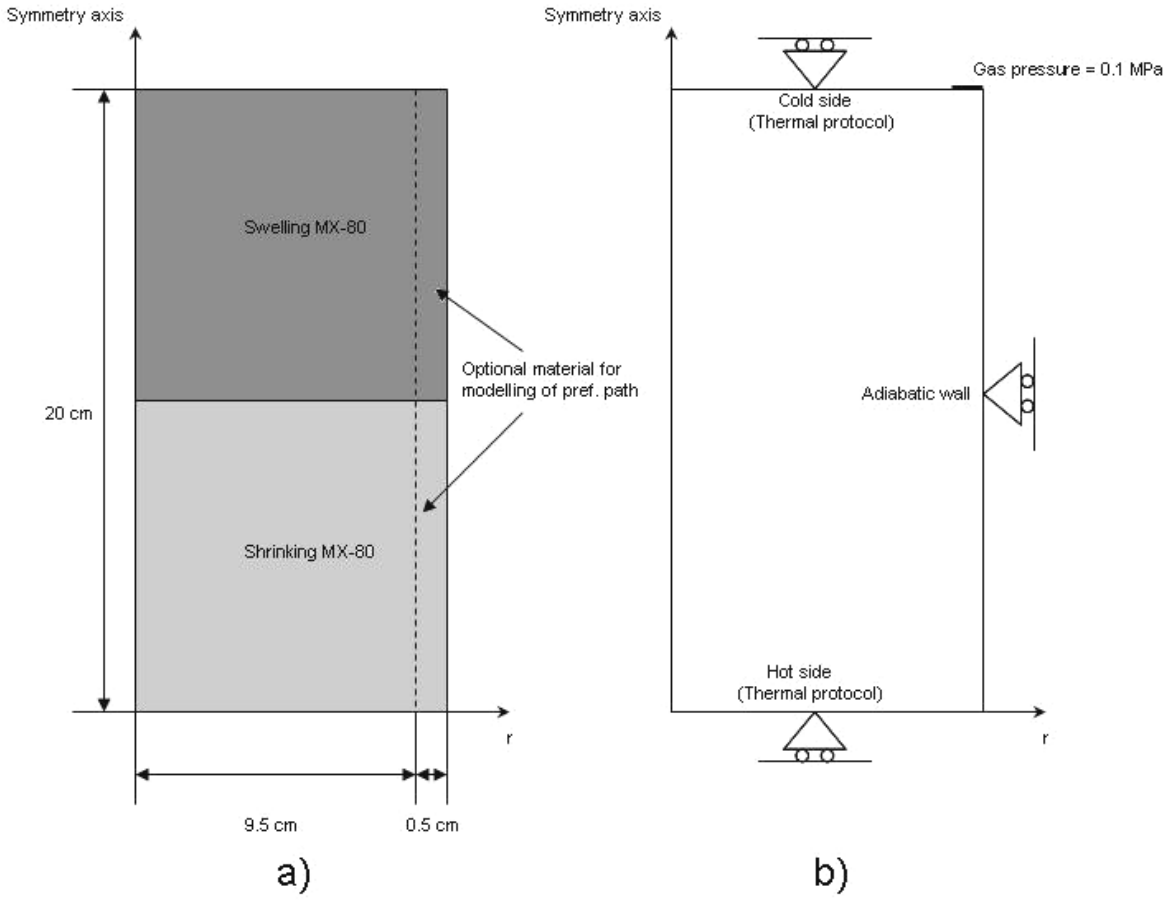

Figure 5: *The model geometry (a) and boundary conditions (b)*

The heating of the sample was modeled using time-dependent temperature boundary conditions on the top and bottom boundaries as described in the modeling program (c.f. Fig. 3). The vertical boundaries were adiabatic. The heating procedure is divided into two phases - the nominal phase (day 0-40) and the optional phase (day 40-80).

All boundaries were roller boundaries, i.e. mechanically fixed in the normal direction.

3.2.8 Choice of a base case model

The various models give different saturation profiles. In figure 6 the progression of the level of desaturation in four models is plotted as a function of time. As a measure of desaturation, or redistribution, we have here chosen the difference between the minimum and maximum value of liquid saturation along the symmetry axis.

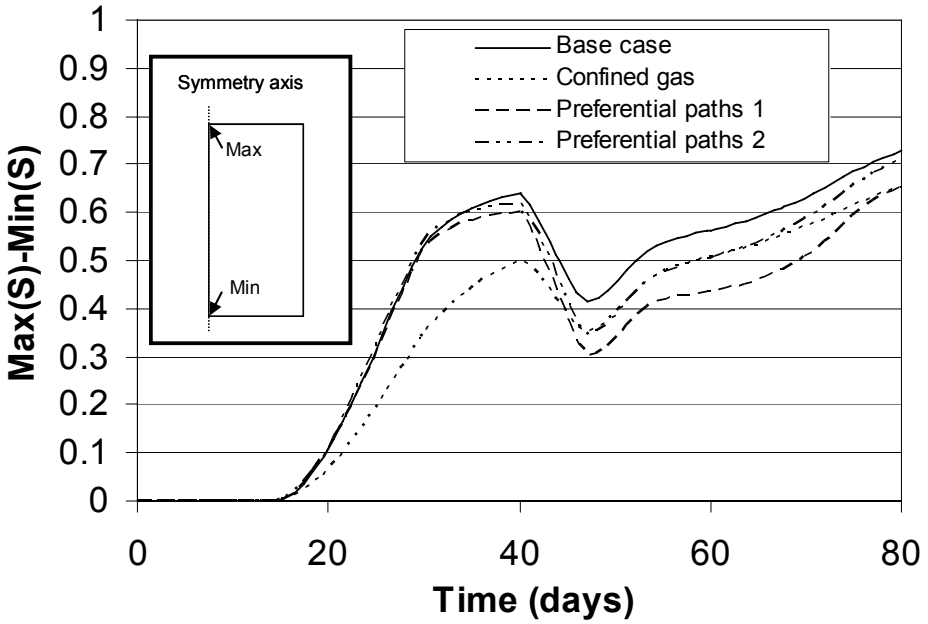

Figure 6. *The evolution of the level of desaturation for various models in the nominal and optional phase. The base case corresponds to a cylindrical specimen with an atmospheric pressure boundary condition, "Confined gas" is a completely isolated model and the models labeled "Preferential paths" are models with a gas pressure boundary and an increased intrinsic permeability within a 5 mm thick circumference to mimic preferential escape paths. The inserted picture shows where the points of highest and lowest liquid saturation are located in the specimen.*

The model labeled "Confined gas" does not allow any gas to escape, which will cause the gas pressure to rise in the cylinder during heating. A higher gas pressure will reduce vapor diffusion from the hotter to the colder part of the cylinder and thereby reduce the level of desaturation. The other models pictured in figure 6 are all exposed to the atmospheric gas pressure boundary described above. The models labeled "Preferential paths" has a higher intrinsic permeability of a factor 100 in the pathway material. This will cause the advective liquid mass flux from hotter to colder parts to increase which in turn will give less desaturation. The effect could be seen already at the end of the nominal phase (day 40) but is more pronounced at the beginning of the optional phase where the temperature gradient becomes smaller and the oppositely directed vapor transport diminishes. The model labeled "Preferential paths 2" has a lowered retention curve (P_0=0.42 MPa) at the lower half of the high-permeability pathway part of the model.

The model chosen as our base case, on which we will focus the following discussion, is the one with uniform material properties, i.e. without particular pathway materials. This choice is made because none of the alternatives tried here gave significantly different results as far as the scan-line predictions are concerned. Although this system in principle is a 2 dimensional model, all calculated properties basically show no variation in the radial direction. Thus, effectively the base case behaves as a 1-dimensional system.

3.2.9 Mechanical processes

Elastic parameters for the thermoelastoplastic constitutive laws are shown in Table 3. Different values are defined for different domains depending on whether swelling or shrinking is expected. The lower half of the experiment that will undergo desaturation is modeled with parameter values valid for shrinking, while the upper half is set for swelling. This type of distinction has appeared to be necessary in order to capture the fundamentally different behavior during drying and wetting, respectively.

Such a division can nevertheless be executed with more or less details. For instance, the temperature is increased during the first 14.5 days of the experiment without subjecting the sample to a temperature gradient. This will induce a certain suction increase throughout the sample during this period, which in turn will lead to a build-up of stresses throughout the sample, if the whole sample is modeled as swelling. This stress level will remain throughout the calculation, even if the parameter setting for the lower part is changed to those defined for shrinking. Such a remaining stress level at the lower part appears to be of limited credibility, although a homogenous but limited stress build-up can be expected during the initial heating period. The lower part was therefore set for shrinking already from the start.

No yield surface was applied since the deviatoric stresses were fairly limited, as least in the swelling domain with decreasing suction levels.

The initial stresses were set to 0.5 MPa (compression) in all three directions.

Table 2. Elastic parameters for swelling and shrinking domain.

Mode	κ_{i0}	κ_{s0}	α_i	α_{ss}	α_{sp}	p_{ref} (MPa)	v	K_{min} (MPa)
Swelling	0.25	0.28	-0.0129	0	-0.17	0.1	0.2	10
Shrinking	0.008	0.16	0	-0.04	0	0	0.2	10

3.3 Results

The scan-lines are shown in Figure 7. The levels of liquid saturation along the symmetry axis of the cylinder at the times defined in the modeling program are pictured in Figure 8. The corresponding temperature profiles are pictured in Figure 9. Calculated radial stresses along the circumferential boundary are shown in Figure 10, while corresponding axial stresses at the upper boundary are shown in Figure 11.

Since the model in practice represents a 1D-problem, no results are shown for scan-line #2 at the height corresponding to the RH-sensor specifically installed at the circumference. The results along this line can be read from Figures 8 and 9 (at height 0.154 m).

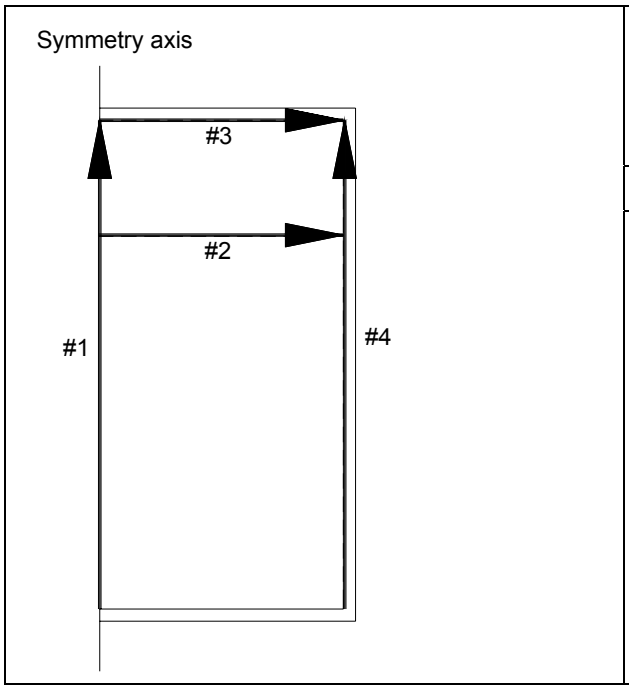

Scan-lines:

#1	#2	#3	#4
T, RH	T, RH	σ_A	σ_R

Figure 7. *Scan-lines.*

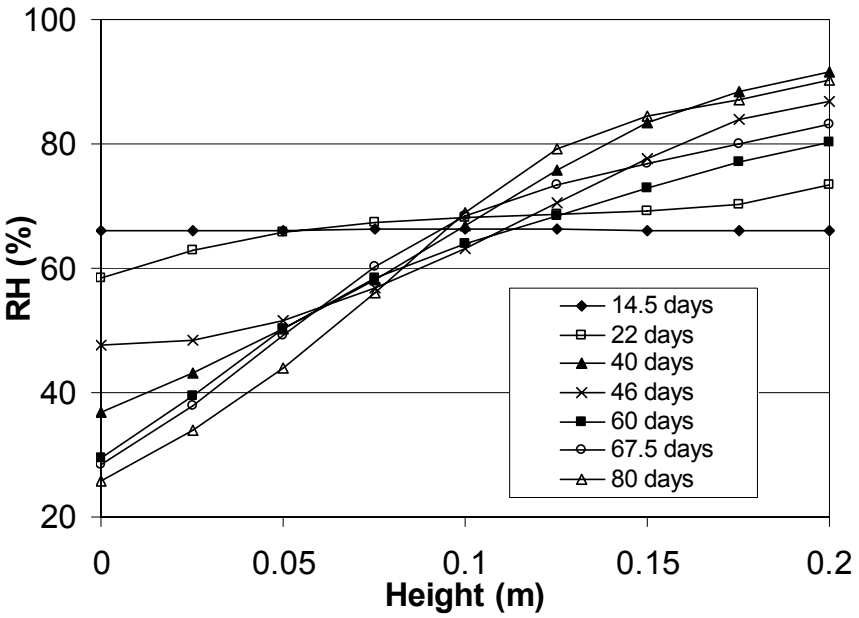

Figure 8. *RH-profiles along the symmetry line of the sample cylinder at the requested time points (nominal and optional phase). Scan-line #1.*

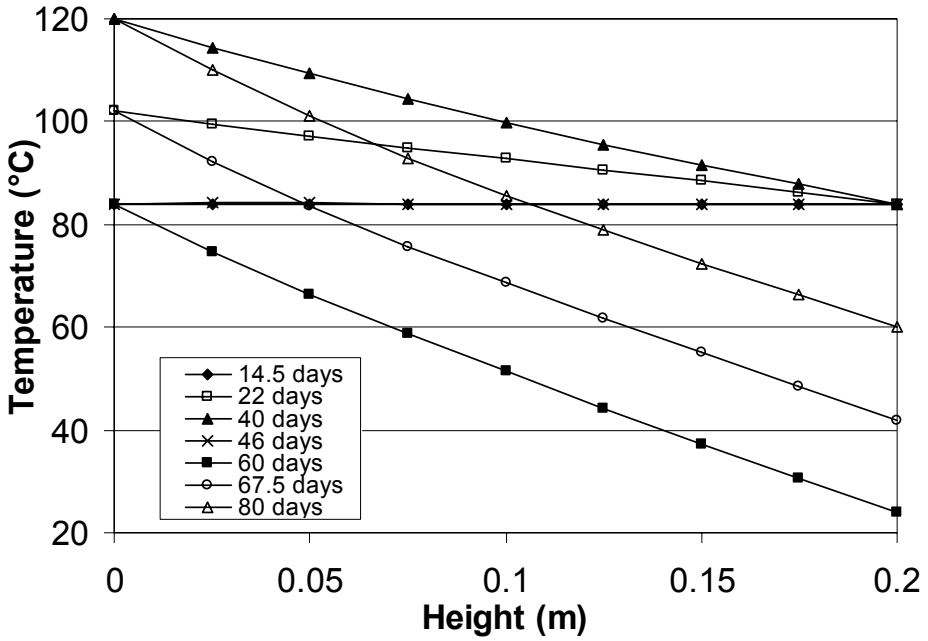

Figure 9. *Temperature profiles along the symmetry line. Scan-line #1.*

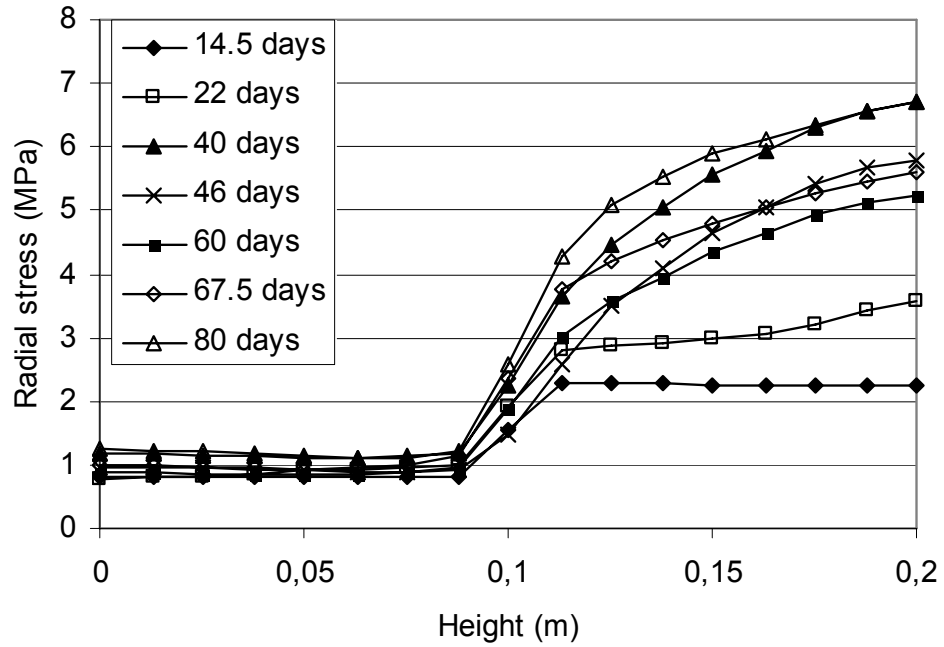

Figure 10. *Radial stresses along circumferential boundary. Scan-line #4. The initial stress offset at sample mid-height is due to the different representation of swelling and shrinking material. c.f. section 3.2.9.*

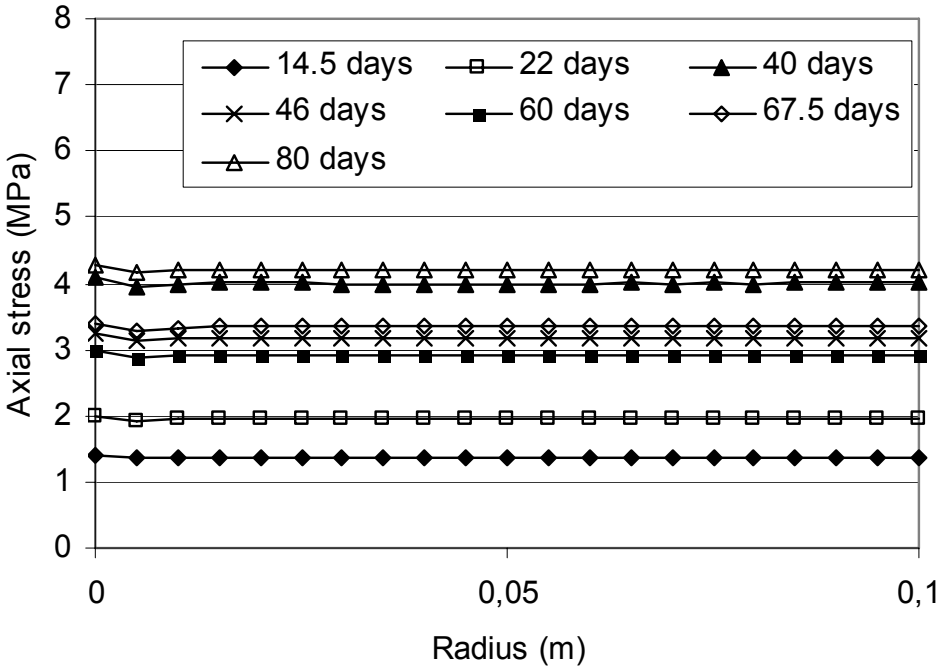

Figure 11. *Axial stresses along the upper boundary. Scan-line #3.*

3.4 Modeling results - discussion

3.4.1 Desaturation

The results indicate that there will be extensive moisture redistribution during the 40 days included in the nominal phase. The redistribution started as soon as the thermal gradient was imposed at day 15 and increased almost linearly with the increasing gradient between day 15 and day 30, as shown in Figure 12. Between day 30 and day 40, the temperature gradient was fixed at 1.8 °C/cm, with continued but less rapid desaturation. At the end of this 10-day period, the system seemed to be approaching steady-state conditions. The slopes of arrows #1 through #4 in Figure 12 indicate the rate of dehydration at the hot end during periods of increasing (#1, #3) and constant (#2, #4) thermal gradients, and allow for the following straightforward observations:

- The highest rates are found when the gradient increases (arrows #1 and #3). These rates are approximately equal, although there are differences in temperature level and in the rate of gradient increase.

- Arrows #2 and #4 show the desaturation rate during periods of constant thermal gradients. The rate given by #4 is a little higher, although the temperature is lower, at least in the beginning just after day 45. There are no signs of temperature dependence of the dehydration rate.

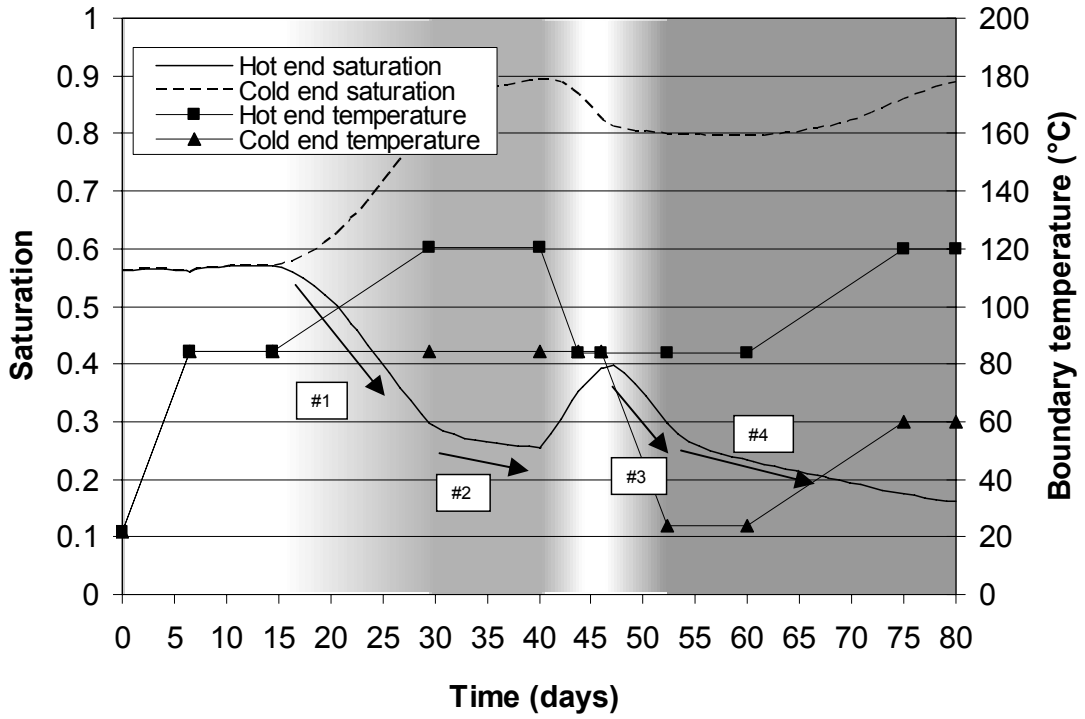

***Figure 12**. Degree of saturation at the hot and cold ends as function of time. The grey-scale indicates the thermal gradient. Arrows 1 and 3 indicate rate of desaturation at the hot end during stages of increasing thermal gradient. Arrows 2 and 4 indicate constant gradient stages.*

The modeling results do not support the notion of gradient thresholds. This is a consequence of how the laws of vapor transport and liquid water transport are formulated in Code_Bright. Modifying the parameter values shown in Table 1 may change the extent and the time-scale of the dehydration process, but qualitatively the results would be the same. In previous TBT modeling work, there has been a tendency to over-predict vapor transport and dehydration. In the present study, parameter values used previously for some of the properties of MX80 bentonite have been modified (updated retention models and more accurately calibrated vapor tortuosity values).

The modeling of the optional phase (day 40 – day 80) was conducted for the sake of completeness, even though dehydration was found already in the nominal phase. Fair comparisons are difficult to make because the point of departure (regarding moisture distribution) of the optional phase is different from that of the nominal phase. However, the following can be observed:

- The desaturation rate during the time of increasing gradient was approximately the same for both phases although the temperature was lower in the optional phase.
- The increase in temperature between day 60 and day 75 did not seem to have much influence on the desaturation rate.

3.4.2 Stresses

Modeling of mechanical processes in this type of experiment is less straightforward than in tests with low thermal load and with continues water uptake to saturated conditions. The previous mock-up test /Gatabin and Billaud, 2005/ could therefore provide useful information to the present modeling task. The recorded stresses in the previous test showed however some irregular characteristics in that the axial stresses exceeded the radial stresses in the upper part. These observations lead to an idea about condensation at the circumference due to preferential paths and radial strains in the upper part. During the modeling work though, two arguments has appeared that questions such a view. The first thing is the difficulty to model a condensation process predominating at the circumference. The second thing was the information that the transmission from the radial pressure sensors in the previous test had been questioned. The idea about radial strains was therefore abandoned. The radial stresses in the upper part of the current experiment were therefore expected to exceed the axial stresses.

The calculated build-up of stresses should be considered as qualitative, since the current formulation of thermoelastoplastic constitutive laws has certain limitations. For instance, the general distribution of radial stresses, with the highest values at the top, and the notion that these surpass the axial stresses, appears to be quite reliable. The actual values should however be regarded as a rough estimate.

3.4.3 Relevance – boundary conditions

The numerical Code_Bright model did not include any components other than the bentonite sample itself. The confinement, i.e. the steel cylinder and the PFTE lining were regarded as perfectly stiff, while in reality thermally induced deformations of the cell will have caused some disturbance to the stress evolution. Approximate and preliminary analyses of the steel/PFTE system show that these disturbances probably are very minor. The axial thermal expansion of the steel cylinder may be about 0.5 mm. Because of the properties of the PFTE lining, the inner diameter will be reduced by about the same amount. This means that changes of the net porosity, if any, are small.

The experiment is not run under gas-tight conditions. There will probably be gas leaks between different parts of the steel assembly and possibly along cables and sensors. In the numerical model, a small portion of the top boundary close the cell edge was kept at atmospheric gas pressure to account for possible gas escape. There is no firm justification for this particular gas boundary approach. For the assumptions made here (in the Code_Bright model) regarding gas phase permeability, this gas escape route turned out to be sufficient to keep the gas pressure within the bentonite sample very close to atmospheric. The model was tested also assuming perfect gas confinement (c.f. Fig. 6), which gave gas pressures of about two atmospheres within the sample, but very small effects on the evolution of the moisture redistribution. If the gas permeability were much lower, then the gas pressure would choke the vapor transport and reduce the moisture redistribution. The experimental results now available of gas flow in bentonite confirm however that the high relative permeability values used here are relevant (see e.g. /Alonso and Alcoverro, 2003/). In addition, in the TBT field experiment, increased gas pressures are not recorded anywhere. Therefore, as far as moisture redistribution is concerned, the treatment of gas and gas escape seems to be relevant, i.e. there are no reasonably realistic gas boundary conditions and gas permeability assumptions (other than, possibly, gas leaks in the hot region at the bottom of the cylinder) that could change the results in any significant way.

4 General remarks on the desaturation process

4.1 Analytical solution of steady-state conditions

Claesson and Sällfors (2005) have recently derived a coordinate independent relation between the liquid saturation level and the temperature for a 1-dimensional isolated system at steady-state conditions. Translated into the notation used in Code_Bright, the relation is expressed as:

$$\frac{dS}{dT} = -\frac{K_T(S,T)}{K_S(S,T)}, \tag{4-1}$$

where

$$K_T(S,T) = n \cdot (1-S) \cdot \tau \cdot D(T) \cdot \frac{\partial \rho_v}{\partial T} \tag{4-2}$$

and

$$K_S(S,T) = \left[\frac{\rho_w \cdot k_r(S) \cdot \bar{k}}{\mu(T)} + n \cdot (1-S) \cdot \tau \cdot D(T) \cdot \frac{\partial \rho_v}{\partial p_l} \right] \cdot \frac{dp_l}{dS}. \tag{4-3}$$

Here τ is the tortousity coefficient for the diffusive vapor transport, *D(T)* the temperature-dependent diffusion coefficient and *n* denotes the porosity. ρ_v and ρ_w are the density of the water vapor and liquid water, respectively. Furthermore, k_r and $\bar{k}$ are the relative (water phase) and intrinsic permeabilities, μ is the dynamic viscosity while p_l denotes the liquid pressure.

Solution of Equation 4-1 gives the steady-state saturation as a function of temperature. Assuming a linear relationship between temperature and the spatial coordinate of the system (which in our case is the dimension along the symmetry axis of a cylinder) the saturation profile is a simple scale transformation of the *S(T)*-curve at steady state conditions. From this fact we infer that many characteristic features of the saturation profile (especially the minimum and maximum values) cannot depend on the actual slope of the temperature profile, but only on the absolute values of the temperature at the endpoints.

Equation 4-1 is an initial value problem. In practice the initial value $S(T_0)$ cannot be known. The relevant solution is the one for which the total amount of water corresponds to the initial amount of water contained in the sample. Examples of solutions for different assumptions of the initial water content are shown in Figure 13. The actual calculation can be performed in any advanced mathematical spreadsheet.

Of course, the temperature profile contains nonlinear features to some degree, due to the fact that the heat conductivity depends on the level of saturation. However, here these effects are small, as demonstrated in Figure 9. Neglecting them should only have a minor effect on the saturation profiles (the error is of the order of the size of the second derivative of the temperature profile).

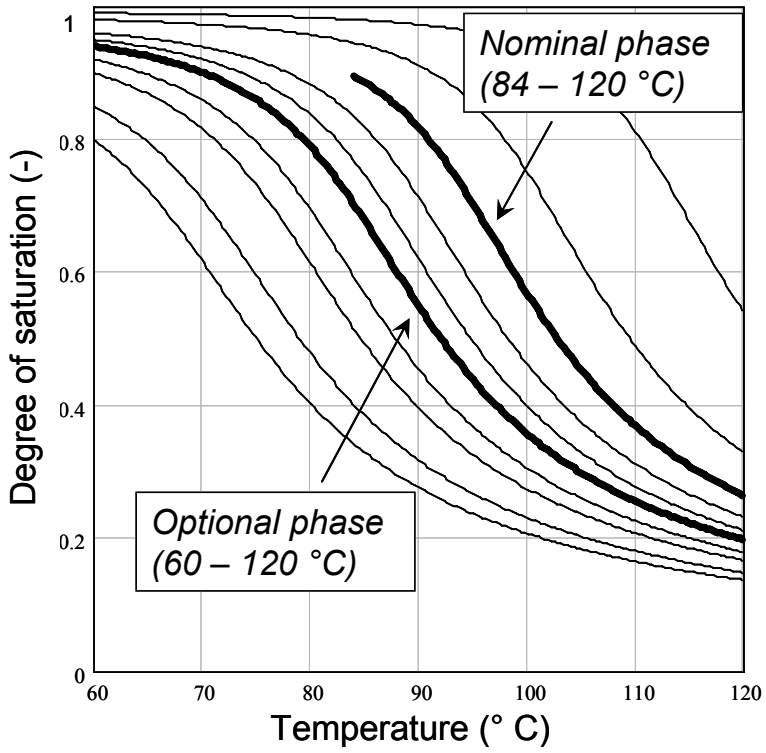

Figure 13. *Solutions of the differential equation 4-1. Applied parameter values and marked distributions correspond to the current mock-up test.*

4.2 Test of method

In order to illustrate the steady-state characteristics of the desaturation, and specifically to show that only the end-point temperatures influence the shape of the saturation profile (except for the obvious scaling), two cylindrical Code_Bright models of MX-80 were analyzed. One model was 5 cm in height and the other 20 cm. Apart from the different sizes, the two models were made identical.

In order to get strictly linear temperature profiles, the heat conductivity was set to a constant value in the two samples. The same time-dependent temperature boundary conditions were used in the two models, giving a four times larger temperature gradient in the shorter sample.

The temperature on the lower base was raised from 20 ºC to 110 ºC in steps. The steps were 10 ºC between 20 ºC and 100 ºC and 5 ºC between 100 ºC and 110 ºC. The upper side of the cylinder was kept at 20 ºC at all times. After the final temperature was established at the lower end of the cylinder (after 41 days), the boundary temperatures were kept constant for a long time (109 days) in order to reach steady-state behavior.

The levels of desaturation as a function of time are pictured in Figure 14. We see that during the first part of the heating procedure, the desaturation is much more pronounced in the shorter specimen, but as the heating proceeds the level of desaturation for the longer specimen gets closer and eventually coincides with the 5 cm-curve at the end of the time period. Thus, the transient behavior of the short sample is much faster than for the longer one, where steady-state behavior is not reached until the end of the

calculation. The complete saturation profiles after 150 days are found in Figure 15, where the coincidence of the two curves confirms that the temperature gradient does not influence the steady-state saturation.

By recalculating the saturations profiles with the constant heat conductivity replaced by the usual linear saturation-conductivity model (Table 1), we will get an estimate of the influence of the nonlinearity of the temperature profiles. The result of these calculations is also found in Figure 14 and 15.

From Figure 15 the following can be concluded:

- The Code_Bright results verified the analytical solution (c.f. constant conductivity cases).
- Also for non-constant heat conductivity assumptions, the temperatures at the end-points rather than the thermal gradient determined the shape of the saturation profile.

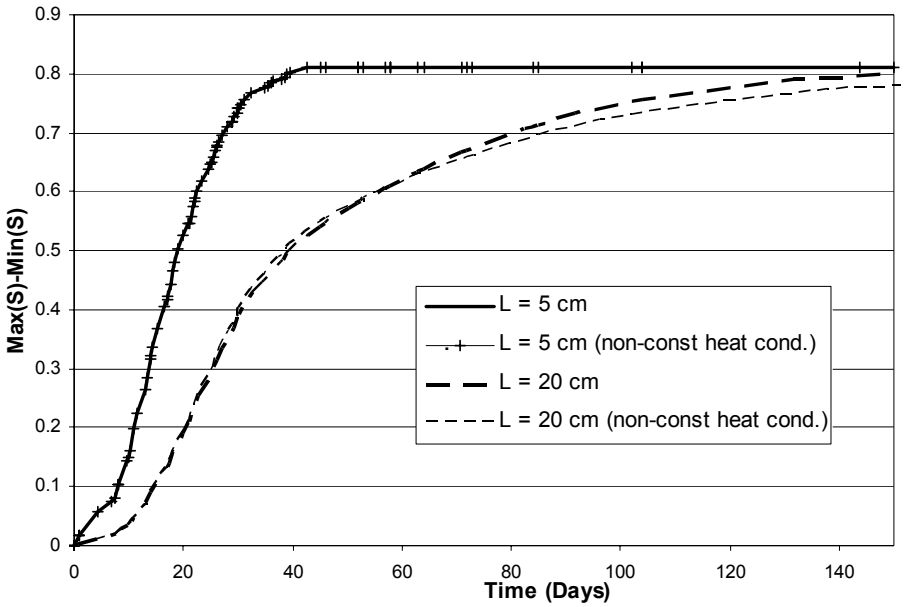

Figure 14. *Desaturation as a function of time for the short and long sample modeled with Code_Bright. The temperature increase is interrupted at day 41 at 110 °C and thereafter the temperature is held constant.*

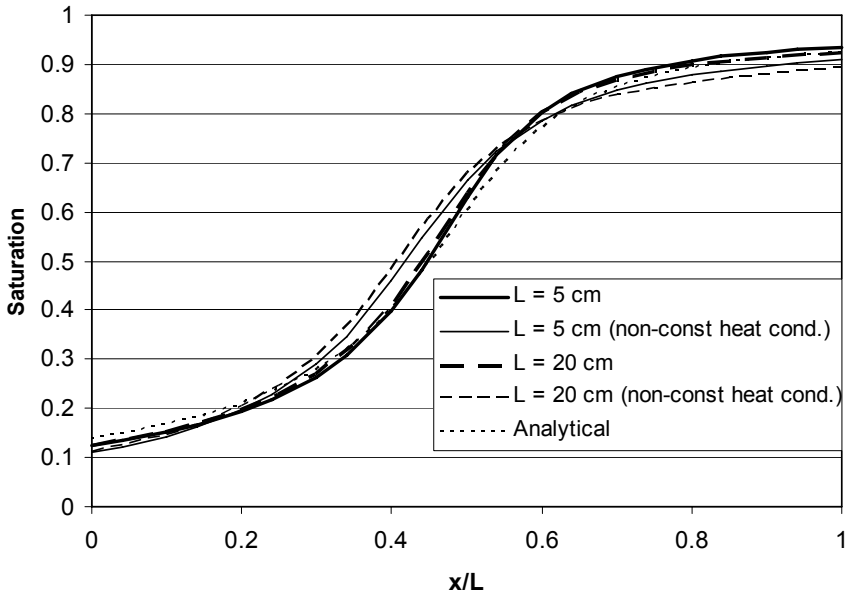

Figure 15. *Liquid saturation profiles at day 150 for the two samples with or without an assumption of constant heat conductivity. The corresponding analytical solution at steady state is plotted as well (assuming a linear temperature profile).*

5 Final remarks

5.1 Gradients

The current models of the TH processes, used in Code_Bright and in the analytical solution described in Chapter 4 do not support the notion of thermal threshold gradients. Moisture redistribution takes place as soon as there are thermal gradients. As far as long-term effects are concerned, the difference in temperature between the hot and cold ends, rather than the gradient determines the extent of desaturation at the hot end. This was demonstrated here both by use of Code_Bright modeling results and by use of the independent analytical solution.

5.2 Temperatures

For the Code_Bright model geometry and the assumption made regarding gas escape and gas permeability, the temperature level was found to have some influence, but not a decisive one. Figure 16a show normalized vapor/liquid transport coefficient ratios as a function of temperature for a number of saturation assumptions. The ratios are normalized such that Sr = 0.3 gives a ratio of 1 at 20 °C. Increasing the temperature from 20 ºC to 120 ºC means lower ratios, i.e. the effects of viscosity reductions overshadow the effects of the built-in dependence on temperature of the vapor diffusivity (Eq. 3-1).

Figure 16b shows the ratios as function of saturation for a number of temperature assumptions.

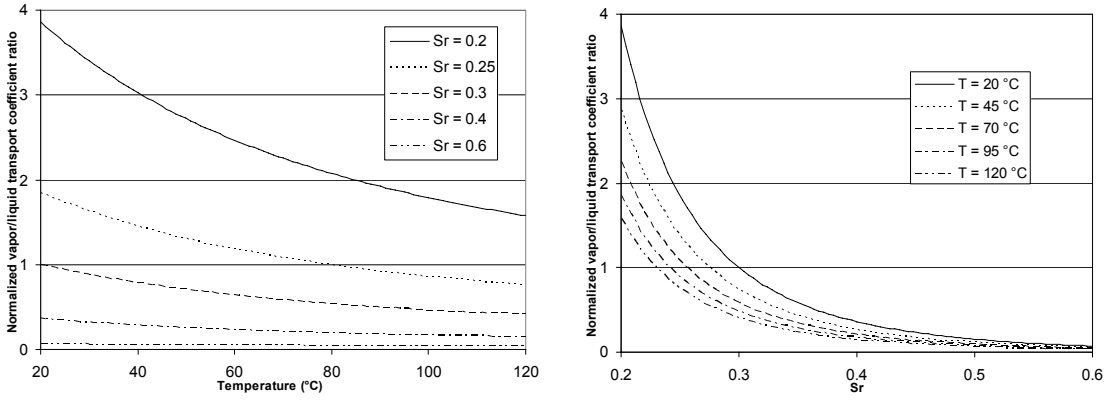

Figure 16. *The ratio is normalized so that it equals 1 at S_r=0.3 and T=20ºC*

Increasing the temperature makes liquid transport, relatively seen, more efficient than the vapor transport. This does not mean that the extent of desaturation at the hot end will be smaller at high temperatures. The gradient of the potential that drives vapor flow, i.e. the vapor mass fraction gradient, will be higher at high temperature because of the increased vapor production, while the suction gradient that drives the liquid flow is not equally sensitive to temperature changes. The net effect is that the desaturation will

be promoted by increasing temperatures, despite decreasing vapor/liquid transport coefficient ratios. Figure 17 shows analytically calculated steady-state saturation profiles for two cases with the same initial saturation and with 60°C difference between the end temperatures. The case with the higher temperature level gives a hot end saturation of about 15% and the low temperature case gives about 20%.

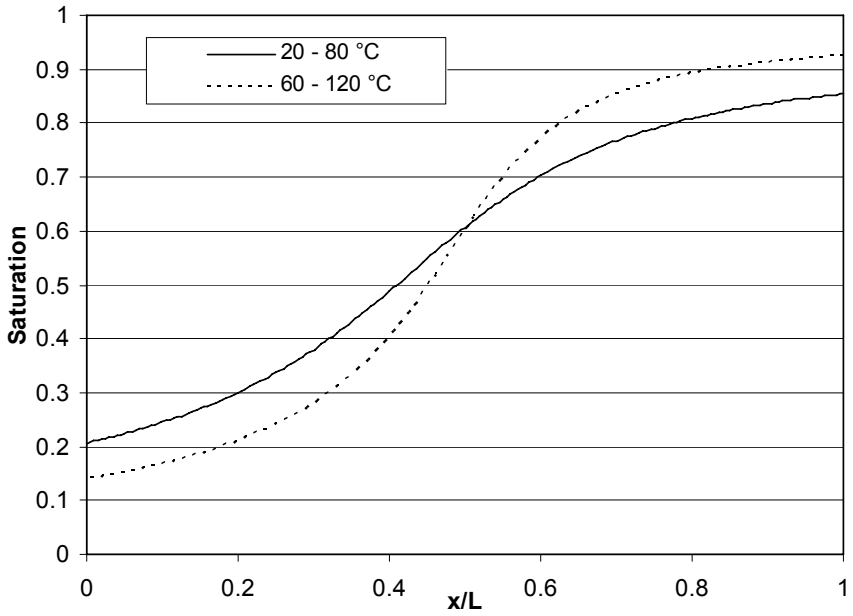

Figure 17. *Analytically calculated steady-state saturation profiles for two cases with identical temperature gradients, identical water contents but different levels of temperature.*

References

Alonso E.E., Alcoverro J., 2003. The FEBEX Benchmark Test. Case definition and comparison of different modelling approaches**.**

CIMNE, 2000. CODE_BRIGHT. A 3-D program for thermo-hydro-mechanical analysis in geological media. Departamento de Ingeneria del Terreno; Cartgrafica y Geofisica, UPC, Barcelona, Spain.

Claesson J., Sällfors G. 2005. Drying and resaturation of the bentonite barrier. New tools for modeling and analysis. In: Engineered Barrier System – Long-Term Stability of Buffer and Backfill. Swedish Nuclear Power Inspectorate. SKI Report 2005:48

Dueck A. 2004. Hydro-mechanical properties of a water unsaturated sodium bentonite. Laboratory study and theoretical interpretation. Division of Soil Mechanics and Foundation Engineering, Lund Institute of Technology, Lund, Sweden.

Fälth B., Hökmark H., 2004. TBT - Evaluation Modeling. Clay Technology AB. Lund.

Gatabin C., Billaud P., 2005. Bentonite THM mock-up experiments. Sensor data report. CEA. France.

Goudarzi R., Åkesson M., Hökmark H. (2005). Äspö Hard Rock Laboratory. Temperature Buffer Test. Sensors data report (period 030326-050101) Report No:5. SKB IPR-05-06

Hökmark H., Fälth B., 2002. TBT- Predictive modeling program rev3. Clay Technology AB. Lund

Åkesson M., Hökmark H. 2005. TBT_2 Predictive modeling Program. Clay Technology AB. Lund.